THESIS APPROVAL

GRADUATE SCHOOL, KASETSART UNIVERSITY

Master of Science (Chemistry)

DEGREE

Chemistry	Chemistry
FIELD	**DEPARTMENT**

TITLE: Ground state and Excited State Intramolecular Proton Transfer on the Enol-Keto Tautomerization of Salicylaldimine Based Chemosensor: Experimental and Theoretical Study

NAME: Miss Nutjarin Klinhom

THIS THESIS HAS BEEN ACCEPTED BY

THESIS ADVISOR

(Assistant Professor Songwut Suramitr, Ph.D.)

THESIS CO-ADVISOR

(Assistant Professor Surachai Thachepan, Ph.D.)

DEPARTMENT HEAD

(Associate Professor Waraporn Parasuk, Ph.D.)

APPROVED BY THE GRADUATE SCHOOL ON _____

DEAN

(Associate Professor Gunjana Theeragool, D.Agr.)

THESIS

GROUND STATE AND EXCITED STATE INTRAMOLECULAR PROTON TRANSFER ON THE ENOL-KETO TAUTOMERIZATION OF SALICYLALDIMINE BASED CHEMOSENSOR: EXPERIMENTAL AND THEORETICAL STUDY

NUTJARIN KLINHOM

A Thesis Submitted in Partial Fulfillment of
the Requirements for the Degree of
Master of Science (Chemistry)
Graduate School, Kasetsart University
2014

Nutjarin Klinhom 2014: Ground State and Excited State Intramolecular Proton Transfer on the Enol-Keto Tautomerization of Salicylaldimine Based Chemosensor: Experimental and Theoretical Study. Master of Science (Chemistry), Major Field: Chemistry, Department of Chemistry. Thesis Advisor: Assistant Professor Songwut Suramitr, Ph.D. 107 pages.

Three Schiff base derivertives, 2-(2-hydroxybenzylideneamino)phenol, 2-(hydroxybenzylidene)aniline and (Benzylideneamino)phenol, were synthesized and characterized by ^{1}H-NMR and FT-IR spectrometer. The photophysical properties of these salicylaldimine derivertives were studied as a function of pH. The result showed the Enol-Keto tautomers in acid-base solution. The effect of solvent polarity on the absorption and fluorescence properties were analyzed as well and the result exhibited the excited state intramolcular proton transfer (ESIPT) in non-polar and aprotic polar solvents. Moreover, the geometries at the ground state were optimized using Density Functional Theory (DFT) calculations with the CAM-B3LYP/6-311G(d,p) level of approximation. The electronic properties were carried out using the Time Dependent Density Functional Theory (TDDFT) at the same method. The effects of the solvents (chloroform and acetonitrile) were added using the polarizable continuum model (PCM) to model the solvation effect. The calculated results were in good agreement with those obtained from the experimental observation. The potential energy profiles of the ground and the lowest excited singlet state were studied on 2-(2-hydroxybenzylideneamino) phenol. The result of potential energy curve showed low activation barrier on the ground state (8.6 kcal/mol), whereas barrierless proton transfers were observed in case of excited state, confirming that intramolecular proton transfer prefer in the first singlet excited states more than ground state. The calculations also indicated S_1/S_0 conical intersection (CI) which provided alternative channel for radiation-less decay to the ground state that was a complete cycle.

_____ _____ ___ / ___ / ___

Student's signature Thesis Advisor's signature

ACKNOWLEDGMENTS

I sincerely appreciate to my thesis advisor, Assistant Professor Dr. Songwut Suramitr for his invaluable help and tremendous support throughout the course of this research. I am most grateful for him because I would not have achieved this far and this thesis would not have been completed without all the support that I have always received from him. I also wish to express my appreciation to my advisory committee Assistant Professor Dr. Surachai Thachepan for his constant encouragement and advice, not only the research methodologies but also many other methodologies in life.

I would like to express my deep gratitude to the Thailand Research Fund. These works were supported from Faculty of science, Kasetsart University. Center of Nanotechnology Kasetsart University, Kasetsart University Research and Development Institute (KURDI), The National Research University Project of Thailand (NRU), Laboratory of Computational and Applied Chemistry (LCAC). I would also like to thank all of staffs at Department of Chemistry, Faculty of Science, Kasetsart University for research facilities.

Finally, I am thankful for everything around me here in Kasetsart University that made me as I am today, all of my friends who give me laughter and make through all difficulties together for past three years. Moreover, I am especially grateful to my family for their advice, encouragement, support, and understanding throughout my graduate study. I promise, I will be the great one in someday.

Nutjarin Klinhom

June, 2014

TABLE OF CONTENTS

Page

LIST OF TABLES

LIST OF TABLES (Continued)

LIST OF FIGURES

LIST OF FIGURES (Continued)

LIST OF FIGURES (Continued)

LIST OF FIGURES (Continued)

LIST OF FIGURES (Continued)

LIST OF FIGURES (Continued)

LIST OF ABBREVIATIONS

E_{exc}	=	Excitation energy
λ_{max}	=	Maximum wavelength
$\angle$	=	Torsional angle, dihedral angle
θ	=	Rotation angle
B3LYP	=	Becke's three parameter hybrid functional using the LYP correlation functional
DFT	=	Density Functional Theory
EC	=	Exchange Correlation
eV	=	Electron Volt
f	=	Oscillator strength
HF	=	Hatree Fock theory
HOMO	=	Highest Occupied Molecular Orbital
LUMO	=	Lowest Unoccupied Molecular Orbital
ICT	=	Intramolecular Charge Transfer
MeOH	=	Methanol
FMOs	=	Frontier Molecular Orbitals
nm	=	Nanometer
PCM	=	Polarizable continuum model
S_0	=	Ground state
S_1	=	First singlet excited state
S_2	=	Second singlet excited state
S_3	=	Third singlet excited state
S_4	=	Fourth singlet excited state
S_5	=	Fifth singlet excited state
TD-DFT	=	Time-Dependent Density Functional Theory
UV	=	Ultraviolet radiation
PECs	=	Potential energy curves
PES	=	Potential energy surface
Å	=	Angstrom (unit of length)

LIST OF ABBREVIATIONS (Continued)

Compound (I)	=	2-(2-hydroxybenzylideneamino)phenol
Compound (II)	=	2-(hydroxybenzylidene)aniline
Compound (III)	=	(Benzylideneamino)phenol
E-form	=	Enol form
K-form	=	Keto form
EtOH	=	Ethanol
DMSO	=	Dimethyl sulfoxide
IRC	=	Intrinsic reaction coordinate
^{1}H-NMR	=	Proton Nuclear Magnetic Resonance
FT-IR	=	Fourier transform infrared spectroscopy
CI	=	Conical intersection
IC	=	Internal conversion
GSIPT	=	Ground state intramolcular proton transfer
ESIPT	=	Excited state intramolcular proton transfer
IMBD	=	Intramolecular hydrogen bonding
TS	=	Transition state
SS-PCM	=	State-Specific Polarizable continuum model

GROUND STATE AND EXCITED STATE INTRAMOLECULAR PROTON TRANSFER ON THE ENOL-KETO TAUTOMERIZATION OF SALICYLALDIMINE BASED CHEMOSENSOR: EXPERIMENTAL AND THEORETICAL STUDY

INTRODUCTION

1. Chemosensor

A chemosensor was a molecular device designed to detect a specific atoms or class of molecules. Research in this field was poised for considerable advances with the advent of diverse methods for analyze detection and new developments in the field of molecular recognition (Swager *et al*., 1998). The development of chemosensors for specific chemical species was a considerably important research area within the field of supramolecular chemistry. One of the most appealing approaches involved the construction of colorimetric chemosensors, specified that would allow the so-called 'naked-eye' detection without resort to any spectroscopic instrumentation. In recent years, designing molecular systems for sensing anions and cations with ''naked-eye'' detection were an attractive goal. Such system generally contained some combination of substrate recognition functionality (receptor) and optical signal reporter group (chromophore), and was designed to permit the detection of substrates via binding-induced changes in absorption properties. Many chemical sensors followed the approach of the covalent attachment of signaling subunits and binding sites as schematically shown in Figure 1.

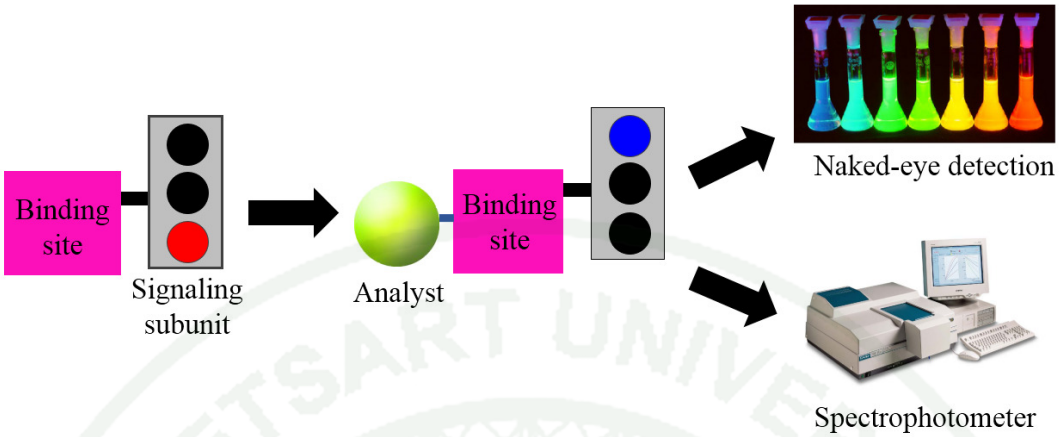

Figure 1 Schematic of chemosensor's function based on the binding site-signaling subunit approach and detection.

Chemosensors based on fluorescent signal changes were commonly referred to as fluorescent chemosensors which was another way which had been widely used as versatile tool in analytical chemistry, biochemistry, etc because it had highly sensitive technique selective versatile technique (Fegley *et al.*, 2012). Fluorescence chemsensors were usually made up of a receptor (ionphore), fluorophore (signal moiety) and a spacer to link them together. The readout of a fluorescent sensor was measured as a change in fluorescent intensity or intensity decay lifetime, or a shift in emission wavelength (Martínez-Máñez and Sancenón, 2003). Fluorescence techniques could accurately measure concentrations one million times smaller pico- and even femtomolar. Quantities less than an attomole ($<10^{-18}$ mole) might be detected which was better than absorption techniques.

2. Schiff base

Schiff base, or an imine functional group, was a compound with a functional group that contained a carbon nitrogen double bond with the nitrogen atom connected to an aryl or alkyl group, not hydrogen. Schiff base was formed from the condensation of an amine group with the carbonyl group of an aldehyde or ketone, as shown in the Figure 2. Schiff bases in a broad sense had a general formula $R_1R_2C{=}NR_3$, where R was an organic side chain. Since the nitrogen of the resulting bond had basic character (indicated by the lone pair shown explicitly on the nitrogen atom in the figure), it could take up a proton to form the conjugated acid of the schiff base, or the protonated schiff base. The formation of a schiff base and its functionality were important in a number of mechanism including in bioreactions.

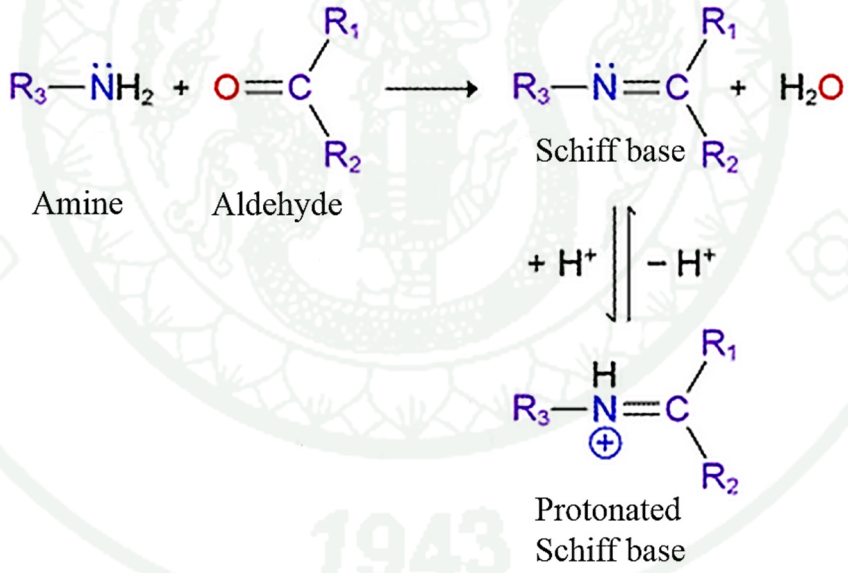

Figure 2 Synthesis of schiff base and the direct production of the protonated form.

Source: Soderberg (2012: section11).…….

Imine or schiff bases were some of the most widely used organic compounds due to their interesting properties. They were used as dyes and pigments, catalysts, liquid crystals, and intermediates in organic synthesis and a broad range of biological

activities such as probes in investigating the structure of DNA. Moreover, schiff base ligands also received significant attention. These compounds were often called ‘‘privileged ligands’’ because they were easy to obtain and had numerous applications (Kaczmarek *et al*., 2010). The applications of schiff base ligand instanced catalytic activity, selective recognition of metal ions, photochromic properties, antibacterial activity, and anticancer activity. For example in biological field, salicylideneaniline derivatives were effective against Mycobacterium tuberculosis H37Rv (Fang *et al*., 2014).

Salicylaldimine schiff bases were paid interest in this work. These compounds exhibited tautomerism of three different forms via enol, keto and zwitterionic forms which were reported to exist in the solid state. Salicylaldimine schiff bases were typical examples of photochromic and thermochromic compounds that continued to attract wide interest because of their technological applications. Photochromism and thermochromism of these compounds were due to their ability to undergo proton tautomerism, i.e., reversible change between enol and keto forms caused by electromagnetic radiation or heat. These properties depended on the molecular planarity, nature of crystal packing, effect of substituent and nature of the solvent. The mechanism of enol-keto tautomerism was demonstrated below.

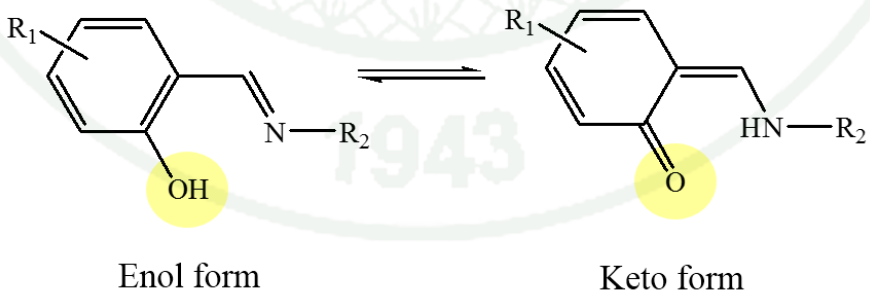

Figure 3 The mechanism of enol-keto tautomerism in salicylaldimine schiff bases.

Source: Chatziefthimiou *et al.*, 2006

3. Excited state intramolcular proton transfer

Excited state intramolecular proton transfer (ESIPT) was the process that involved the shifting of the proton in the excited state that consisted of proton donor (hydroxyl group –OH or amino group $–NH_2$) and proton acceptor group (carbonyl oxygen –C=O or imine nitrogen –N=) in close proximity in order to form the intramolecular hydrogen bonding (IMHB). This was the necessary condition for ESIPT. The basic photophysical process of the ESIPT was illustrated in Figure 4.

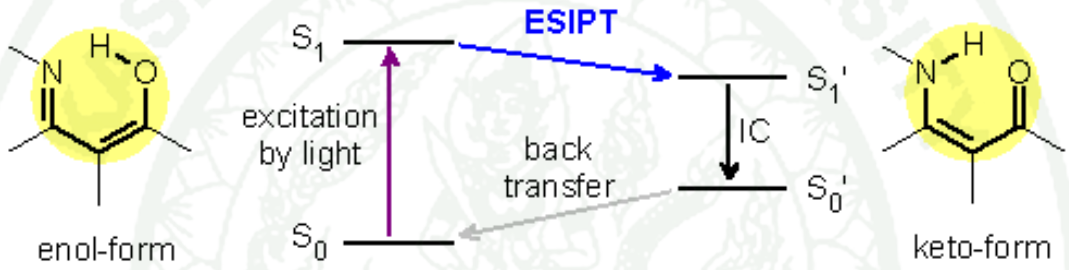

Figure 4 Schematic illustration of excited state intramolecular proton transfer.

Source: Kim *et al.*, 2010

ESIPT was a photo-induced enol-to-keto tautomerization via proton transfer in the excited state. The ESIPT chromophores existed in cis-enol form at the ground state, in which the intramolecular hydrogen bond was formed. Upon photoexcitation, the singlet excited state of the enol form was populated. Noted that no geometry relaxation occured during the excitation, which was the mandate of the Franck–Condon principle. Then an ultrafast ESIPT process occured and the cis-keto form at the singlet excited state was produced, which was stabilized by the intramolecular hydrogen bond. Since the ESIPT was much faster than the fluorescence process (radiative decay) (Shigemitsu *et al*., 2012), the fluorescence observed for the ESIPT chromophores often occured due to the keto tautomer, although exceptions did exist (Zhao *et al*., 2012).

In general, stoke shift was the difference between positions of the band maxima of the band maxima of the absorption and emission spectra of the same electronic transition. Large Stokes shifted fluorescence emission, about 6,000-12,000 cm^{-1}, was the most remarkable photophysical property of the ESIPT chromophores compared to the normal fluorophores such as fluorescein, rhodamine or boron-dipyrromethene (BODIPY) (Wang and Pang, 2013). The large stokes shift was a desired feature for fluorophores because the self-absorption or the inner filter effect could be avoided and the fluorescence analysis could be improved with this kind of fluorophores. Another unique feature of the ESIPT chromophores was the transient character of the ground state of the emissive species of the ESIPT chromophores, i.e. the keto tautomer. Figure 5 showed large bathochromic stokes shift about 8,000 cm^{-1} of 2-(2-hydroxy-4-phenyl)benzothiazole arising from transformation in excited state of enol tautomer.

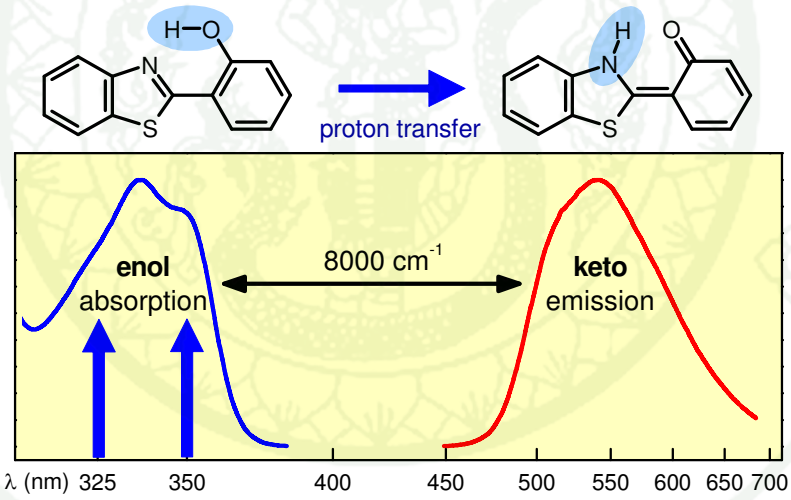

Figure 5 Large stokes shift of 2-(2-hydroxy-4-phenyl)benzothiazole.

Source: Elsaesser and Kaiser, 1986

Several characteristics hinted for ESIPT: (i) a nearly perfect planar ground-state structure with an hydrogen bond; (ii) a large Stokes shift; (iii) electronic transitions with an intramolecular charge-transfer (CT) nature; (iv) significant changes of the optical spectra upon pH variations; and (v) theoretical calculations indicating a possible ESIPT (Laurent *et al*., 2014). So, schiff bases with the proton donor close to nitrogen was considered.

In recent years, ESIPT had received an increasing attention because of its wide applications in such systems as UV-light polymer stabilizers, laser dyes, molecular switches fluorescence sensors, and particularly in biological systems. Mechanism of ESIPT process was currently being used to understand the photophysics of some molecules that showed such interesting characteristics. Several computational reports published in recent years (Doroshenko *et al*., 2012; Padalkar *et al*., 2013; Jayabharathi *et al*., 2014) had allowed a remarkable advance toward a full understanding of the ESIPT process, providing the ground for interpreting the quickly growing amount of experimental results. However in ESIPT mechanism, there were a number of questions that could not be answered exclusively by experimental means so it called for a detailed theoretical investigation. For example, what the structure of the S_1/S_0 systems was, why the ESIPT processes occurred, what the origin of ESIPT mechanism was, what non-radiative transition of ESIPT molecules was, computational quantum chemistry study on relevant model systems was a promising way to reveal the mechanism of the proton transfer through the intramolecular hydrogen bond (IMHB) process.

4. Quantum chemical calculations

Computational chemistry was a branch of chemistry that used computer simulation to assist in solving chemical problems. It used methods of theoretical chemistry, incorporated into efficient computer programs, to calculate the structures and properties of molecules. Computational results normally completed the information obtained by chemical experiments, in some case it could predict yet unobserved chemical phenomena. In addition, the experiments could not be explained with the electronic structure. Theoretical studies were an important way to approximate the electronic structure determinations, geometry optimizations, vibrational characteristics absolute infrared intensities, definition of transition structures and reaction paths, electron and charge distributions, potential energy surfaces (PES), rate constants for chemical reactions (kinetics), electron-donating and electron-accepting ability, thermodynamic calculations heat of reactions and energy of activation of molecular system with common computer software. Therefore computational quantum chemistry was one of the challenging tasks in calculating the electronic structure and predicting properties of variety for molecules. This approach could be provided molecular models and guided the design of novel molecules.

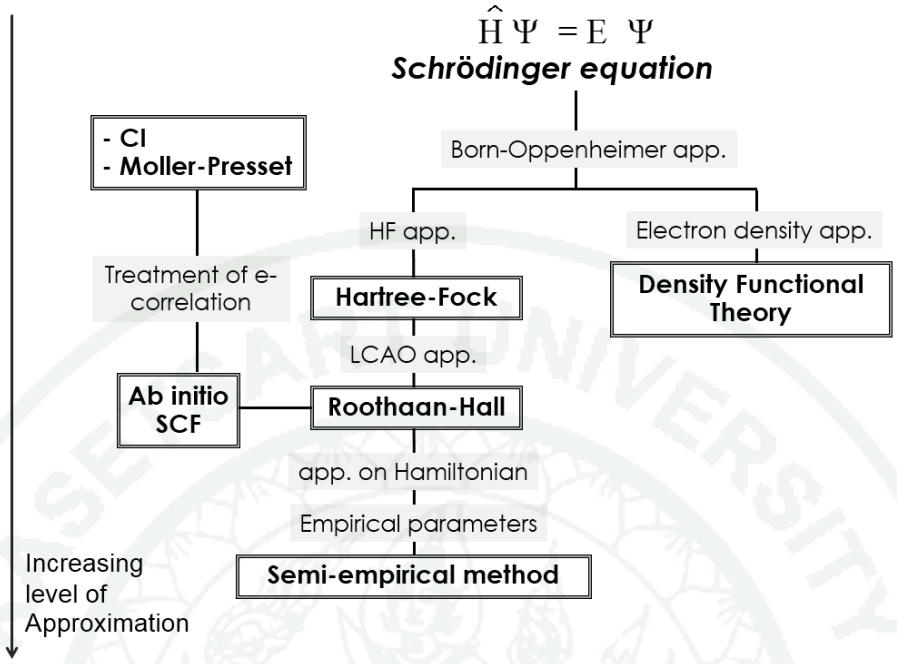

Figure 6 Diagram of several methods of quantum chemical calculation increasing level of approximation.

Source: Hehre, 2003

For quantum chemical calculation, it could be divided into different method according to the approximation explained in Figure 6. Quantum chemical calculations based on semi-empirical, *ab*-initio and density functional theory (DFT) or higher levels of theory. *Ab* initio quantum chemistry methods were computational chemistry methods based on quantum chemistry. The term *ab* initio was first used in quantum chemistry by Robert Parr and coworkers, including David Craig in a semi-empirical study on the excited states of benzene (Par *et al*., 1950). *Ab* initio translated from Latin means "from first principles." This refered to the fact that no experimental data was used. Hartree-fock theory (HF) was the simplest *Ab* initio calculation. It formed the wavefunction-based method foundation for more elaborate electronic structure methods. Hartree-fock relied on the following approximations: the Born-Oppenheimer approximation (electrons act independently of nuclei) and the independent electron approximation (electrons experience the field of all other electrons as a group, individually). The

Hartree-fock methods were able to give good results which provided a reasonable basis set and an appropriate correlation treatment taken into account. Semi-empirical quantum chemistry methods were based on the Hartree–fock formalism, but made many approximations and obtained some parameters from empirical data. It was less accurate than *ab* initio methods but also much faster thus it was applicable to large molecular systems and in certain circumstances fairly good theoretical results. Density Functional Theory (DFT) was considered an *ab* initio method, but different from other *ab* initio methods because the wave-function was not used to describe a molecule, instead the electron density was used.

DFT was among the popular and versatile methods available in condensed matter physics, computational physics and computational chemistry so this method was used in this work. DFT had been very popular for calculations in solid-state physics since the 1970s. However, DFT was not considered accurate enough for calculations in quantum chemistry until the 1990s, when the approximations used in the theory were greatly refined to better model, the exchange and correlation interactions. Hybrid exchange correlation functionals were widely used in the DFT formalism, to get a better fit with experiments. Popular forms of hybrid DFT methods included Becke's three parameter hybrid functional (Becke *et al*., 1993) using the Lee Yang Parr (LYP) (Lee *et al*., 1988) correlation functional (B3LYP). A new hybrid exchange–correlation functional named CAM-B3LYP was proposed by Yanai, Tew and Handy in 2004 (Yanai *et al*., 2004). It combined the hybrid qualities of B3LYP and the long-range correction demonstrating CAM-B3LYP yields atomization energies of similar quality to those from B3LYP, and also performing well for charge transfer excitations in a dipeptide model, which B3LYP underestimated enormously.

Time-dependent density functional theory (TDDFT) extended the basic ideas of ground state density functional theory (DFT) to the treatment of excitations or more general time-dependent phenomena. TDDFT was used to investigate the properties and dynamics of many-body systems in the presence of time-dependent potentials, such as electric or magnetic fields. Many researchers focused on Time-dependent density functional theory (TDDFT) method in order to investigate excitation energies,

frequency-dependent response properties, and photo absorption spectra, electronic properties with geometry relaxation effects in excited states (Jacquemin and Perpète, 2006). Nowadays, TDDFT still had some limitations, even though it could be helpful in understanding fundamentals of the electronic and optical characteristics of conjugated polymers and guiding the experimental efforts toward compounds with enhanced characteristics. However, the level of accuracy and computational time of a simulation was dependent on the model and basis set used.

Because of the application of excited state intramolecular proton transfer for chemosensor in accordance with the foregoing, recently, a number of papers had been published reporting in ESIPT mechanism in several molecules. Photoisomerization was not completely clear for salicylaldimine compounds and only few photophysical properties and photoisomerization which mechanism had been studied on experiment and theoretical calculation. These were the main motivations for starting this research. In this work, we focused on ground state and excited state intramolecular proton transfer (GSIPT and ESIPT) mechanism on Salicylaldimine Schiff bases. Salicylaldimine and its derivertives were synthesized and characterized by ^{1}H-NMR, IR spectroscopy. The absorption and emission properties were also investigate in organic and acid-base solution. Moreover quantum calculation was used to get insight into the molecules. The structural and optical properties were predicted using quantum chemical calculations with the CAM-B3LYP employing 6-311G(d,p) basis set by a suite of Gaussian 09 program. We had mainly optimized the ground state and excited-state geometries of Salicylaldimine Schiff bases. In addition, we gained important information about its spectra i.e. absorption, fluorescence and vibrational frequency by the theoretical calculation, and then discussed the role of intramolecular hydrogen bonding (IMHB) in the ESIPT process in detail. Meanwhile, we also carried out the calculations of some compound and focused on the mechanism for nonradiative transition in the excited state. The obtained calculation results were in good agreement with the experimental data and led to understanding in deep detail about salicylaldimine and its derivertives that could be designed and improved in new chemosensor.

OBJECTIVES

There are four main objectives of this work which were

1. To synthesize and characterize three salicylaldimine Schiff base derivatives; 2-(2-hydroxybenzylideneamino)phenol (Compound I), 2-(hydroxybenzylidene)aniline (Compound II) and (Benzylideneamino)phenol (Compound III).

2. To study the intramolecular proton transfer of salicylaldimine derivatives by photophysical properties considering on pH effect and solvent effect.

3. To investigate the structural geometry and electronic properties of salicylaldimine derivatives by Density Functional Theory (DFT) and Time Dependence Density Functional Theory (TDDFT) calculations.

4. To consider the potential energy curves (PECs) of 2-(2-hydroxybenzylidene amino)phenol, Compound I, on the Ground State Intramolecular Proton Transfer (GSIPT) and Excited State Intramolecular Proton Transfer (ESIPT) by DFT and TDDFT calculations.

LITERATURE REVIEW

In this section, literatures associating with this research were collected to create the main idea that use to plan this project. The application of Schiff bases used as chemosensors including the study of intramolecular bonding on ground state and excited state were reviewed.

Chemosensors played important roles in many chemical, environmental and biological systems. They were useful for monitoring analytes. So far, a large number of chemosensors had been constructed. Many literatures reported the design, synthesis and sensing action of novel receptors for cations bearing structure moieties like imines (Wang *et al*., 2010), coumarin (Kim *et al*., 2009), pyrrole (Xu *et al*., 2006). However, the functional groups such as hydroxyl (-OH) (Zhang *et al*., 2003), urea ($(NH_2)_2C=O$) (Cho *et al*., 2003), thiourea $(NH_2)_2C=S$) (Lee *et al*., 2002), amide (-CONH) (Kim *et al*., 2005) acted as binding site for anions.

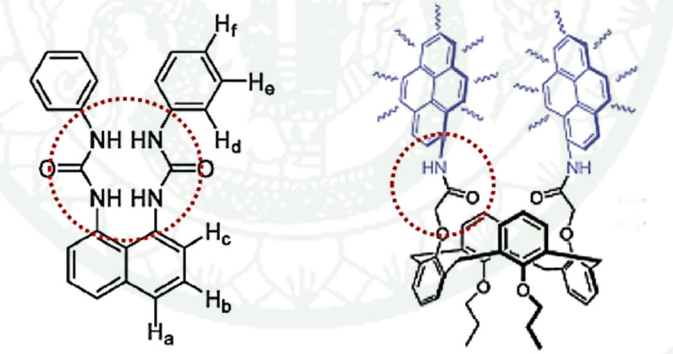

Urea ($(NH_2)_2C=O$) Amide(–CONH)

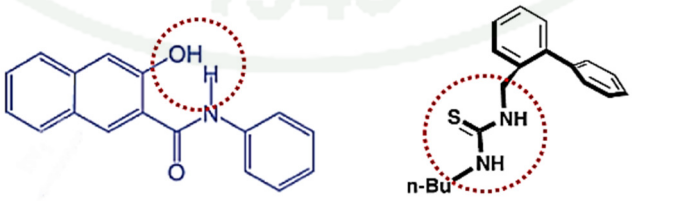

Hydroxide (–OH) Thiourea ($(NH_2)_2C=S$)

Figure 7 For example binding site belonging to chemosensors.

In present work, salicylaldimine deriveritives were chosen to study since they had been attracted significant interested in widespread useful such as fluorgenic agent, pesticides, herbicidal agents, ionoselective electrodes for the determination of cations and anions in analytical samples (Kaczmarek *et al*., 2010). The following example showed the usability of schiff base as chemosensors.

Domotor *et al*. (2014) reported that a novel schiff base was easily synthesized by the condensation reaction of 2-aminophenol and p-hydroxyphenylbenzothiazole (p-HBT) and could be used as detection of aluminum in ethanol as well as in aqueous solution. Among the detected metal ions, only Al^{3+} could induced a significant enhancement in fluorescence intensity. In addition, the binding details of probe-Al^{3+} complex were investigated by means of DFT computational studies, implying the fluorescence intensity enhanced by the inhibition of the ESIPT process and further the formation of a large electron conjugation system. The process was shown in Figure 8.

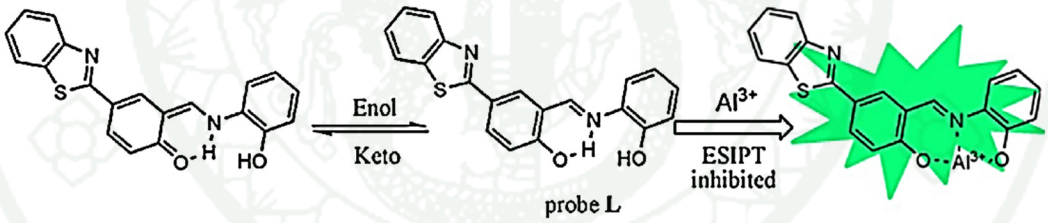

Figure 8 Structures of enol and keto forms of probe and proposed binding mode.

Source: Domotor *et al*. (2014)

Wang *et al*. (2011) reported the application of salicylaldehyde salicylhydrazone for fluorescent indicators for Mg^{2+} and Zn^{2+} in living cell. Salicylaldehyde salicylhydrazone in free solution could be take place ESIPT and displayed non-fluorescence. After addition Mg^{2+} showed the fluorescence peak at 460 nm in dimethylformamide (DMF)-water solvent and showed fluorescence peak at 488 nm in the present of Zn^{2+} for ethanol-water. The mechanism of ESIPT on salicylaldehyde salicylhydrazone and the chemosensing process were shown in Figure 9.

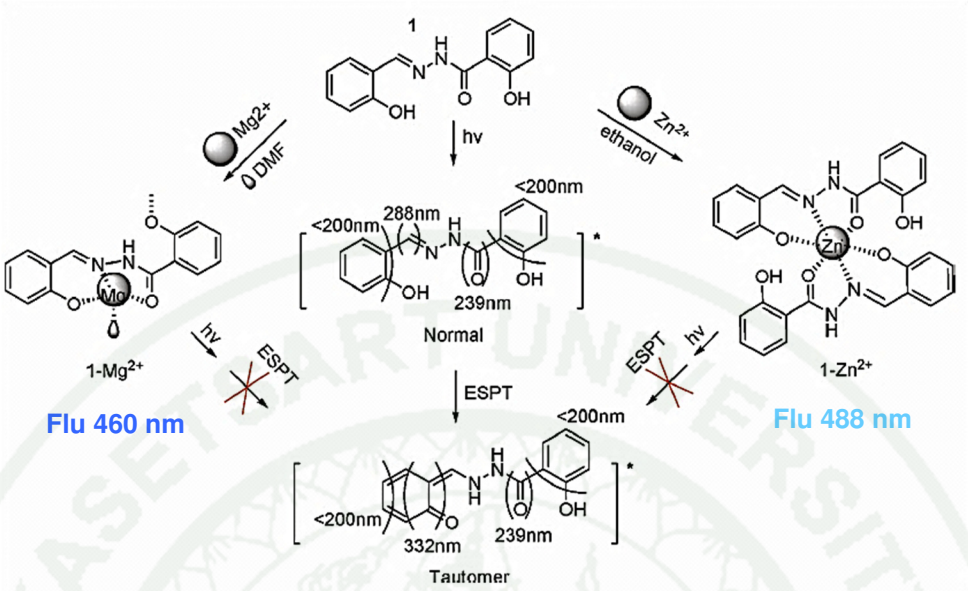

Figure 9 Process of salicylaldehyde salicylhydrazone used as fluorescence chemosensor in ethanol and DMF solution.

Source: Wang *et al*. (2011)

Wu *et al*. (2014) showed a facile naphthalene-based schiff base chemosensor, 1-((pyridin-2-ylmethylimino)methyl)naphthalen-2-ol (NS), was designed and synthesized for selective detection of Zn^{2+} ions. NS alone was almost non-fluorescent in neutral aqueous solution which was assigned to the isomerization while a fluorescence enhancement of 10-fold at 446 nm could be realized upon addition of 5.0 equiv. of Zn^{2+} with excitation at 352 nm indicating that NS formed a complex with Zn^{2+} and the transformation of *cis–trans* isomerization had been restricted. Figure 10 showed a proposed structure of the probe–Zn^{2+} complex.

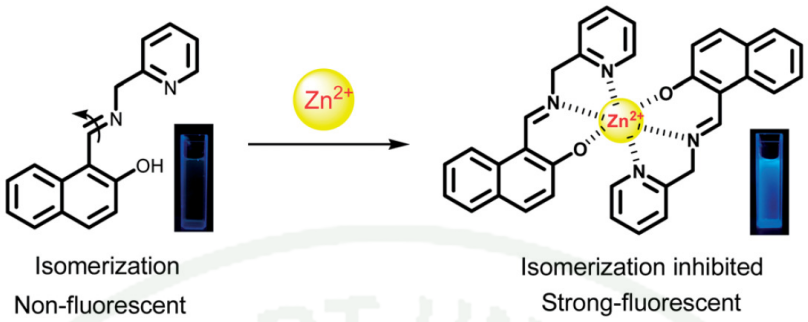

Figure 10 A proposed structure of the probe-Zn^{2+} complex.

Source: Wu *et al*. (2014)

Kim *et al*. (2012) showed salicylimine-based fluorescent chemosensor was developed utilizing turn-on fluorescence enhancement. Upon treatment with aluminium ions, the fluorescence of the sensor was enhanced at 510 nm due to formation of a 1:1 complex between the chemosensor and the aluminium ions at room temperature. As the concentration of Al^{3+} was increased, the fluorescence gradually increased. The application was used for biological imaging. Figure 11 showed how the receptor and complex binding.

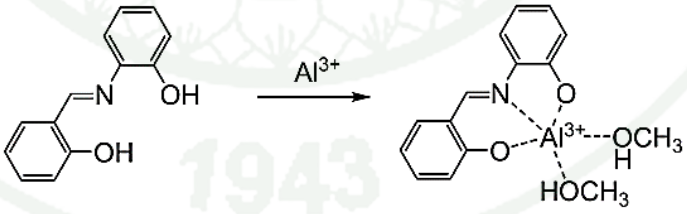

Figure 11 Chemical structures of the receptor o-phenolsalicylimine and a 1:1 complex of receptor and Al^{3+} in CH_3OH:H_2O.

Source: Kim *et al*., 2012

Prabhu *et al*. (2012) also showed salicylaldimine based chemosensor was examined for anions and cations. Visual changes were showed towards biological relevant anions like F^- and OH^- as well as various cations such as Fe^{3+}, Co^{2+}, Ni^{2+}, Cu^{2+} and Sn^{2+}. The stoichiometry of the complex formed between the receptor with anions and cations were investigated by Job's plot method. Receptors bound with anions in a 1:1 stoichiometry and with cations either in 2:1 stoichiometry. Proposed cyclic structure formed between the anion or cation and the receptors was shown in Figure 12**.**

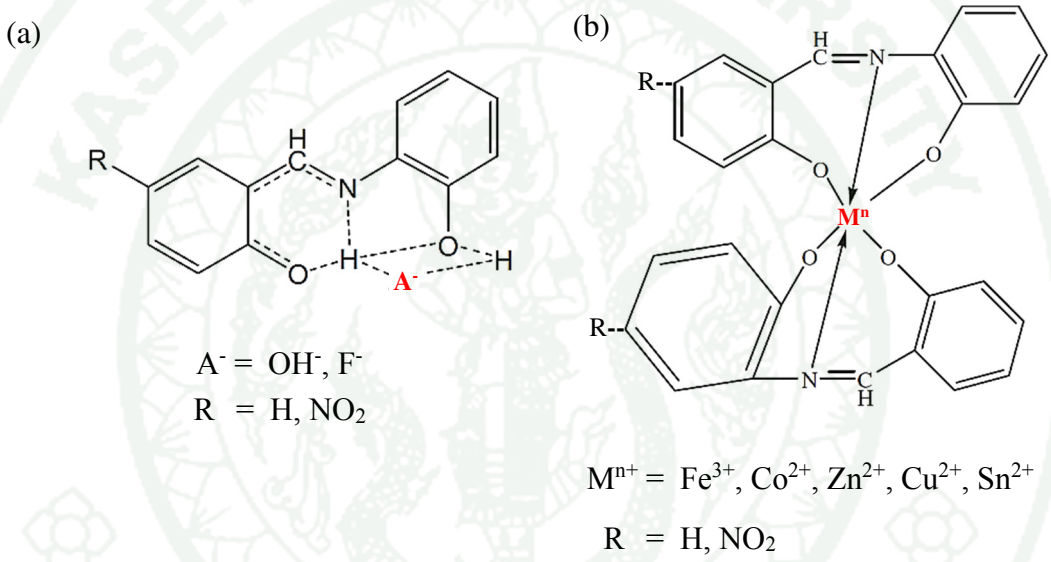

Figure 12 (a) Proposed hydrogen bonding interaction between receptor with anion. (b) Proposed structure of the 2:1 complex formed between the receptors and cation.

Source: Prabhu *et al*. (2012)

It could be seen the especially same finding that many reviews exhibited on the molecules which could be used as suitable chemosensors for cations and anions. The important of specifications for chemosensors should have a binding site, proton transfer occurrence and non-fluorescence while they were not binding with the target guests.

Weller and Elektrochem (1956) who were the first described on excited-state intramolecular proton transfer (ESIPT) that was a photoinduced procedure in which a proton jumped across the intramolecular hydrogen bond (IMHB) from a proton donor group to a proton acceptor. Weller introduced the domain of photochemistry to a new arena of research, namely the excited state intramolecular through the unique experiments with methylsalicylate proton transfer (ESIPT) reaction. Since then the study of photoinduced proton transfer (PT) process across intramolecular hydrogen bonds (IMHBs) had been a potential avenue for a wide expanse of fundamental as well as applicative research.

Koll (2003) reported the intramolecular proton transfer in schiff bases. Koll observed the change of UV-Visible spectra with solvent polarity, strong acid-base solution and thermochromic properties of compounds. The results showed that structure of tautomeric forms were dependent on resonance and showed quite large flexibility on variable factors. Proton transfer forms revealed that absorption bands were shifted to long wavelength when increasing polarity of solvents, increasing base solution and low temperature. These results were concluded that tautomeric forms of schiff bases being in equilibrium of molecule was different. In schiff bases, each of tautomers were strongly influenced by resonance internal π-electronic coupling between zwitterionic and keto structures. Almost equal participation of both forms led to effective resonance between them and stabilization of intramolecular hydrogen bond in this way. It was responsible for the increased stability of so called resonance assisted hydrogen bonds. Figure 13 showed resonance interaction between enol, keto and zwitterionic of the structure.

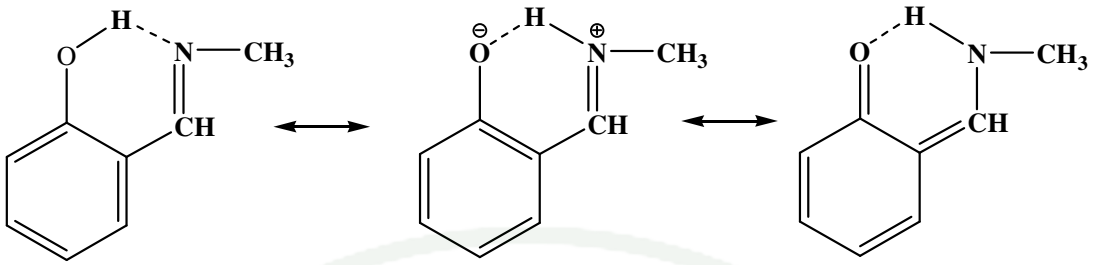

Figure 13 Resonance interaction between zwitterionic and keto of 2-(methylaminomethyl)phenol

Source: Koll (2003)

However the mechanism of salicylaldimine schiff base could not be observed on the molecular level by experimental such as excited state behavior, transition state energies character and enol-keto tautomerization so it needed expensive and high technology in extremely short timescales such as femtosecond spectroscopy for experimental part. Because of the significant mechanism, we required to understand in the depth of these molecules. Quantum chemical calculation was the application skill to approximate chemistry problems. Therefore, theoretical calculations were a useful complementary tool for the understanding of absorption and emission spectra, photophysical properties, enol-keto tautormerization mechanism via proton transfer in ground state and excited state on salicylaldimine derivatives. The comprehension of system behavior were particularly important for chemosensor and the novel materials.

Suramitr *et al*. (2010) showed that the electronic excitation transitions of carbazole-based oligomers, could be investigated by using density functional theory (DFT) and time-dependent (TDDFT) methods. Absorption and fluorescence energies had been obtained from TD-B3LYP/SVP calculations performed on S_1 optimized geometries and results were in agreement with experiment data. They also discussed and concluded advantages of theoretical calculation, which provided critical structural

and electronic understanding of excitation relaxation phenomena that could be exploited in design novel optical material.

Tomasi *et al*. (2005) and Jacquemin *et al*. (2007) indicated that the solvent effects on absorption and emission spectra were relevant. Time dependent density functional theory (TDDFT) methodology allowing excited state optimizations with the inclusion of bulk solvent effects had been proposed and applied comparing gas-phase and solvent effect. The results showed that the low-lying excited states using the TDDFT had been the subject of an intense study and a detailed understanding of its photochemistry. In addition, the wavelengths of absorption and emission had been compared to the available experimental values and the results were successful.

Yang *et al*. (2008) and Meeto *et al*. (2008) found that TDDFT was used for the vertical excitation energies and absorption properties calculation and the optimized geometry in the ground state was employed to perform this vertical TD calculation. The compounds were performed by single point calculations at the optimized geometries of the ground state. The excitation energy, calculated based on the optimized structures on the ground state, the electronic transitions were studied for first and second singlet-singlet state. The implicit assumption underlying this approximation was that the lowest singly excited state could be described by only one singly excited configuration in which an electron was promoted from the Highest Occupied Molecular Orbital (HOMO) to the Lowest Unoccupied Molecular Orbital (LUMO) were given in Suramitr *et al*. (2005 and 2007) to understand the electron delocalization.

In recent years, many researchers had studied on ESIPT process by theoretical calculation. As the popular theoretical method, DFT had been used efficiently and accurately in studying the mechanism of many compounds, which the results from this method well reproduced the experimental results. In addition, TDDFT method had been confirmed to be an effective candidate to investigate the electronic spectra and electronic excited state. The following was the model of the computational chemistry to study the intramolecular hydrogen bonding (IMBD) system of schiff bases molecule.

Beyramabadi *et al*. (2011) showed computational theory studied on tautomerization of 4-(2-thiazolylazo)-resorcinol, employing density functional theory and the polarizable continuum model (PCM). B3LYP hybrid functional and the 6-311+G(d,p) basis set was used in this research. In addition tautomerization mechanism was investigated in gas phase, chloroform and dimethyl sulfoxide (DMSO) solutions for analysis of the solvent effects. The calculated results showed that enol form was stable in the ground state, and conversion from the enol to the keto form occurred very rapidly after excitation. Enol tautomer was more stable than the keto tautomer in the gas phase, while solute-solvent interactions favored the keto tautomer in polar solvents. Also, by increasing of the polarity of the solvent, stability and percentage of the keto tautomer increased in comparison with the enol tautomer.

Annaraj *et al*. (2014) reported electronic properties on two schiff bases compounds, 6,60-(1E,10E)-1,10-(propane-1,3-diylbis(azan-1-yl-1-ylidene))bis(ethan-1-yl-1ylidene)bis (3-(prop-2-ynyloxy)phenol) and (E)-2-(1-(2-hydroxyethylimino) ethyl)-5-(prop-2-ynyloxy)phenol compared with the available experiment data. B3LYP/6-311+G(d,p) level of theory was used in this research. The vibrational frequencies and potential energy curves for the intramolecular proton transfer in the ground (GSIPT) and excited (ESIPT) states were also generated in gas phase and dimethyl sulfoxide. The results showed the enol forms were more stable than the corresponding keto forms in gas phase. However, in solution phase, the keto forms were found to be more stable than the respective enol forms. In gas phase, the GSIPT went through low activation barrier, whereas in excited state spontaneous proton transfer occured. In presence of DMSO solvent, the energy barrier for GSIPT for the enol to keto conversion in ground state reduced to 1.2 kcal/mol. The calculated vibrational frequencies and UV–Visible spectra were compared with those obtained from experiments.

Kim *et la*. (2007) exhibited fluorescence quenching behaviors of four known excited-state intramolecular proton transfer (ESIPT) molecules were studied by semiempirical and *ab* initio calculations. The ESIPT compounds studied in this work were assorted into two sets depending on the N-containing ring structure (5- and 6-

membered rings). It had been found that twisted intramolecular charge transfer (TICT) process in the excited keto state (K*) after ESIPT, one of the possible quenching pathways of ESIPT fluorescence, was significantly influenced by the geometrical properties of intramolecular hydrogen bond associated with the N-containing ring structure. The compounds with 5-membered ring had efficient ESIPT emission with large barrier to fluorescence-quenching TICT state, due to appropriate stabilization of planar K* through intramolecular H bond. For the compounds with 6-membered ring, however, ESIPT emission was completely quenched due to significantly lowered barrier resulting from too short H-bond length. Elaborate calculations were shown that the structure of N-containing proton donor ring played a crucial role in intramolecular H-bond stabilization in the K* state and thus determined the ESIPT emission differently.

Moghadam *et al*. (2014) showed the computational results of the photophysics of N-salicilydenemethylfurylamine (SMFA). Excited state reaction coordinates and the consequent energy profiles of this schiff base had been investigated with the CC2 method, which was a simplified version of singles-and-doubles coupled cluster theory. The results displayed the primary UV-induced reaction which was proton transfer from the hydroxyl group to the imine group. This reaction was predicted to be essentially barrier-less and thus extremely fast. The photochromic species SMFA formed in this process absorbed strongly in the visible range of the spectrum. It represented a typical example of a so-called ESIPT system.

Moreover they also reported that the characteristic features of such systems were strong and broad absorption in the UV-Visible range, and very fast radiation-less returned to the ground state whereas such systems effectively converted the photon energy into vibrational energy (heat), as was well known for commercially used photostabilizers and photoscreens. The calculations in this research indicated two S_1/S_0 conical intersections (CIs) which provided non-adiabatic gates for radiation-less decay to the ground state for SMFA. At the CIs, two barrier-free reaction coordinates directed the excited system to the ground state of enol-type minimum. According to calculation results, a trans-keto type structure obtained from photoexcitation of the enol, could be

responsible for the photochromoic effect of SMFA. The trans-keto form produced by UV excitation of enol form was a strong UV-Visible and should be highly photostable. Upon strong UV irradiation, a significant concentration of the trans-keto form of SMFA could be produced. The ground state of the trans-keto form was metastable ($\Delta E = 0.84$ eV). The thermal back reaction from trans-keto to the more stable enol form had to overcome a barrier of about 1.1 eV and was therefore expected to be rather slow. Thus, UV irradiation of SMFA might result in a mixture of enol form and its photoproduct trans-keto form.

For the excited-state intramolecular proton transfer (ESIPT) reaction of salicylidene aniline, which incorporated transfer of a hydroxy proton to the imine nitrogen through an intramolecular six-membered-ring hydrogen-bonding system, numerous research had been investigated for example Ortiz-Sánchez *et al*. (2008), Sporkel *et al*. (2013) and Jacquemin *et al*. (2014). Nonetheless, salicylidene-o-Amino phenol with double hydrogen proton had never been studied. So, in this study we studied the photophysical properties of salicylidene-o-aminophenol (Compound I), and salicylialdimine derivatives (Compound II and III) which were synthesized by amine aldehyde condensation (Xia and Chen, 2006). This study was separated into two parts which composed of experiment and calculations. This was promising work that helped to understand a fundamental of the compound and profound molecular system for known materials as well as in guiding the experimental efforts toward novel compound with enhanced characteristics.

MATERIALS AND METHODS

1. Chemicals

- 2-Aminophenol (C_6H_7NO, Sigma Aldrich)
- Salicylaldehyde ($C_7H_6O_2$, Sigma Aldrich)
- Benzaldehyde (C_6H_5CHO, Sigma Aldrich)
- Aniline (C_6H_7N, Sigma Aldrich)
- Dimethyl sulfoxide ($(CH_3)_2SO$), A.R. grade, ACI Labscan)
- Ethyl alcohol (EtOH, A.R. grade, ACI Labscan)
- Ethyl acetate ($CH_3COOC_2H_5$, A.R. grade, ACI Labscan)
- Acetonitrile (CH_3CN, A.R. grade, ACI Labscan)
- Methyl alcohol (MeOH, A.R. grade, ACI Labscan)
- Dichloromethane (CH_2Cl_2, A.R. grade, ACI Labscan)
- Acetone ($(CH_3)_2CO$), A.R grade, ACI Labscan)
- Sodium hydroxide (NaOH, Lab. grade, Labscan)
- Hydrochloric acid (HCl, Lab. grade, Labscan)
- Sodium Sulfate, Anhydrous (Na_2SO_4, A.R. grade, ACI Labscan)

2. Apparatus

2.1 Nuclear Magnetic Resonance analyses (NMR) were recorded on an INNOVA UNITY VARIAN spectrometer which operated at 400.00 MHz for ^{1}H-NMR in deuterated chloroform-d ($CDCl_3$). Tetramethylsilane (TMS) used as an internal reference.

2.2 Fourier Transform Infrared analyses (FT-IR) was used to characterize the molecule using Bruker Equinox 55. Small amount of dried sample powder was mixed together with 0.500 g of KBr. The mixture powder was pressed to a flat round piece and then scanned with IR radiation to collect the percentage the transmittance in the range between 4000-1000 cm^{-1}

2.3 UV-Vis analyses were carried out with Jasco V-670 UV/Vis/NIR spectrophotometer. The spectra were measured using 1 cm quartz cells at the room temperature. A stock solution (10^{-3} mol/L) of samples was diluted to a suitable volume in order to obtain the required concentration (10^{-4} mol/L) in several solvents, ethyl acetate, dichloromethane, ethyl alcohol, methyl alcohol, acetonitrile and dimethyl sulfoxide.

2.4 Fluorescence analysis was obtained using Perkin Elmer Instruments LS55 fluorescence spectrophotometer. The excitation wavelength for compound (I), (II) and (III) were 350, 340 and 350 nm, respectively. The fluorescence spectra were measured in the range of 200-700 nm. All compound solutions for fluorescence measurements were prepared at the concentration of 10 μM in several solvents, ethyl acetate, dichloromethane, ethyl alcohol, methyl alcohol, acetonitrile and dimethyl sulfoxide.

3. Synthesis

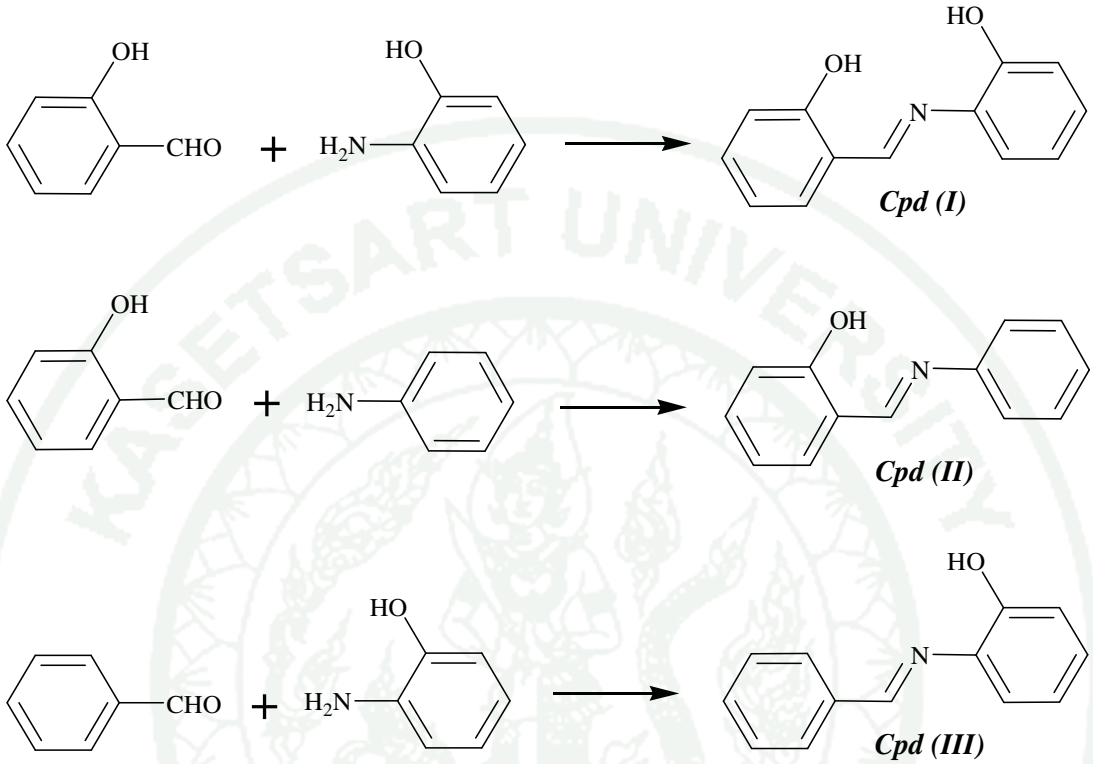

Figure 14 Synthesis of Compound (I), (II) and (III).

Compound (I), (II) and (III) were synthesized by mixing a solution aniline (5.00 mmol) in ethanol (20 mL) and a solution of aldehyde (5.00 mmol) in ethanol (20 mL). The reaction mixture was refluxed about 80 °C for 2 h. The reaction progress was checked by thin layer chromatography (TLC) to monitor the completed product. The two substrates and product were spotted on a sheet of TLC (20 x 20 cm, silica gel 60 with F_{254}) known as a stationary phase and hexane: ethanol (1:1) as a mobile phase. The solution was evaporated to 15 mL. After cooling down to room temperature, crystals were form. The crystals products were filtered and washed with cooled ethanol and then dried in air. The products were characterized by ^{1}H-NMR and FT-IR data. The mechanism of this reaction was shown in Figure 15.

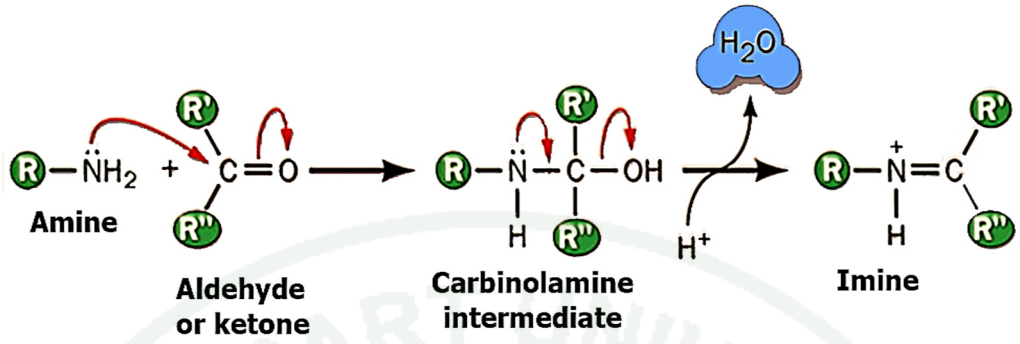

Figure 15 Amine aldehyde condensation mechanism.

In acid or base reaction, protonation of the carbonyl activated and made it more susceptible to attack by a neutral nucleophilic like the N of a primary amine. At first, amine which was the N nucleophile attacked at the electrophilic C of the C=O group with the electrons. Removal of the proton neutralized the positive charge on the N and formed the carbinolamine intermediate. To form the imine, we needed to dehydrate. Before -OH left, it needed to be protonated so a simple acid or base reaction occurred. The electrons of the N used to help pushing out the leaving group occurred a neutral water molecule and left iminium ion. Deprotonation of the iminium N revealed the imine product and regenerated the acid catalyst.

4. Theoretical calculation

Calculation part were brought to investigate intramolecular hydrogen bonding mechanism. Compounds which had proton donor adjacent to a proton acceptor could be given intramolecular proton transfer in ground and excited state. Figure 16 as shown below depicted the possibility pathway in ground state and excited state intramolecular proton transfer process of Compound (I), Salicylidene-o-aminophenol, which Enol form, $Keto_A$ and $Keto_B$ were represented the structures on ground state while Enol*, $Keto_A$* and $Keto_B$* were represented the structures in excited state.

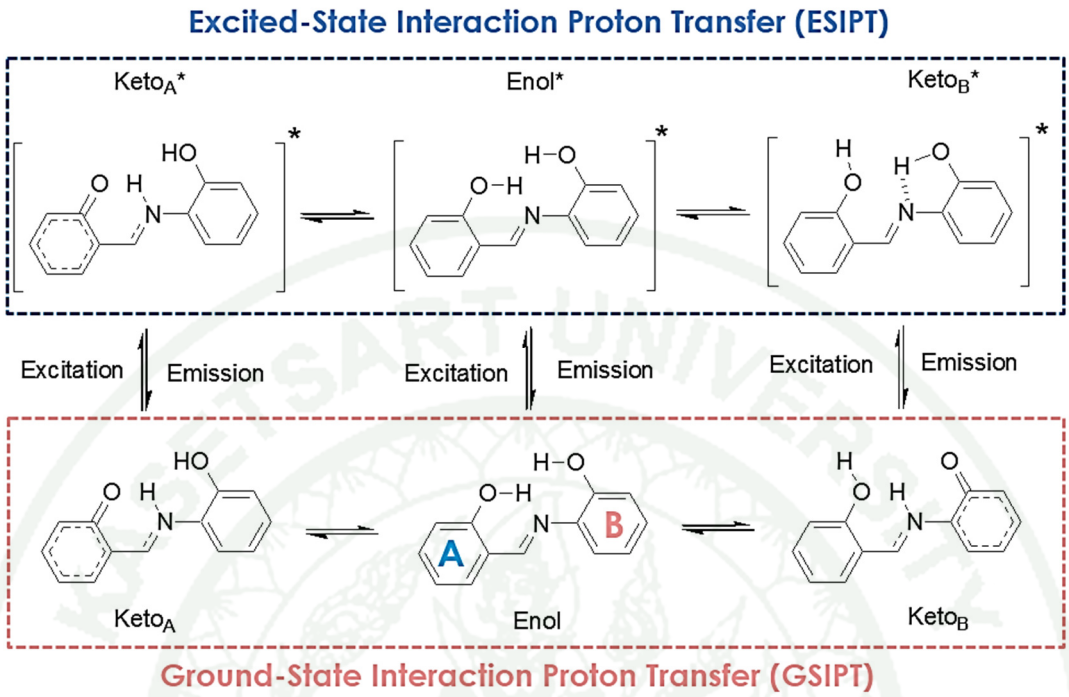

Figure 16 Mechanism of enol-keto tautomerization via GSIPT and ESIPT of Compound (I).

For ground state intramolecular proton transfer (GSIPT), the molecular structure of compounds were carried out based on DFT. The three parameter hybrid functional of Becke with the correlation functional of Lee, Yang, and Parr had been chosen. The ground state (S_0) geometries were fully optimized without restricting the symmetry using hybrid functional with long-range corrections state CAM-B3LYP together with 6-311G(d,p) level of theory to determine the most stable conformation. The vibrational frequencies at the optimized structures were computed using the same method to verify that the optimized structures corresponded to local minima on the energy surface. The vertical excitation energies of the ground state equilibrium geometries were calculated with TDDFT. The low-lying first singlet excited state (S_1) of each conformer was relaxed using the TDDFT to obtain its minimum energy geometry. The difference between the energies of the optimized geometries in the first singlet excited state and the ground state was used in computing the vertical emission. The schematic of calculation excitation and emission energy were shown in Figure 17.

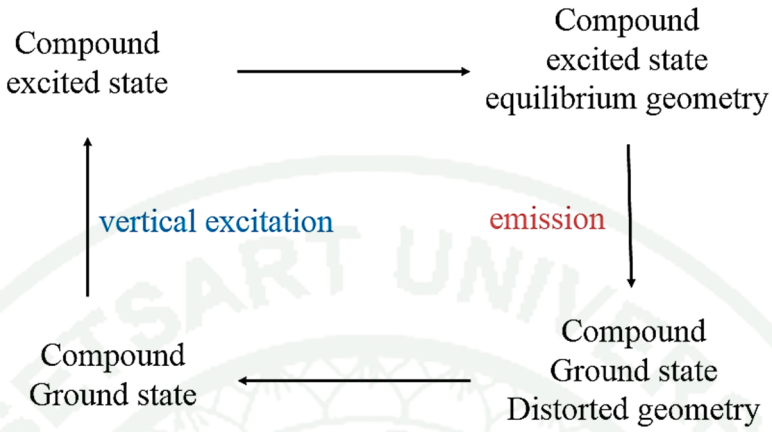

Figure 17 The scheme for calculation of excitation and emission.

The solvent effects on the absorption and emission properties were also taken into account. All the computations in solvents were carried out using the Polarizable Continuum Model (PCM). The conductor polarizable continuum model (CPCM) was one of the most common and effective model among the theoretical methods for considering solvent effect which conducted employing parameters and iterative computation methods (Zhang *et al*., 2008) to contain the solvation effect. Therefore, the solvent effect on electronic spectra with a continuum solvent model were estimated on the molecules.

The potential energy surfaces (PECs) were considered to study GSIPT and ESIPT and conical intersection (CI) mechanism. TDDFT had been successfully used to study other related ESIPT systems (Aquino et al., 2005; Ortiz-Sanchez et al., 2006). PECs were explored taking the O-H elongation and the ∠C-C-N-C dihedral angle as driving coordinates for the proton transfer and the rotation, respectively. An approximation to the geometry and energy of the CI had been obtained minimizing the energy of the S_1 state using TDDFT monitoring its excitation energy.

All calculations were performed using the GAUSSIAN 09 computational program (Frisch *et al*., 2009). GaussView5.0.8 program was used to prepare input molecules using its advanced 3D structure builder and examined calculation results, graphically visualization features such as display molecular orbitals and other surfaces, view spectra, animate normal modes, geometry optimizations and reaction paths (Dennington *et al*., 2008). Electronic DFT based methods had been used to explore the topology of the ground S_0 and TDDFT optimizations performing for S_1 states. Single electronic spectra, absorption spectra, and charge distribution between the ground and excited states were obtained from TD-DFT data and calculated with GaussSum 2.0 (O'Boyle *et al*., 2005).

RESULTS AND DISCUSSION

Experiment

1. Synthesis and characterization

In the present work, three compounds were synthesized by facile condensation of aldehyde and amine. Compound (II) and Compound (III) were synthesized in order to compare properties with Compound (I). The spectral data may be selected as displayed below. The ^{1}H-NMR and FT-IR spectra were shown in Appendix A and B, respectively.

1.1 Synthesis of Compound (I)

Compound (I) was prepared from salicylaldehyde (0.53 mL, 5.00 mmol), 2-aminophenol (0.546 g, 5.00 mmol). It was obtained with a yield of 0.981 g, 92.3% as an orange product as shown in Figure 18a. ^{1}H-NMR spectra the follow signal were observed:

^{1}*H*-NMR ($CDCl_3$, δ *ppm*): 12.26 (s, 1H, Ar-O*H*), 8.69 (s, 1H, -C*H*=N), 7.42 (t, J_1=7.4, J_2=7.6 Hz, 2H, Ar-*H*), 7.22 (t, J_1=7.7, J2=7.9 Hz, 1H, Ar-*H*), 7.15 (d, J=7.7, 1H, Ar-*H*), 7.06-6.94 (m, 4H, Ar-*H*), 5.78 (s, 1H, -O*H*)

FT-IR (KBr, cm^{-1}): 3,455 (O-H, stretching); 3,046 (-HC=N, stretching); 2,947 (-C-H, stretching); 1,632 (C=N, stretching); 1,464 (C=C, stretching); 1,415 (–HC=N, bending) 1,367 (C-N, stretching); 1,222 (C-O, stretching)

1.2 Synthesis of Compound (II)

Compound (II) was prepared from salicylaldehyde (0.53 mL, 5.00 mmol), aniline (0.46 mL, 5.00 mmol). It was obtained with a yield of 0.859 g, 90.1% as yellow product as shown in Figure 18b. ^{1}H-NMR spectra the follow signal were observed:

^{1}H-NMR ($CDCl_3$, δ *ppm*): 13.25 (br, 1H, Ar-O*H*), 8.63 (s, 1H, C*H*=N), 7.45-7.36 (m, 4H, Ar-*H*), 7.31-7.27 (m, 3H, Ar-*H*), 7.03 (d, J=9.0 Hz, 1H, Ar-*H*), 6.95 (t, J_1=7.5, J_2=7.6 Hz, 1H, Ar-*H*)

FT-IR (KBr, cm^{-1}): 3,227 (O-H, stretching); 3,078 (-C-H, stretching); 3,024 (-C-H, stretching); 3,058 (H-CN, stretching); 1,616 (C=N, stretching); 1,589 (C=C, stretching); 1,608 (C=C, stretching); 1,275 (C-O, stretching); 1,184 (C-N, stretching)

1.3 Synthesis of Compound (III)

Compound (III) was prepared from benzaldehyde (0.51 mL, 5.00 mmol), 2-aminophenol (0.546 g, 5.00 mmol). It was obtained with a yield of 0.8471 g, 87.3% as beige color product as shown in Figure 18c. ^{1}H-NMR spectra the follow signal were observed:

^{1}H-NMR ($CDCl_3$, δ *ppm*): 8.71 (s, 1H, C*H*=N), 7.93 (d, J=7.5 Hz, 1H, Ar-*H*), 7.92 (d, J=7.6 Hz, 1H, Ar-*H*), 7.52 (d, J=7.2 Hz, 2H, Ar-*H*), 7.48 (s, 1H, Ar-*H*), 7.31 (d, J=8.0 Hz, 1H, Ar-*H*), 7.23 (t, J_1=7.7, J_2=7.7 Hz, 2H, Ar-*H*), 7.03 (d, J=8.7 Hz 1H, Ar-*H*), 6.91 (t, J_1=7.7, J_2=7.7 Hz, 1H, Ar-*H*)

FT-IR (KBr, cm^{-1}): 3,342 (O-H, stretching); 3,078 (-C-H, stretching); 3,024 (-C-H, stretching); 3,041 (H-CN, stretching); 2,895 (C-C, stretching); 1,626 (C=N, stretching); 1,481 (C=C, stretching); 1,288 (C-N, stretching); 1,249 (C-O, stretching)

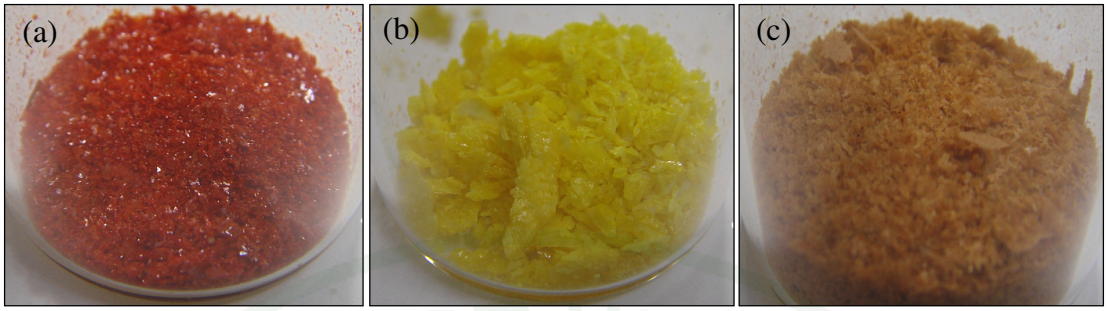

Figure 18 Photographs of (a) Compound (I) (b) Compound (II) and (c) Compound (III).

2. Photophysical properties

Photophysical properties of Compound (I), (II) and (III) were investigated by UV-Visible and fluorescence spectroscopy in acetonitrile solution. The absorption properties, emission properties, stokes shift and peak area of emission spectra were considered in order to study ESIPT on salicylaldimine derivertives.

2.1 Absorption and emission properties

Photophysical properties of all compound were investigated by UV-Visible and fluorescence spectroscopy in acetonitrile solution. The absorption and fluorescence spectra were depicted in Figure 19 and 20, respectively. The maximum wavelengths both of absorption and emission band were reported in Table 1.

In the Figure 19, the maximum wavelength (λ_{max}) of UV-Visible spectrum for Compound (I) was at 270 and 351 nm. Absorption spectrum of Compound (III) was similar to Compound (I) located at 273 and 349 nm whereas Compound (II) was unlike other compounds. It showed main absorption maximum peak at 272, and 339 nm and there were also small peaks at 301 and 317 nm. It could be seen that electronic absorption spectra of Compound (I), (II) and (III) showed two transitions that were absorption band at 270 (Compound I), 272 (Compound II) and 273 (Compound III) nm corresponding to the excitation of the aromatic π electrons. While band at 340

(Compound I), 334 (Compound II) and 349 (Compound III) nm was attributed to π-π* transition of CH=N linkage of azomethine groups.

Three compounds of salicylaldimine derivatives (I), (II) and (III) were excited with the radiation at 350, 340 and 350 nm, respectively. The spectra showed two emission bands in acetonitrile solution (Figure 20). Due to the fact that excited state intramolecular proton transfer (ESIPT) process in electronically excited singlet states can be easily recognized by the appearance of a second band to the red of the normal band in the fluorescence spectrum. Normal band was due to emission from S_1 state of the molecule in the form which was thermodynamically the most stable in S_0 state and second band was due to emission from its tautomer, formed by ESIPT (Jayabharathi *et al*., 2013). For the results, Compound (I) displayed bands at 420 and 547 nm. Compound (II) and (III) displayed the similar characteristics. Emission wavelengths of Compound (II) showed at 405 and 549 nm while 411 and 504 was of Compound (III). In these results, Compound (I), (II) and (III) exhibited dual fluorescence in acetonitrile solution indicating that intramolecular proton transfer took place through the excited state, exciting from normal form by each appropriate to the energy of radiation.

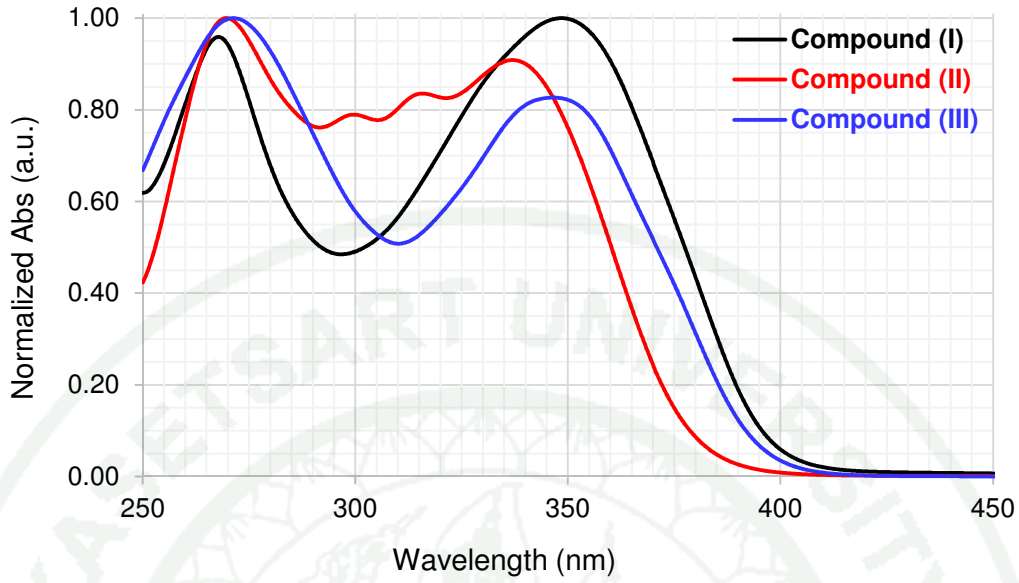

Figure 19 Absorption spectra of Compound (I), (II) and (III) measured in acetonitrile solution.

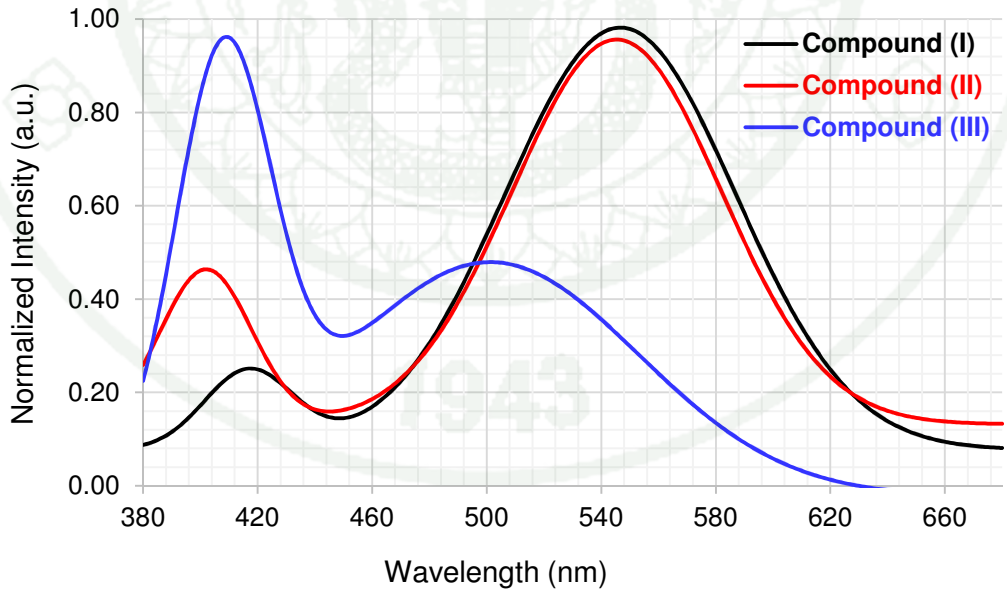

Figure 20 Emission spectra of Compound (I), (II) and (III) measured in acetonitrile solution (excitation wavelength at 350, 340 and 350 nm, respectively).

2.2 The stokes shift

The difference of main peak wavelength between absorption and emission called “stokes shift” was calculated for three prepared compounds in acetonitrile solution. Both of excitation and emission spectra of each structure were shown in Figure 21, 22 and 23 as well as data were recorded in Table 1. The results showed small stokes shift attributed to normal tautomer while large stokes, longer wavelength, obtained from ESIPT compound which attributed to the excited state keto tautomer originating from the excited state normal tautomer. The comparison of large stokes shift showed that Compound (I) and (II) had equal stoke shift value as large as 196 nm (10,208 cm^{-1}) and 215 nm (11,725 cm^{-1}). The Stokes shift of Compound (III) was 155 nm (8,812 cm^{-1}) which was the smaller stokes shift than others. However all compounds exhibited a large stroke shift which it has been reported over 8,000 cm^{-1} (Wang and Pang, 2014). This property was important for fluorescence chemosensor arising from ESIPT.

Furthermore, a peak area on dual emission spectra was calculated using Origin Pro8 program. The percentage of each peak area in 100 was related with a number of E-form and its tautomer (K-form) which was transformed in the excited state. Comparing of three structures, we found that Compound (I) and (II) were likely to transform E-form into K-form. Compound (I) producing ratio of E-form/K-form was 6.7 : 93.3% while compound (II) was 14.9 : 85.1%. Otherwise Compound (III) showed E-form higher than K-form as 36.2 : 63.8% . It concluded that Compound (III) exhibited the probability for transformation in excited state less than Compound (II) and (I), respectively.

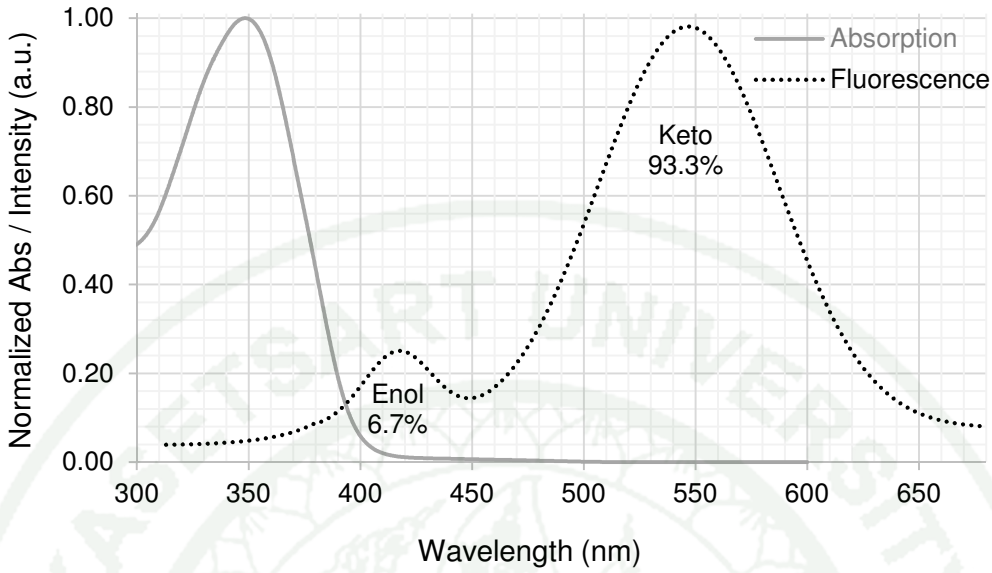

Figure 21 Compound (I) spectra demonstrating the concepts of excitation and emission properties including ratio of occurrence between two tautomers.

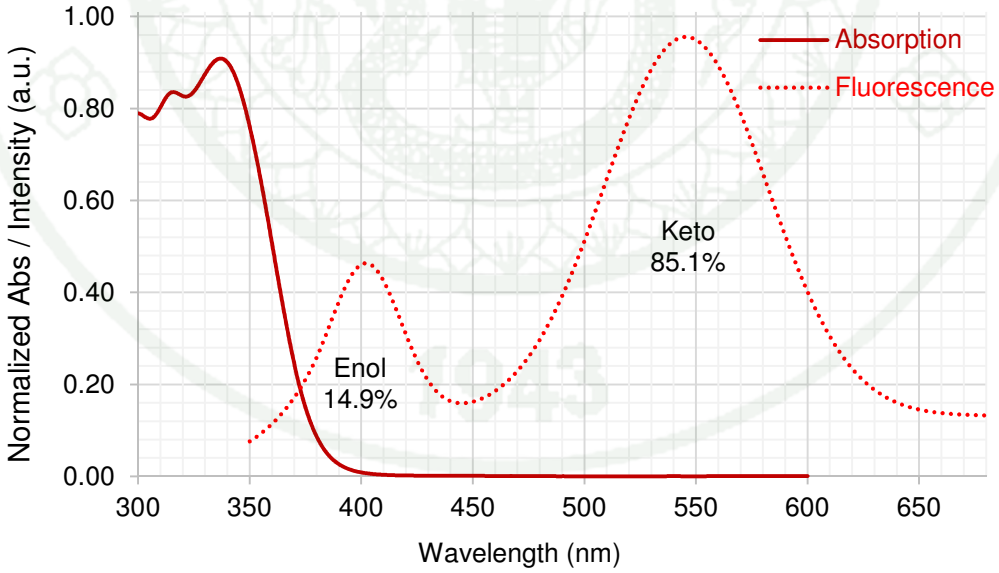

Figure 22 Compound (II) spectra demonstrating the concepts of excitation and emission spectra properties ratio of occurrence between two tautomers.

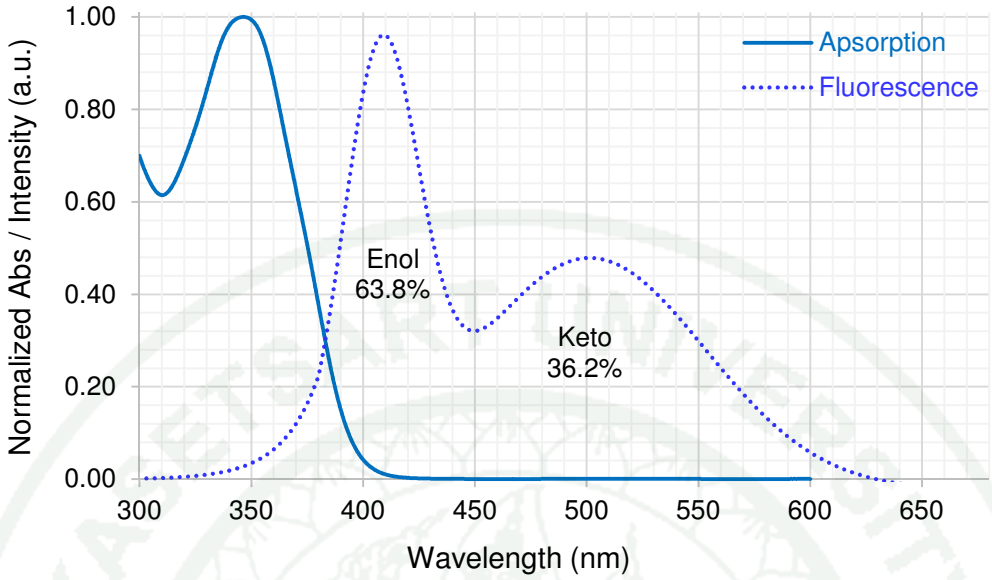

Figure 23 Compound (III) spectra demonstrating the concepts of excitation and emission spectra properties ratio of occurrence between two tautomers.

Table 1 Photophysical data of Compound (I), (II) and (III) in acetonitrile solution.

Compound	Absorption λ_{max} (nm)	Emission λ_{max} (nm)	%Ratio Enol-Keto	Stokes shift	
				λ (nm)	Wave number (cm^{-1})
Compound (I)	351	420	6.7	69	4,681
		547	93.3	196	10,208
Compound (II)	334	405	14.9	71	5,249
		549	85.1	215	11,725
Compound (III)	349	411	63.2	62	4,322
		504	36.8	155	8,812

λ_{max} = maximum wavelength

3. Effect of pH on photophysical properties

The UV-Visible absorption of Compound (I), (II) and (III) was measured at different pH range from pH=5 to pH=12. Emission spectra were investigated along pH=3 to pH=13 as well. All of them were measured in 6:4 aqueous buffered acetonitrile solution as the solvent for studying the pH responsive properties of salicylaldimine schiff bases. UV-Visible absorption and emission spectra were shown in Figure 24-29.

The UV-Visible absorption spectra for Compound (I) as shown in Figure 24 exhibited a significant band 325 nm at pH=5, 6 and 7 which the intensity of the absorption decreased from pH=5 to pH=7. For pH=8 to pH=12 showed onwards, the absorption band experienced a new red shift that was located at 380 nm increasing from pH=8 to pH=12 while band at 325 did not appear. For the emission spectra which were excited at 350 nm as depicted in Figure 25. Compound (I) exhibited only emission peak 435 nm at pH=5 and then decreasing to pH=7. At pH=6, it showed dual emission, a new absorbance with a maximum wavelength of 506 nm was shown and still existed band at 435 nm while pH=7, it showed only longer wavelength at 506 nm with the highest intensity. For pH=8 to pH=12, the spectra showed a single band at 506 nm which fluorescence intensity increasing as function on base solution while band at 436 disappeared from the spectra.

It was evident that the anion chromophore revealed more red shifted absorption than related normal chromophore (Koll, 2003). So this experimental result on pH effect implied that in the acid solution Compound (I) presented E-form (phenol form) whereas anion form predominated in basic solution with the longer absorption (phenolate form). The UV-Visible spectra at pH=6 and 7 showed one absorbance from E-form excitation while emission spectra at pH=6 showed two emission band for E- and K-form. At pH=7 showed the highest intensity band at 506 nm from emission of K-form. In consideration of these results indicating that only pH=6 and pH=7 exhibited the ESIPT process. The isosbestic points at about 346 for Compound (I) confirmed the equilibrium among three species that explained by resonance interaction between enol, zwitterionic and keto tautomer.

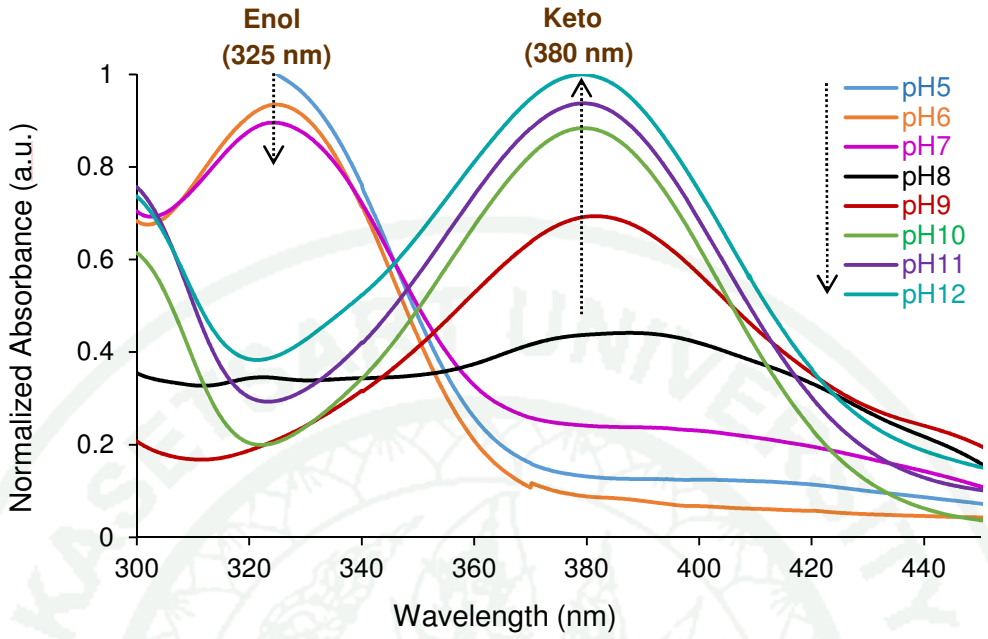

Figure 24 Absorption spectra of Compound (I) over the pH range from 5.0 to 12.0.

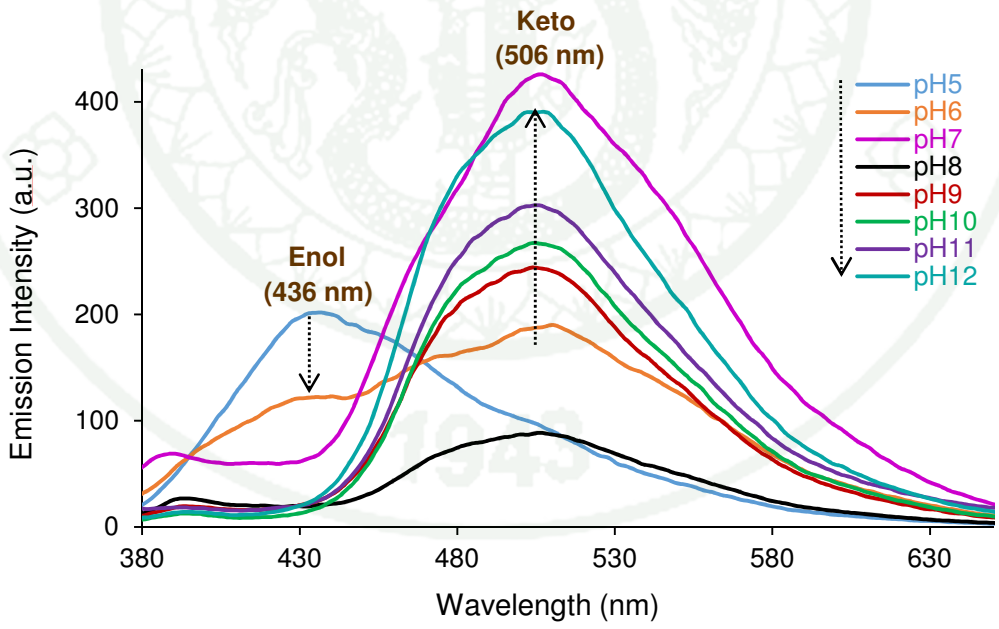

Figure 25 Emission spectra of Compound (I) at different pH.

Similar to Compound (II), the spectra showed a significant absorption band at 327 nm in pH=6, 7 and 8 with decreasing from pH=6 to pH=8. For pH=8 appeared a small band at 382 nm which implying keto tautomer. Absorbance at pH=9 to pH=12 showed single peak at λ_{max} value 380 nm and this band attained to maximum value at pH 12. For emission property of Compound (II) exhibited the same pattern along with Compound (I). At pH=3 to pH=5, a single emission band appeared at 435 nm while higher concentration of hydroxide (pH=7 to pH=13) appeared a peak at 505 nm.

The difference of conformation on low and high pH solution for all compounds confirmed two different isomers in acid-base solution. The band with lower wavelength, higher energy, could be attributed to the emission from enol tautomer as shown in acidic solution (pH<8). As the emission band at longer wavelength, lower energy could conceivably be assigned to keto tautomer in alkali solution (pH>8), Salicylaldimine based compounds showed longer emission band in present of keto tautomer. Apparently, isoemission point for Compound (I) and (II) was apparent around 470 nm which indicated the equilibrium between the keto and the enol form. The similarity of absorption and emission properties implied the structure of Compound (I) and (II) were coherent.

For Compound (III) was different from Compound (I) and (II). In pH=6 to pH=9, Compound (III) showed only one peak at 286 nm with no peak observed at higher range than 300 nm. At pH=10 to pH=12, the band displayed a longer λ_{max} located 430 nm with increased absorption by increasing pH (from pH=10 to pH=12). The emission band of Compound (III) in the acid solution showed peak at 438 nm. For base solution, band showed at 467 nm with disappearing band at 438 nm.

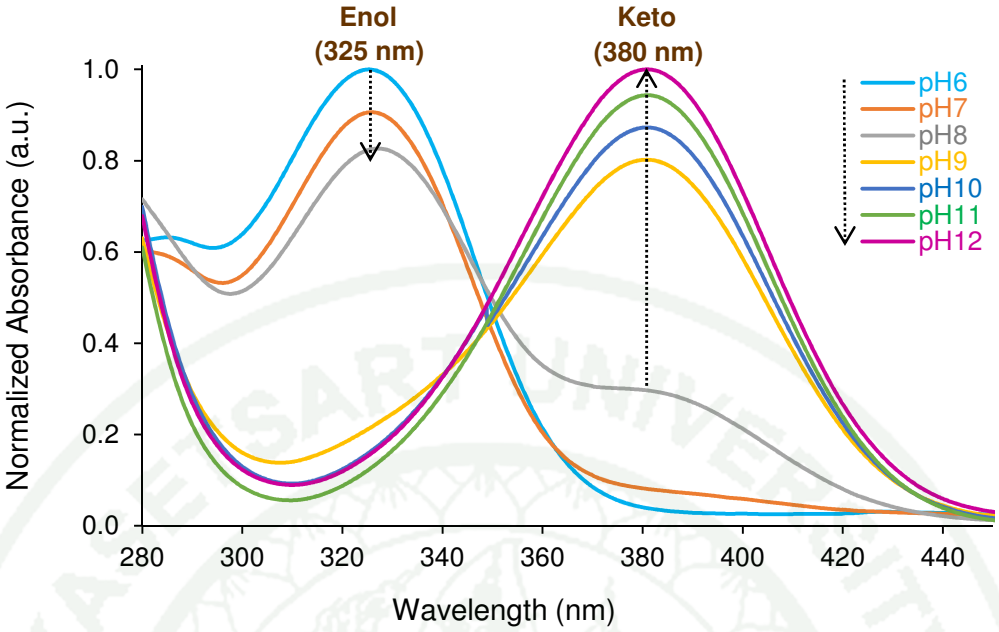

Figure 26 Absorption spectra of Compound (I) over the pH range from 6.0 to 12.0.

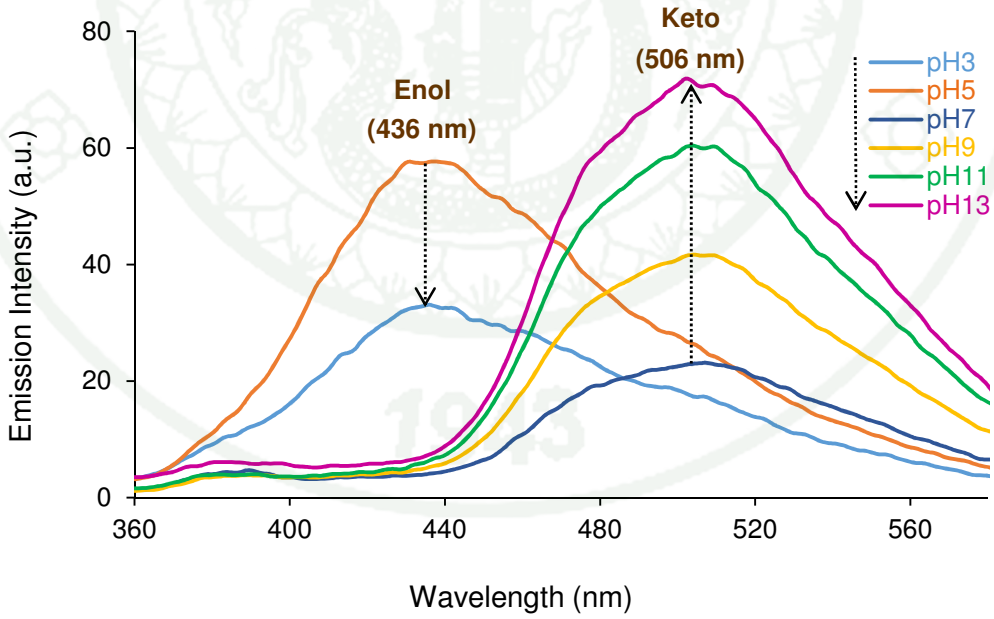

Figure 27 Emission spectra of Compound (II) at different pH.

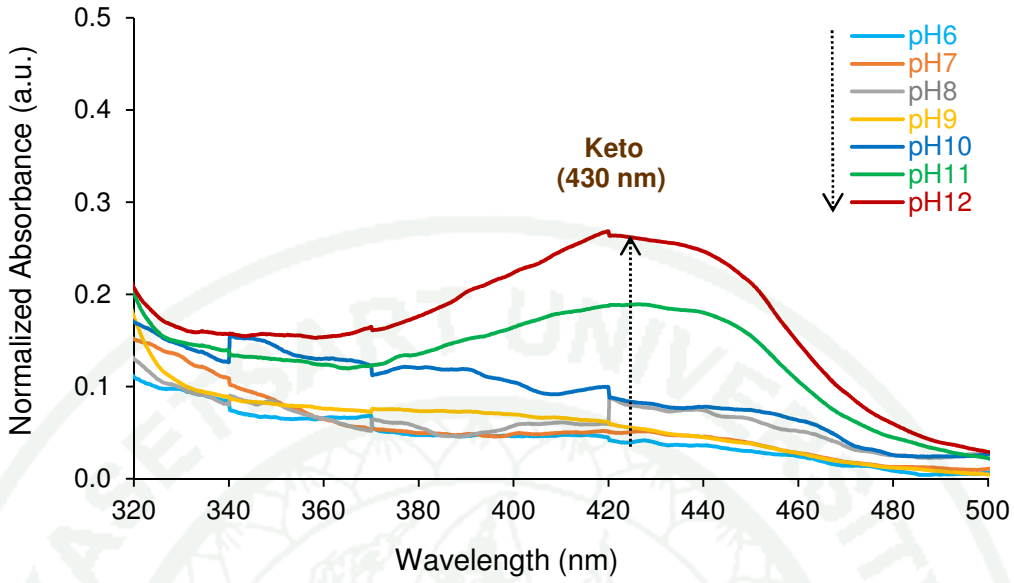

Figure 28 Absorption spectra of Compound (III) over the pH range from 6.0 to 12.0.

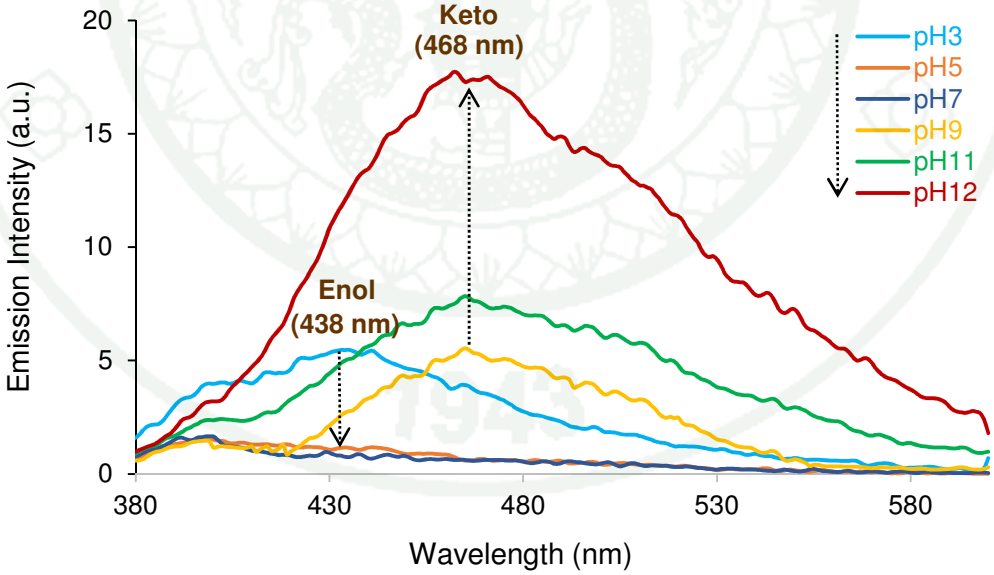

Figure 29 Emission spectra of Compound (III) at different pH.

The ratios of the emission intensities were plotted at I_{504}/I_{436} belonging to Compound (I) and Compound (II) and I_{462}/I_{436} belonging to Compound (III) against the pH in the buffer:ACN (6:4) solution as shown in Figure 30. It displayed that Compound (I) and (II) showed the relationship between two parameters. This intensities ratio for Compound (I) and (II) increased from low to high value associated with pH change from 3 to 13. For Compound (I) at pH=7, the I_{Keto}/I_{Enol} intensity began to increase while Compound (II), I_{Keto}/I_{Enol} intensity began to increase at pH=5. Compound (III) showed low I_{Keto}/I_{Enol} intensities about the same level at pH=3 to pH=7. From pH=9 to pH=12, I_{Keto}/I_{Enol} intensities evenly showed in higher level which pH=9 was the highest value. These results concluded that acid–base solution led to two different forms of Compound (I) and (II). On Compound (III) could be said that it could not occur ESIPT process or difficult to occur. The different substituents onto the benzene ring of the molecule had responsive characteristics on pH value.

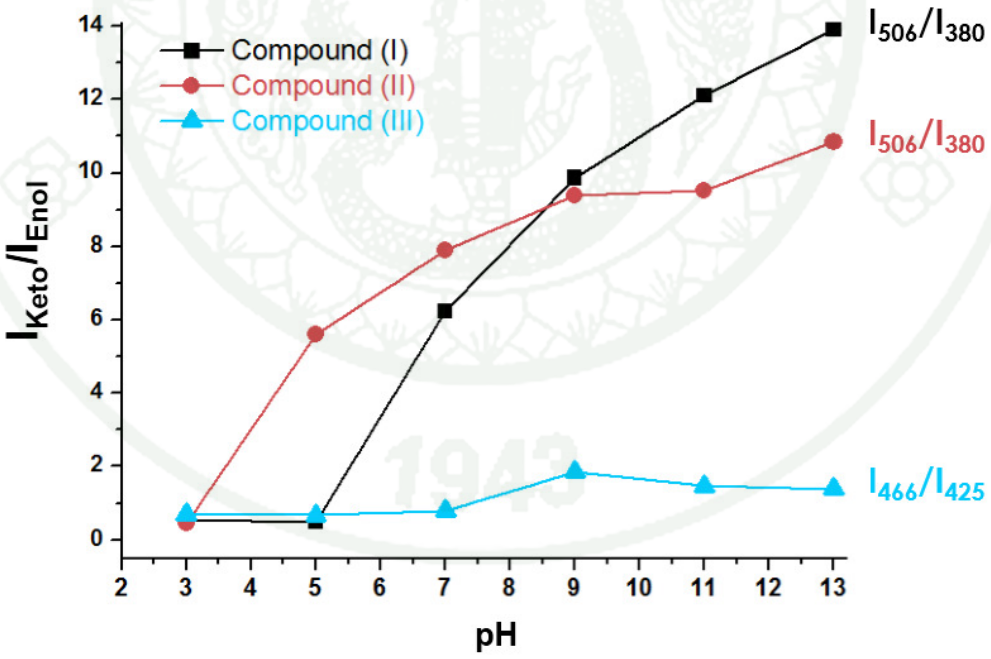

Figure 30 Plot of the emission intensities ratio (I_{Keto}/I_{Enol}) of Compound (I), Compound (II) and Compound (III) to pH variation with excitation wavelength 350, 340 and 350 nm, respectively.

4. Solvatochromism

Solvatochromism was studied by UV-Visible and emission spectrophotometer. Only Compound (I) was investigated in non-polar, aprotic as well as protic solvents including diethyl ether (EE), chloroform ($CHCl_3$), dichloromethane (DCM), ethyl acetate (EA), dimethyl sulfoxide (DMSO), ethanol (EtOH), methanol (MeOH) and acetonitrile (ACN) of which the polarities were different from each other. Absorption spectra in the region 250-500 nm and emission spectra in the range of 380-680 nm were displayed in Figure 32 and 33. Data results were recorded in Table 3. Compound (I) in different polarity of solvents under the ambient condition were seen in Figure 30. It exhibited the transparent color in the non-polar solvents, diethyl ether (EE) and ethyl acetate (EA) solution, and exhibited more yellow color in higher polarity solvents (DCM to DMSO). For the polar protic solvents, EtOH and MeOH, they showed the intense yellow.

Change in absorption wavelength arised from an interaction between solvent and solute so the different polarity of solvents affected to absorption and emission properties (Sadhan and F.N.I, 1963). Corresponding with absorbance spectra result as could be seen in Figure 31, it showed distinct maximum wavelength that appeared around 350-360 nm in various solutions. In view of non-polar solvents such as chloroform and diethyl ether, Compound (I) showed maximum peak at 350 nm in diethyl ether and 355 nm in chloroform solution. In aprotic solvents (DCM, ACN and DMSO), the maximum band were at 357, 349 and 357 nm, respectively. It was observed that Compound (I) in the high polarity of aprotic solvents, (DMSO ε= 46.8) and protic solvent (EtOH, ε= 24.6 and MeOH, ε= 32.6) exhibited extra larger red shifted at approximately 450 nm. These extra bands were due to the stabilizing interaction between the hydroxyl containing solvent and the phenol group of salicylaldimine based so that there was greater delocalization of the π electron cloud of the aromatic system.

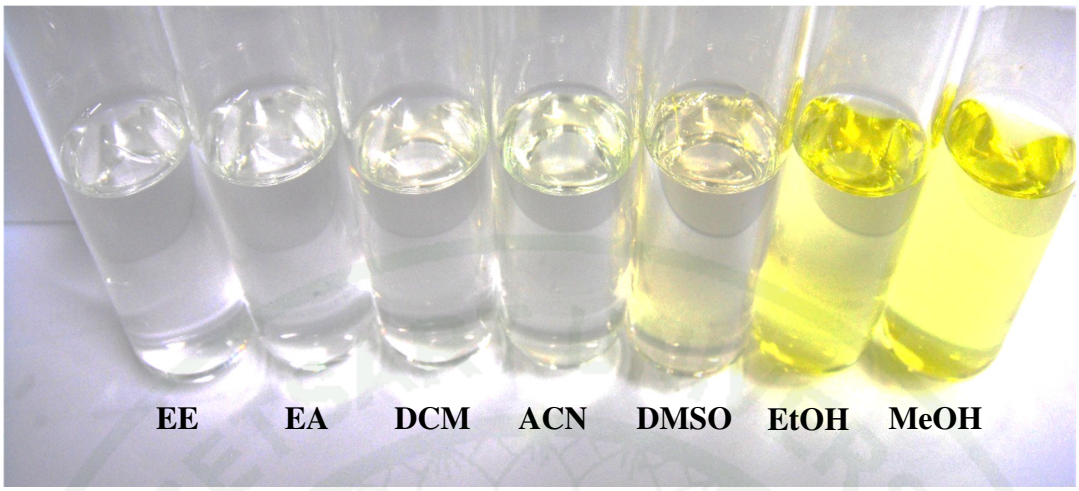

Figure 31 Compound (I) in various solvents under the sun light at room temperature.

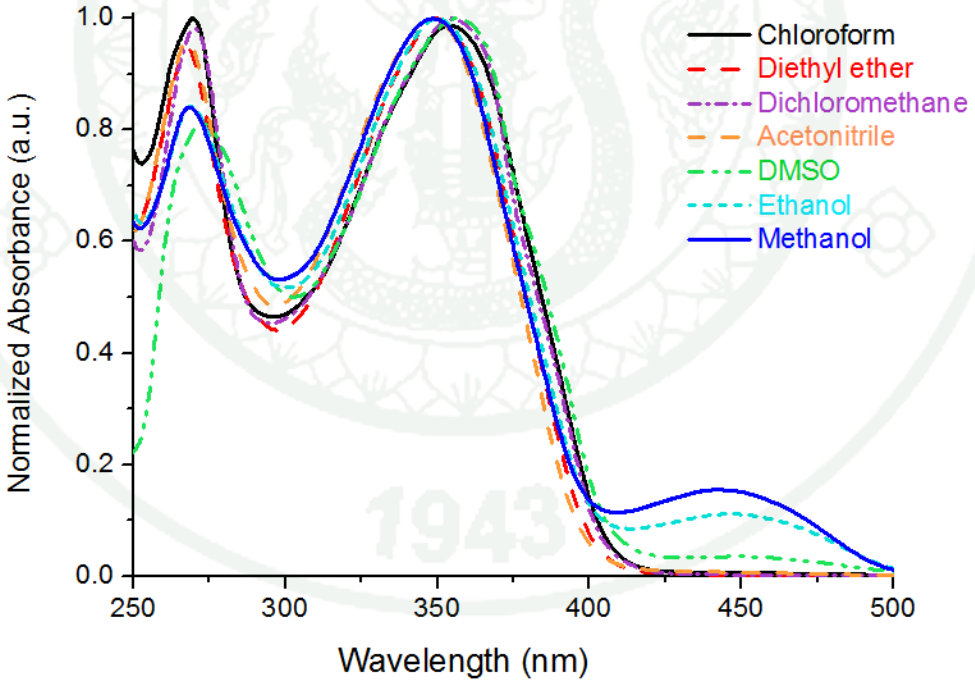

Figure 32 Absorption spectra of Compound (I) in various solvents.

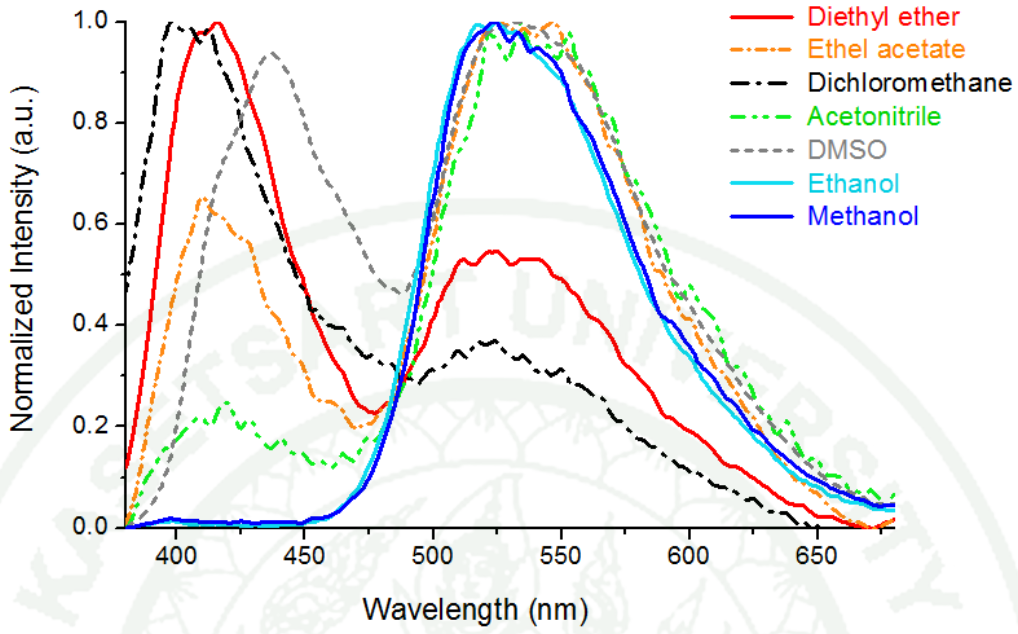

Figure 33 Emission spectra of Compound (I) in various solvents.

The emission spectra of Compound (I) in different kind of solvents as shown in Figure 33 were also obviously different. The emission characteristics observed apparently dual emission wavelengths in non-polar solvent (diethyl ether and ethyl acetate) aprotic solvents (dichloromethane, acetonitrile and DMSO). They displayed a normal stokes-shifted emission band in range of 404-437 nm and another one showed large stokes shift in range of 525-540 nm. Dual emission was due to ESIPT which excitation of isomer I (Figure 34a) led to the formation of keto-isomer II (Figure 34b) demonstrating ESIPT process. However in hydroxylic solvents, a short wavelength emission band disappeared. They exhibited single emission at 525 and 530 nm in ethanol and methanol, relatively. These corresponded to the results obtained earlier data for absorption spectra at 450 nm. Absence of dual emission in these compounds was caused by the presence of intermolecular hydrogen bonding with solvent molecule leading to the stabilization of solvated isomer III (Figure 34c) in which ESIPT was impossible. In other words, salicylaldimine based exhibited single emission peak as a result of hydrogen bonding perturbation by protic solvent molecules that could prevent proton transfer in the excited state.

Table 2 UV-visible absorption and emission wavelength (nm) of Compound (I) in different polarity of solvents.

Solvent	Absorption Wavelength	Emission Wavelength
Non polar		
Diethy ether (ε =4.24)	355	413, 530
Chroloform (ε =4.71)	350	-
Ethyl acetate (ε =6.02)	-	420, 536
Polar aprotic		
Dichloromethane (ε =8.93)	357	404, 525
Acetonitrile (ε =37.7)	349	419, 540
DMSO (ε =46.8)	357	437, 534
Prolar protic		
Ethanol (ε =24.8)	350	525
Methanol (ε =32.6)	349	530

ε = Dielectric constant of solvents

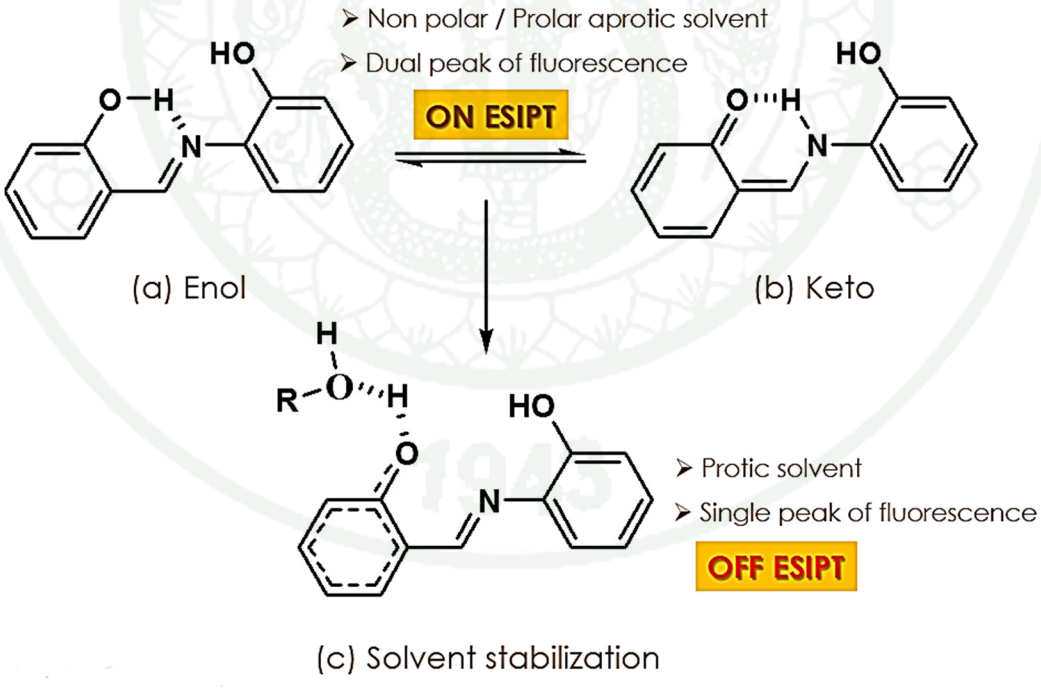

Figure 34 Intramolecular hydrogen bond in various isomeric forms of Compound (I).

From the experimental section, Compound (I) showed the photophysical properties similar to Compound (II) while Compound (III) differed from others. Compound (I) and (II) had the same hydroxyl group on phenol of aromatic ring A. It indicated that only hydroxyl group on phenol A influenced over ESIPT process. However, in case of Compound (I), there were two moieties O2-H1-N6 and O9-H10-N6 where intramolecular proton transfer were likely to occur. On experimental part, some questions did not be explain such as how salicylaldimine schiff bases showed dual emission with normal and large strokes shift, why Compound (I) did not show the simultaneous double intramolecular proton transfer process, how intramolecular hydrogen bonding induced the proton transfer in the excited state and particularly on experimental part could not explain the ESIPT process in term of energy level. Next, we examined theoretical tools these outcomes, which allowed us to bring forward an explanation of the observed data. Quantum chemical calculation with the selected method was described in details in the ESIPT and answered these questions. The results successfully rationalized the optical signatures of ESIPT dyes possessing a dual enol-keto fluorescence signature.

Quantum Chemical Calculations

1. Ground state intramolecular proton transfer of Compound (I), (II) and (III)

1.1 Ground state optimized structures and molecular geometries

The preliminary of this part looked for the most stable structure for the E-form (enol form), E-form (keto form) and TS-form (transition state) of Compound (I), (II) and (III), corresponding to different orientations with respect to benzene ring and hydroxyl group. Several conformers were considered in the structures as depicted in Appendix C to find the lowest structural energy. Quantum calculation was investigated in order to understand structural properties of these molecules. All structures as shown in Figure 35 were optimized at the ground state (S_0) for E-form and K-from. Density functional theory was used with CAM-B3LYP functional as well as a combination of 6-311G(d,p) basis set. As mention above these molecules were considered as tautomers which accompanied by a switch of E-form (a single bond) and K-form (adjacent double bond) via transition state. Transition state of their tautomers was also done by QST3 option for calculation. The optimized structures of Compound (I), E-form, K-form and its transition state, were shown in Figure 36 and the optimized structure for Compound (II) and (III) were shown in Appendix D. Some of most important geometrical parameters including bond lengths, bond angles and torsional angles were collected in Table 3, 4 and 5 for Compound (I), (II) and (III), respectively.

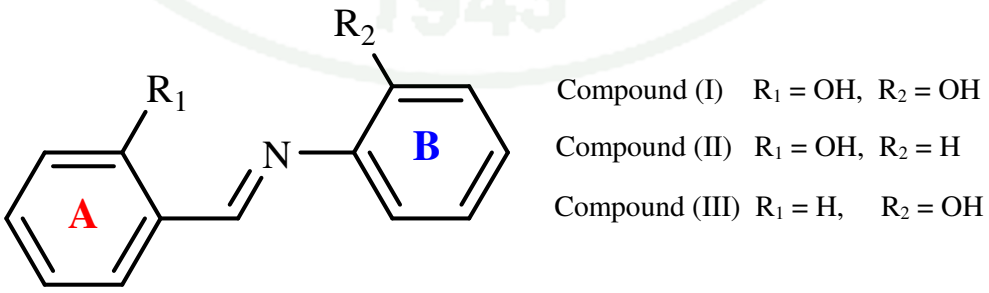

Figure 35 Molecular structure of Compound (I), (II) and (III) of salicylaldimine derivertives with benzene rings label.

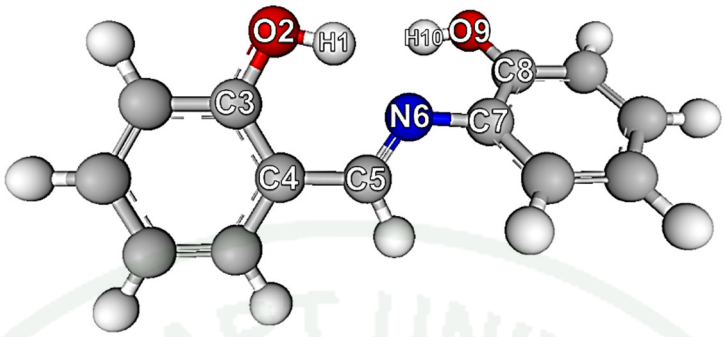

(a) Enol form

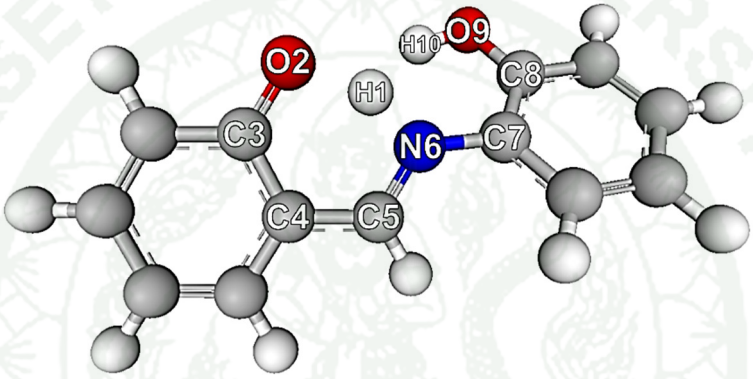

(b) TS-form

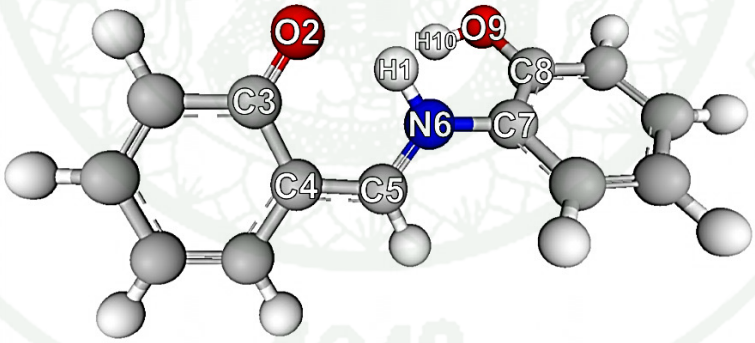

(c) Keto form

Figure 36 Optimized structures of (a) E-form, (b) TS-form and (c) K-form of Compound (I) with atom numbering which calculated in gas phase by CAM-B3LYP with 6-311G(d,p) basis set.

Table 3 Selected optimized geometry parameters for Compound (I) obtained from full optimization by CAM-B3LYP at 6-311G(d,p) (bond length in angstrom angle in degree). The mean of % relative error values was also listed.

Structural parameters	Enol form		TS form	Keto
	Calculated	X-ray	Calculated	Calculated
Bond length (Å)				
H1-O2	0.98	0.86	1.29	1.56
O2-C3	1.34	1.34	1.28	1.26
C3-C4	1.41	1.43	1.44	1.45
C4-C5	1.45	1.42	1.41	1.39
C5=N6	1.28	1.28	1.31	1.32
N6-C7	1.41	1.41	1.40	1.41
C7-C8	1.40	1.39	1.40	1.40
C8-O9	1.35	1.35	1.36	1.35
O9-H10	0.97	0.93	0.97	0.96
N6-H1	1.76	-	1.20	1.06
Bond angle (°)				
∠C4-C5-N6	122.9	122.8	119.6	121.2
∠C5-N6-C7	121.2	126.4	126.8	127.5
∠H1-O2-C3	107.5	-	102.7	103.0
∠C8-O9-H10	107.8	-	111.3	111.5
∠O2-H1-N6	146.8	-	151.8	144.6
Torsional angle (°)				
∠C3-C4-C5=N6	3.3	1.3	2.5	-0.5
∠C4-C5=N6-C7	177.1	179.9	177.8	177.4
∠C5=N6-C7-C8	145.6	-	146.1	140.3
∠C3-C4-C7-C8	-46.4	-	-36.0	-36.7
% Relative error	2.50	N/A	-	-

* Tunc *et la*., 2009

Table 4 Selected optimized geometry parameters for Compound (II) obtained from full optimization by CAM-B3LYP at 6-311G(d,p) (bond length in angstrom, angle in degrees).

Structural parameters	Enol form	TS form	Keto form
Bond length (Å)			
H1-O2	0.99	1.31	1.67
O2-C3	1.33	1.28	1.25
C3-C4	1.41	1.44	1.46
C4-C5	1.45	1.41	1.39
C5=N6	1.28	1.3	1.32
N6-C7	1.41	1.41	1.41
C7-C8	1.39	1.39	1.39
C8-O9	-	-	-
O9-H10	-	-	-
N6-H1	1.74	1.17	1.04
Bond angle (°)			
∠C4-C5-N6	122.6	119.8	122.8
∠C5-N6-C7	120.6	125.7	127.2
∠H1-O2-C3	107.7	103.6	103.9
∠C8-O9-H10	-	-	-
∠O2-H1-N6	147	151.6	140.3
Torsional angle (°)			
∠C3-C4-C5=N6	-0.5	0.4	0.2
∠C4-C5=N6-C7	178	178.9	179.3
∠C5=N6-C7-C8	140.3	152.2	159.8
∠C3-C4-C7-C8	-50.2	-32.9	-24.3

Table 5 Selected optimized geometry parameters for compound (III) obtained from full optimization by CAM-B3LYP at 6-311G(d,p) (bond length in angstrom, angle in degrees).

Structural parameters	Enol form	TS form	Keto form
Bond length (Å)			
H1-O2	-	-	-
O2-C3	-	-	-
C3-C4	1.4	1.4	1.4
C4-C5	1.47	1.45	1.45
C5=N6	1.27	1.28	1.29
N6-C7	1.41	1.39	1.38
C7-C8	1.40	1.44	1.45
C8-O9	1.35	1.28	1.25
O9-H10	0.97	1.43	1.83
N6-H1	2.06	1.16	1.05
Bond angle (°)			
∠C4-C5-N6	123	124.1	124.1
∠C5-N6-C7	122	132.6	133.5
∠H1-O2-C3	-	-	-
∠C8-O9-H10	105.7	89.5	86.1
∠O2-H1-N6	117.9	133.1	120.6
Torsional angle (°)			
∠C3-C4-C5=N6	-5.5	0.1	0
∠C4-C5=N6-C7	178	180	180
∠C5=N6-C7-C8	157.9	180	180
∠C3-C4-C7-C8	-32.7	0.1	0

Compound (I) with hydroxyl ortho-substituent (-OH) on both of benzene rings displayed the most stable conformation in E-form which two hydroxyl substituents were facing each other (Figure 36a). However, both of aromatic rings showed nonplanar as seen in Figure 37a. Torsional angles ∠C3-C4-C5=N6, ∠C4-C5=N6-C7, ∠C5=N6-C7-C8 as shown in Table 3 were 3.3°, 177.1° and 145.6°, respectively. The torsional angle between two planar of benzene rings ∠C3-C4-C7-C8 was 46.4° indicating that two aromatic rings, A and B, were not planar arrangement. Figure 37b showed Compound (I) with hydrogen bonding label as well (blue and purple dotted lines) which enol-keto tautomerization could occur in two ways in their each planar. One was tautomerization through 6-membered transition and another was through 5-memberd transition.

(a)

(b)

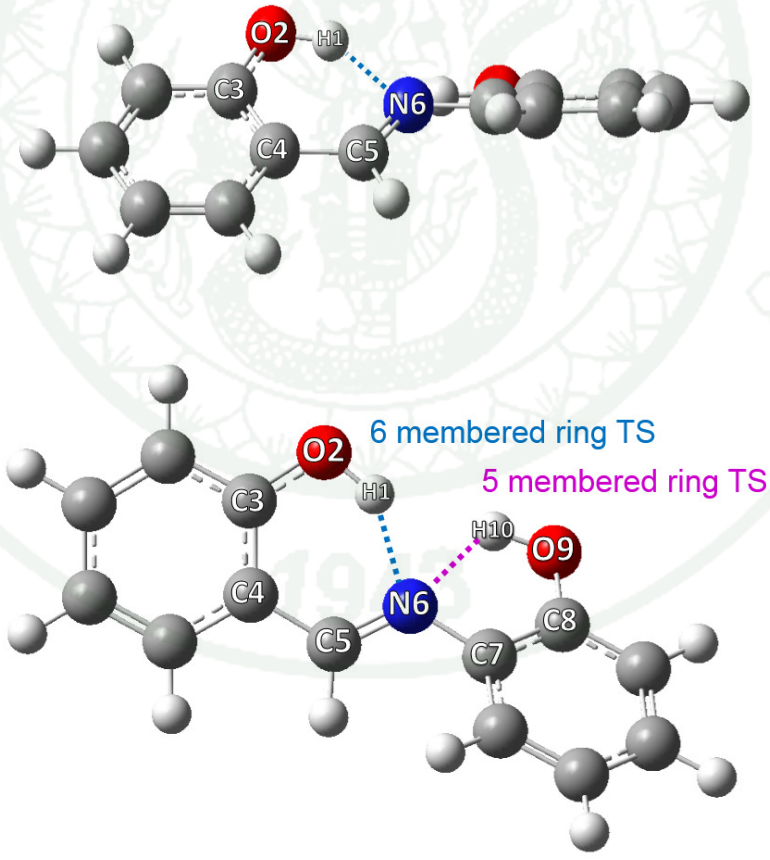

Figure 37 (a) Side and (b) Front view of Compound (I) optimized structure obtained from CAM-B3LYP with 6-311G(d,p) basis set in gas phase and N-H linkage (blue and purple dotted lines) exhibiting the hydrogen bonding.

To confirm the hydroxyl group on phenol ring of Compound (I) turned inside to each other, conformational analysis was used to find it out. Potential energy with a change of torsion angle ∠C4-C3-O2-H1 (θ) and ∠C7-C8-O9-H10 (φ) of hydroxyl group were performed with CAM-B3LYP/6-311G(d,p). Conformational results as displayed in Figure 38 showed that 0° of ∠C4-C3-O2-H1 and 0° of ∠C7-C8-O9-H10 was the lowest energy. This conformational result also showed ∠C4-C3-O2-H1 rotation was higher activated energy when compared to ∠C7-C8-O9-H10 with relative energies 13.8 and 6.7 kcal/mol, respectively. These indicated that the strength of N···H hydrogen bond for O2-H1···N6 was higher than O9-H10···N6. It concluded that intramolcular proton transfer through D-(Donor)-H-A(Acceptor) on phenol ring B (O9-H10···N6) was remote possibility when compared with D-(Donor)-H-A(Acceptor) on phenol ring A (O2-H1···N6).

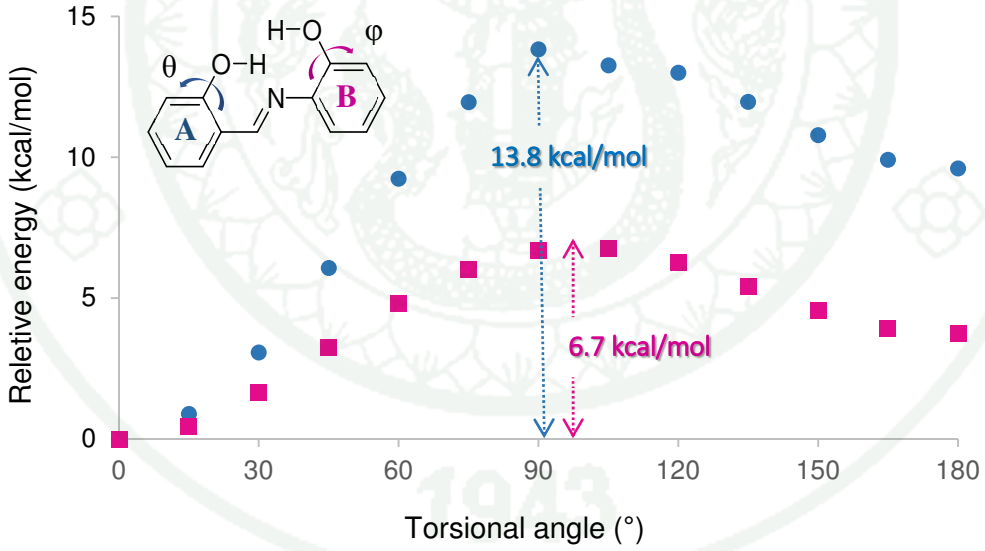

Figure 38 Potential energy surface obtained from CAM-B3LYP/6-311G(d,p) for E-form of Compound (I) in the ground state with respect to two rotational angles indicated in the structure. The inserted structure represents torsion angle around C-O bond with φ = 0◦ and θ = 0◦.

The mean of %relative error was calculated for Compound (I) and compared to X-ray data (Tunc *et la*., 2009) as recorded in Table 3. The mean of % relative errors of E-form was 2.50%. The small discrepancies between the experiment and values were because of the change in phase. Crystal data corresponded to molecules in solid phase, whereas theoretical data corresponded to molecules in gas phase. Single isolated molecule was considered in the theoretical calculations, whereas the results of X-ray study were associated with molecular packing. Even though some differences were observed, in general, there was good matching between the calculated geometrical parameters and data obtained from the X-ray structure. Hence it was mentionable that CAM-B3LYP method employing 6-311G(d,p) basis set could be applied for calculated this system.

For Compound (II), E-form showed the most stable conformer which was hydroxyl group (-OH) turned inside to N atom of imine (-C=*N*) in arrangement of 6-memberd ring (N6-C5-C4-C3-O2-H1) with the torsional angle between two benzene rings which was 50.2°. Compound (III) was the same way with Compound (I), the hydroxyl group turned inside to N (C=*N*-) in arrangement of 5-memberd ring (N6-C7-C8-O9-H10) with torsional angle between A and B benzene, 32.7°, showed the lowest energy in gas phase. The optimized results of Compound (I), (II) and (III) in gas phase deduced that the E-form in the ground state prefered the H-bonded planar conformation owing to the resonance-assisted hydrogen bond stabilization.

1.2 Mechanism of Ground State Intramolecular Proton Transfer (GSIPT) of Compound (I)

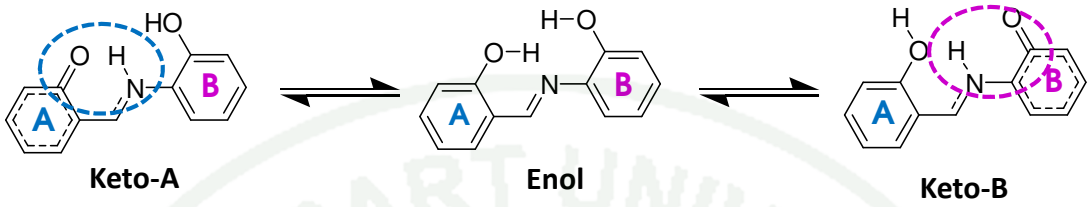

Figure 39 Compound (I) in enol form and possible conformational tautomerization on the ground state (S_0).

On the ground state, enol and keto tautomers could be converted to each other via an intramolecular proton transfer (IPT) reaction. Enol-keto tautomerization focused on Compound (I) which was proposed in two pathways because of nitrogen atom of azomethine closing to two hydroxyl groups (-OH groups) on phenyl rings as shown in Figure 39. The energies of enol to keto on the ground state and its transition state were carried out by means of CAM-B3LYP/6-311G(d,p) level of theory. Figure 40 depicted the enol-keto tautomerization on the ground state via two pathway; A and B, together with the energy barrier in term of kcal/mol.

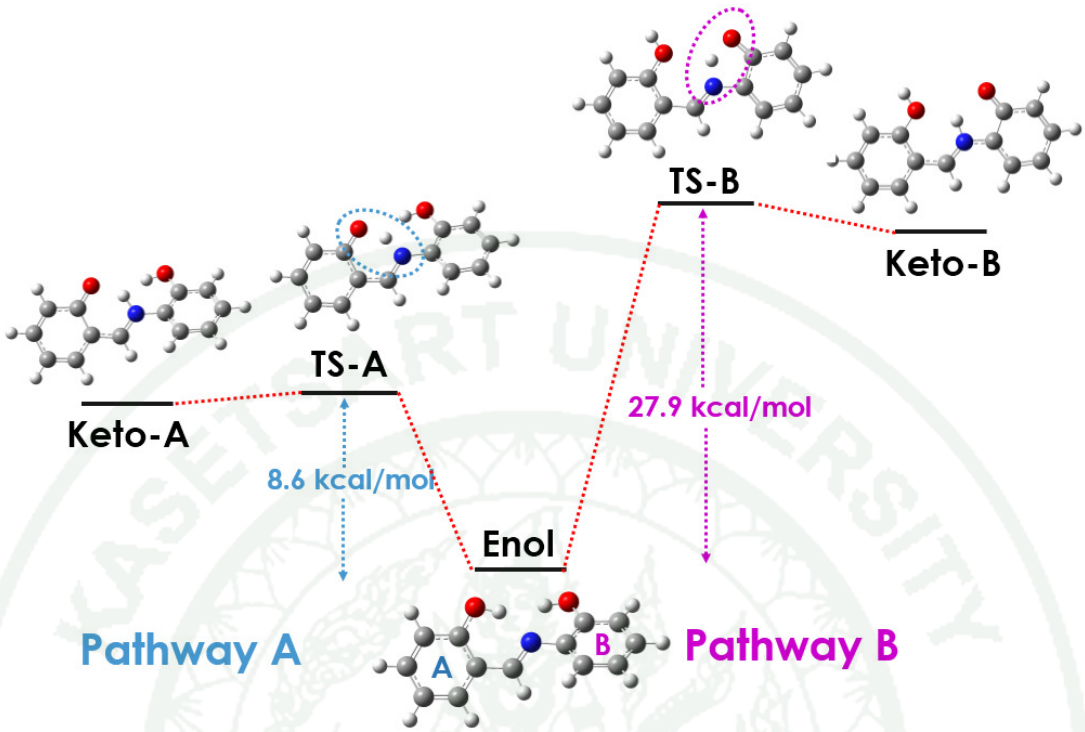

Figure 40 Transition state involving hydrogen transfer corresponding to enol-keto tautomerization via Pathway A and Pathway B.

The difference between Pathway A and B was proton transfer in Pathway A generated six-membered ring in the transition state as shown in the blue dotted circle while Pathway B showed proton transfer via 5-membered ring transition state as shown in the purple dotted circle. Enol form was the minima energy as a reference. The calculated result showed hydrogen transfer from O-H donor to the N acceptor with the relative energy 8.6 kcal/mol for Pathway A while hydrogen transfer for Pathway B consumed 27.3 kcal/mol. So we summarized that proton transfer through six-membered ring easily occurred when compared to proton transfer through five-membered transition. This result confirmed the photophysical experiment of Compound (I) resembled Compound (II) due to GSIPT prefer six-membered ring formed by the transition state.

1.3 Effect of polarity solvent and to Ground state Intramolecular proton transfer

The changes in the physicochemistry properties were considered to arise from the intramolecular proton transfer (IPT) in ground state. It was evident that the polarity and H-bonding strength of solvent affected the stabilization of ground state tautomers. In order to reveal the contribution of the intramolecular hydrogen bonding (IMHB) in hydroxyl schiff bases, the activated energy was investigated to study in the energy detail of three conformations including E-form, K-form and TS-form by CAM-B3LYP method with 6-311G(d,p) level of basis set in gas phase, chloroform and acetonitrile solution. The relative energies, as recorded in Table 6, were calculated as the total energies differences between of transition state and the initial form and the between of transition state and keto form in kcal/mol. Figure 41 and 42 was plotted which graphs obtained the data from Table 6 to easily described results.

Table 6 Relative energies of Compound (I), (II) and (III) in E-form, TS-form and K-form obtained from full optimization from CAM-B3LYP at 6-311G(d,p) level of basis set in gas phase and solutions.

Compound	Relative energies (kcal/mol)			
	Enol	**TS (ΔE enol→keto)**	**Keto**	**ΔE (keto→enol)**
Gas phase				
Compound (I)	0.0	8.6	8.3	0.3
Compound (II)	0.0	7.6	6.3	1.3
Compound (III)	0.0	20.1	18.6	1.5
Chloroform				
Compound (I)	0.0	7.7	7.0	0.7
Compound (II)	0.0	6.2	4.4	1.9
Compound (III)	0.0	17.2	14.4	2.8
Acetonitrile				
Compound (I)	0.0	7.4	6.5	0.9
Compound (II)	0.0	5.8	3.7	2.1
Compound (III)	0.0	16.3	12.8	3.4

*Chloroform ε = 4.71, Acetonitrile ε = 37.7

The calculated data showed the relatives energies which was usable to convert the E-form into the K-form through ground state transition. The result exhibited the difference of energies barrier not only conformation but also phase. For comparison in all of Compound (I), (II) and (III) with different substituents as depicted in Figure 41, enol form showed the most stable conformer over gas phase and solvent phase. In gas phase, Compound (III) showed the highest energies barrier (20.1 kcal/mol) while Compound (I) and (II) showed similar energy barrier of transition state 8.6 and 7.6 kcal/mol, relatively. Compound (III) was IPT through 5-membered ring used more energy barrier than IPT through 6-memberd ring. In other words, it was difficult to change conformation so this concluded that IPT via 5-membered ring transition state and 6-membered ring transition state affected the transformation of tautomers. Similarly to chloroform and acetonitrile solution, Compound (III) showed the highest transition energy following Compound (I) and (II), respectively.

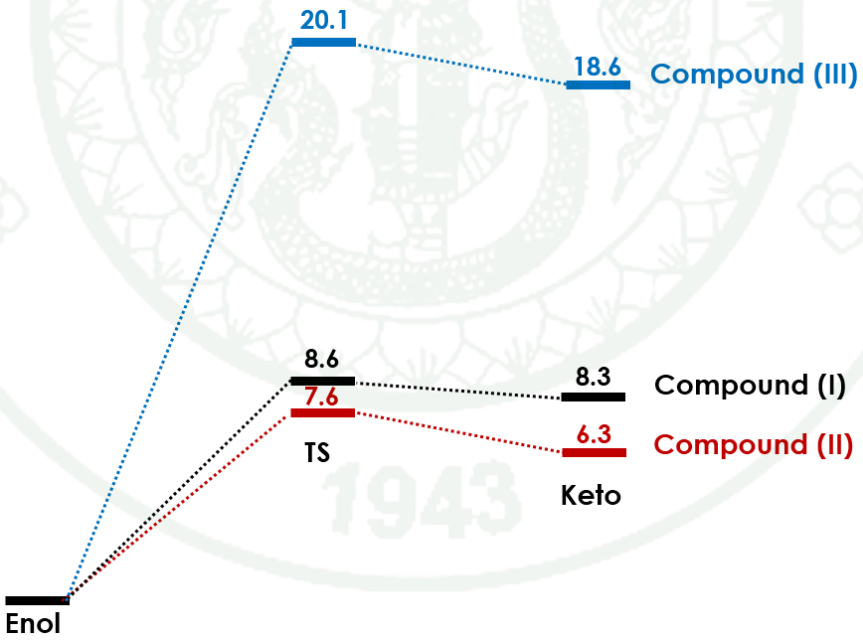

Figure 41 Relative energies of Compound (I), (II) and (III) on ground state in gas phase by CAM-B3LYP with a 6-311G(d,p) basis set for comparison on different substituent in structure.

The solvent molecules played a key part in tautomerism (Beyramabadi *et al.*, 2011). So we carried out in solvent phase in order to evaluate the effect of solvent on GSIPT. Compound (I), (II) and (III) were calculated in chloroform (ε=4.7113) and acetonitrile (ε=35.688). Because three compounds showed the same trend so Compound (I) represented in Figure 42. The relative energies of the TS-form with respect to E-form was 8.6, 7.7 and 7.4 kcal/mol in the gas phase, chloroform and acetonitrile, respectively. The barrier height depended on dielectric constant of solvent which it decreased from gas phase to acetonitrile. In addition, the results found that the relative energy barrier from K-form back into E-form increased 0.3, 0.7 and 0.9 kcal/mol from gas phase to acetonitrile indicating that in higher dielectric constant solvent, K-form was more stable. It was owing to interaction between solvent and molecule that the solvent with larger dielectric constant resulted in larger stabilization energy for the polar species. In consequence, dielectric constant of solvent contributed to effective on the intramolecular proton transfer inducing the equilibrium in enol-keto tautomerization in various solvents.

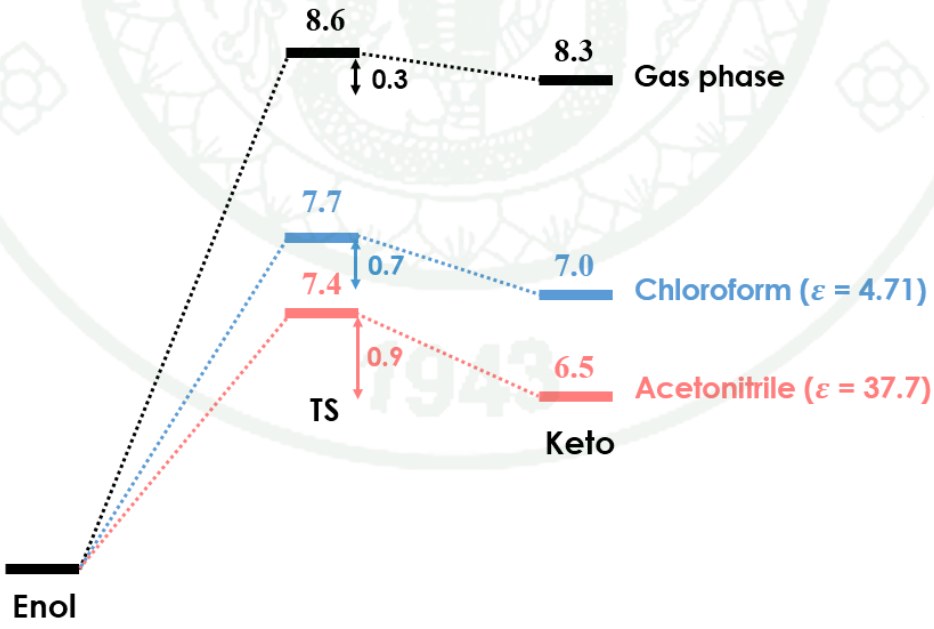

Figure 42 Relative energies of Compound (I) on ground state in gas phase, chloroform and acetonitrile solution by CAM-B3LYP with a 6-311G(d,p) basis set for comparison on different solvents.

2. Excited state intramolecular proton transfer

The relationship between the molecular conformations of Compound (I) on the ground and excited state was illustrated in Figure 43. The most stable form of the ESIPT molecule in the ground state was in equilibrium between different conformers arising from tautomerism and rotamerism (Jayabharathi *et al*., 2014). The normal planar form featured an intramolecular hydrogen bond between hydroxyl function and the basic nitrogen atom of the imine group. The enol conformer could undergo proton transfer to form its tautomer (keto form). Upon excitation of the enol form to its first excited singlet state (*enol**) underwent an excited state intramolecular proton transfer to yield the planar tautomer (*cis-keto**) accompanied with large stokes shifted fluorescence emission. However, in case of enol conformers could transfrom to form their ketoB form so ketoB was difficult to take –O-HA out before hydrogen transfer through 5 membered ring to produce ketoB*. Therefore, the process of pathway B was not revealed. Several research (Kim *et al*., 2007; Spörkel *et al*., 2013; Ahmad *et al*., 2014) have been proved the typical ESIPT producing the tautomeric form could be coupled with the intramolecular charge transfer (ICT) state with a rotation around C-C bond to produce a non-planar configuration (*tran-keto**) between two rings. The *tran-keto** state could be deactivated back to its ground state via radiationless relaxation.

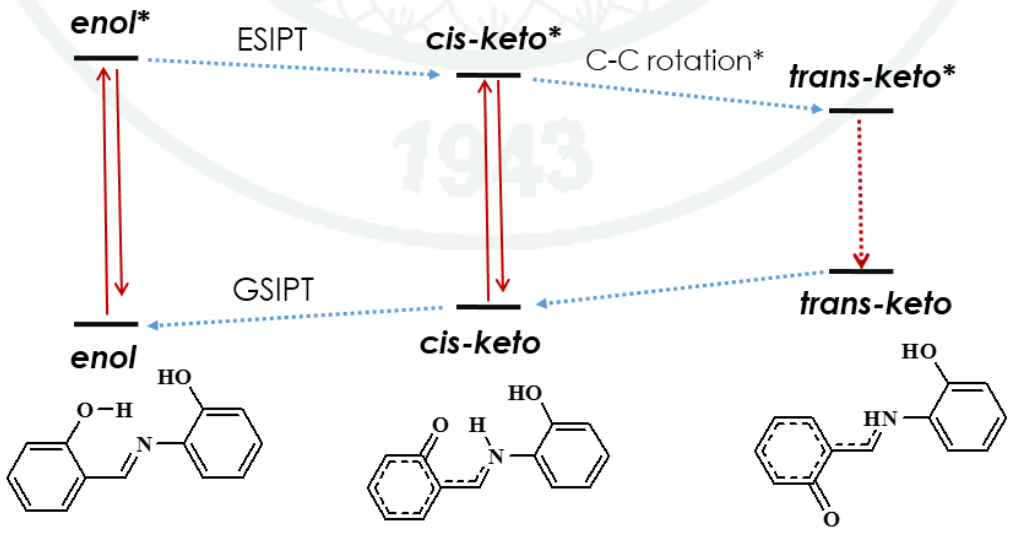

Figure 43 Mechanism of GSIPT and ESIPT of Compound (I).

2.1 UV-Visible absorption properties

Electronic transitions of Compound (I), (II) and (III) were carried out to confirm the configuration for ground state geometry optimization as well as explained the mechanism in ESIPT process. The vertical excitation energies were calculated by Time Dependent Density functional Theory (TDDFT) method taking the optimized structures obtained at the same level of theory (CAM-B3LYP/6-311G(d,p)) for gas phase as well as acetonitrile solution for E- and K-form. The conductor polarizable continuum model (CPCM) was employed to take the acetonitrile solvation effect into account. The calculated excitation energies of Compound (I), (II) and (III) with oscillator strengths for the transition from ground state (S_0) to fifth excited state (S_5) were summarized in Table 7, 8 and 9 along with the experimental value in acetonitrile solution.

The highest oscillator strength exhibited $S_0 \rightarrow S_1$ transition corresponding transition to the excitation from the highest occupied molecular orbital (HOMO) to the lowest unoccupied molecular orbital (LUMO). All of these states were assigned to π-π^* transition. It was interesting that the calculated results corresponding to the maximum wavelength observed in UV-Vis spectrum from experiment. Even though calculated results showed slight blue-shifted than experimental values, all could be acceptable. In case of gas phase, calculated band was near the experiment spectra while the absorption wavelength obtained by calculation including the solvation effect of acetonitrile solution was closer. Simulated band with high oscillator strength compared with experiment underestimated with an error 18 nm (5.17%), 25 nm (8.87%) and 20 nm (5.76%) belonged to Compound (I), (II) and (III), respectively which could be acceptable. (Acceptable tolerances was less than 60 nm)

Table 7 Excitation energies (E_{ex}), absorption wavelength (λ_{max}) and oscillator strength (f) of enol and keto form of Compound (I) calculated using the TDDFT/CAM-B3LYP/6-311G(d,p) level of theory in gas phase and acetonitrile solution.

Electronic transition	Gas phase				Solvent phase				Expt[c]
	E_{ex} (eV)	E_{ex} (nm)	f[a]	Transition state[b]	E_{ex} (eV)	E_{ex} (nm)	f[a]	Transition state[b]	
Compound I									
Enol form									
$S_0 \rightarrow S_1$	3.88	320	0.44	H→L (91%)	3.76	330	0.74	H→L (92%)	348
$S_0 \rightarrow S_2$	4.38	283	0.04	H-1→L (81%)	4.34	286	0.10	H-1→L (81%)	
$S_0 \rightarrow S_3$	4.83	257	0.02	H-2→L (59%)	4.82	257	0.05	H-2→L (66%)	
$S_0 \rightarrow S_4$	5.11	242	0.25	H-3→L (45%)	5.02	247	0.30	H-3→L (52%)	268
$S_0 \rightarrow S_5$	5.60	221	0.03	H→L+1 (27%)	5.57	223	0.11	H→L+1 (38%)	
Keto form									
$S_0 \rightarrow S_1$	3.41	364	0.32	H→L (97%)	3.24	382	0.52	H→L (97%)	
$S_0 \rightarrow S_2$	3.84	323	0.01	H-3→L (77%)	3.97	313	0.04	H-3→L (66%)	
$S_0 \rightarrow S_3$	4.42	281	0.29	H-1→L (76%)	4.32	287	0.48	H-1→L (63%)	
$S_0 \rightarrow S_4$	4.92	252	0.09	H-2→L (71%)	4.84	256	0.10	H-2→L (71%)	
$S_0 \rightarrow S_5$	5.46	227	0.05	H→L+1 (45%)	5.45	227	0.06	H→L+1 (37%)	

[a] Oscillator strength [b] H = HOMO, L = LUMO, H-1 = next highest occupied molecular orbital and LUMO [c] Experimental result

Table 8 Excitation energies (E_{ex}), absorption wavelength (λ_{max}) and oscillator strength (f) of enol and keto form of Compound (II) calculated using the TDDFT/CAM-B3LYP/6-311G(d,p) level of theory in gas phase and acetonitrile solution.

Electronic transition	Gas phase				Solvent phase				Expt[c]
	E_{ex} (eV)	E_{ex} (nm)	f^a	Transition state[b]	E_{ex} (eV)	E_{ex} (nm)	f^a	Transition state[b]	
Compound II									
Enol form									
$S_0 \rightarrow S_1$	3.98	312	0.43	H→L (93%)	3.86	321	0.75	H→L (95%)	337
$S_0 \rightarrow S_2$	4.45	279	0.10	H-1→L (69%)	4.41	281	0.15	H-1→L (78%)	
$S_0 \rightarrow S_3$	4.94	251	0.26	H-3→L (43%)	4.87	255	0.30	H-3→L (51%)	270
$S_0 \rightarrow S_4$	5.06	245	0.00	H-2→L (41%)	5.06	245	0.00	H-2→L (44%)	
$S_0 \rightarrow S_5$	5.72	217	0.06	H-4→L (36%)	5.67	219	0.10	H-4→L (33%)	
Keto form									
$S_0 \rightarrow S_1$	3.23	384	0.38	H→L (98%)	3.33	399	0.60	H→L (98%)	
$S_0 \rightarrow S_2$	3.65	340	0.00	H-2→L (92%)	3.85	320	0.00	H-2→L (93%)	
$S_0 \rightarrow S_3$	4.41	281	0.44	H-1→L (93%)	4.49	287	0.62	H-1→L (92%)	
$S_0 \rightarrow S_4$	4.93	252	0.01	H->L→1 (40%)	5.02	248	0.00	H-3→L (40%)	
$S_0 \rightarrow S_5$	5.52	225	0.00	H→L+2 (56%)	5.61	224	0.09	H→L+2 (39%)	

[a] Oscillator strength [b] H = HOMO, L = LUMO, H-1 = next highest occupied molecular orbital and LUMO [c] Experimental result

Table 9 Excitation energies (E_{ex}), absorption wavelength (λ_{max}) and oscillator strength (f) of enol and keto form of Compound (III) calculated using the TDDFT/CAM-B3LYP/6-311G(d,p) level of theory in gas phase and acetonitrile solution.

Electronic transition	Gas phase				Solvent phase				Expt[c]
	E_{ex} (eV)	E_{ex} (nm)	f[a]	Transition state[b]	E_{ex} (eV)	E_{ex} (nm)	f[a]	Transition state[b]	
Compound III									
Enol form									
$S_0 \rightarrow S_1$	3.87	320	0.47	H→L (89%)	3.79	327	0.97	H→L (95%)	347
$S_0 \rightarrow S_2$	4.68	265	0.01	H-1→L (44%)	4.59	270	0.00	H-4→L (94%)	
$S_0 \rightarrow S_3$	4.85	256	0.32	H-1→L (41%)	4.70	264	0.21	H-1→L (84%)	
$S_0 \rightarrow S_4$	5.02	247	0.01	H-2→L (57%)	4.96	250	0.03	H-2→L (72%)	271
$S_0 \rightarrow S_5$	5.66	219	0.06	H→L+2 (47%)	5.64	220	0.06	H-3→L (75%)	
Keto form									
$S_0 \rightarrow S_1$	2.51	495	0.47	H→L (99%)	2.42	513	0.64	H→L (97%)	
$S_0 \rightarrow S_2$	3.50	355	0.00	H-2→L (95%)	3.90	318	0.00	H-2→L (95%)	
$S_0 \rightarrow S_3$	4.05	306	0.31	H-1→L (97%)	4.07	304	0.45	H-1→L (95%)	
$S_0 \rightarrow S_4$	4.52	274	0.00	H→L+1 (65%)	4.58	271	0.03	H-3→L (80%)	
$S_0 \rightarrow S_5$	4.90	253	0.02	H→L+2 (78%)	4.93	251	0.03	H→L+2 (75%)	

[a] Oscillator strength [b] H = HOMO, L = LUMO, H-1 = next highest occupied molecular orbital and LUMO [c] Experimental result

When considering deeper point, we found that the fault between theoretical calculation and experimental results may be attributed to model structure used as an input in simulation and natural form of tautomers in solution. In the calculation enol and keto form were used as input while indeed schiff bases molecule in the solution could be converted E→K form in equilibrium. For more understanding, a comparison of excitation wavelength gained from computation calculation and experimental spectrum in acid-base solation was illustrated as seen in Figure 44 for Compound (I). The result showed excitation wavelength with the highest oscillator strength for case of enol exhibited close to the maximum absorption peak from experiment in acid solution with 5 nm (1.5% relative error) error for both gas and solvent phase. In the case of keto, no error were exposed between simulated in base solution and analytical results as well as gas phase showed insignificant error with 18 nm (4.8%).

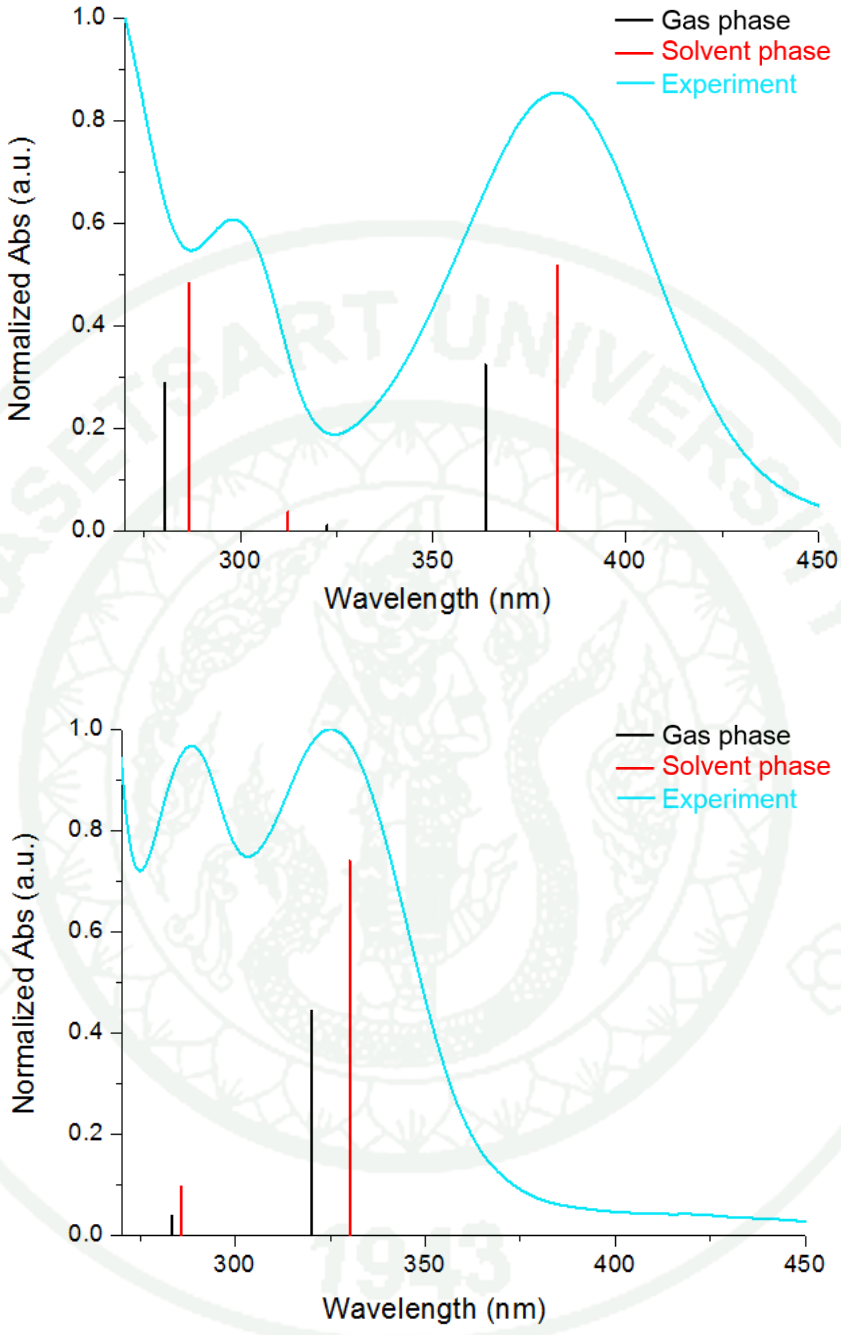

Figure 44 Simulated absorption spectra for Compound (I) with TDDFT/CAM-B3LYP/6-311G(d,p) of (a) E-form and (b) K-form in gas phase (black line) and method with SS-PCM to include solvent effect of acetonitrile (red line) compared with experimental UV-Visible spectrum in (a) acid and (b) base solution (blue line).

2.2 Molecular orbital analysis

The electron density of frontier molecular orbitals (FMOs), HOMO (Highest Occupied Molecular Orbital) and LUMO (Lowest Unoccupied Molecular Orbital) were obtained interesting information from the output of a calculation. In particular, it could be visualized molecular orbitals, electron density and electrostatic potentials. In the 1990s the nodal plane concept of π-system molecular orbital to rationalize the phenomenon of ESIPT was first developed by Nagaoka and Nagashima and since then it had been successfully substantiated to various systems. These work frontier molecular orbitals were used to understand the nature of excited state in these molecules. Hereinbefore, simulated electronic property showed that the S_1 state of Compound (I), (II) and (III) mainly corresponded to the orbital transition from HOMO to LUMO (π-π^* character). The FMO contour maps with the HOMO and LUMO energies enol and keto tautomer of Compound (I), (II) and (III) were presented in Figure 45, 46 and 47. The HOMO and LUMO of Compound (I) was represented to explain.

E-form	**K-form**
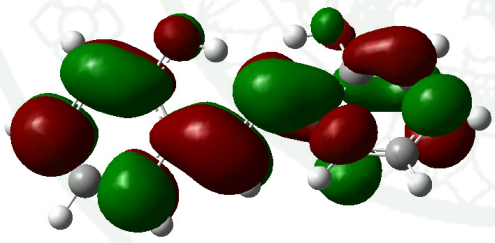	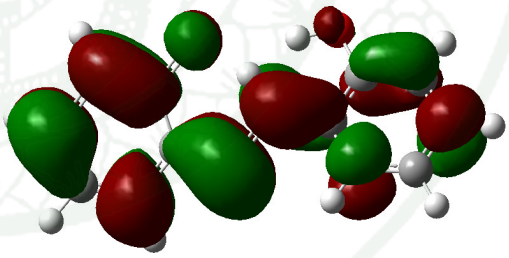
LUMO (-0.224 eV)	**LUMO (-0.229 eV)**
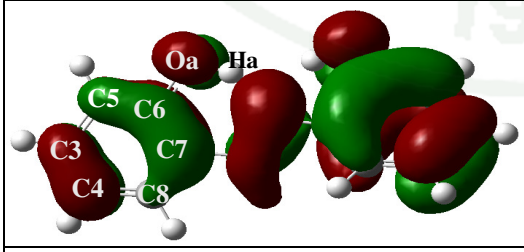	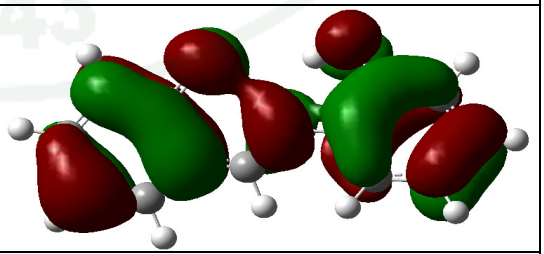
HOMO (-0.326 eV)	**HOMO (-0.324 eV)**

Figure 45 The theoretical frontier molecular orbitals of Compound (I) using the TDDFT/CAM-B3LYP/6-311G(d,p) level of theory in acetonitrile solution.

The analysis of HOMO and LUMO showed that HOMO was a π-orbital with bonding character primarily across C3–C4 and C5-C6-C7-C8 atom, whereas anti-bonding character acrossed C6–Oa bond for both E- and K-forms. As observed in HOMO orbital of E-form, the hydroxyl oxygen consisted of a large electron density projection over Oa atom along with bonding character along Od–Ha bond. Thus, the transfer of proton did not lead to any further stabilization through electronic redistribution. Whereas the LUMO orbital on the E-form was of π^* character and excitation of electron from HOMO to LUMO led to specific localization of π electron density spread over the entire molecular framework with excitation of the electron from HOMO to LUMO pushing the π-electronic density toward the N atom of the molecule. LUMO E-form possessed a high electron density on N atom and there was a lower distribution of electron density on Oa atom in comparison to HOMO. This meant that the acidic character of the phenol group and the basic character of the azomethine group changed in the excited state thereby induced the ESIPT, O–H bond was weakened and N–H bond was formed. On the other hand, HOMO orbital of keto tautomer showed high electron density on O atom. This electronic distribution led to proton transfer from the K- to the E- tautomer in the ground state.

The energies of theoretical FMOs were also computed for the most stable structure of Compound (I), (II) and (III). The HOMO and LUMO energies of Compound (I) were calculated as -0.326 a.u. and -0.224 a.u. (E-form) and -0.324 a.u. and -0.229 a.u. (K-form). Hence HOMO-LUMO energy gap (ΔE_{L-H}) was 2.80 and 2.59 eV. For Compound (II), HOMO-LUMO energy gap (ΔE_{L-H}) was 3.11 (E-form) and 2.54 (K-form) eV. HOMO-LUMO energy gap for Compound (III) (ΔE_{L-H}) was 2.72 (E-form) and 2.13 (K-form) eV.

E-form	K-form
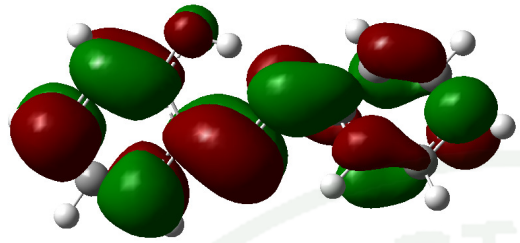	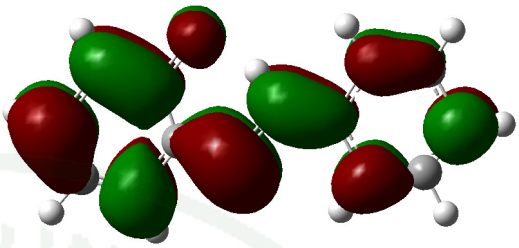
LUMO (-0.223 eV)	**LUMO (-0.233)**
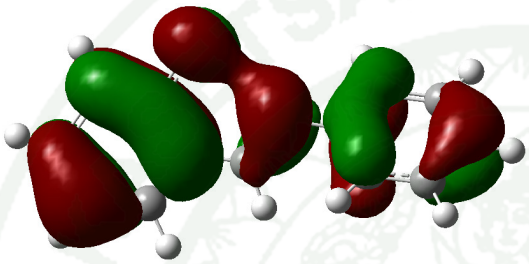	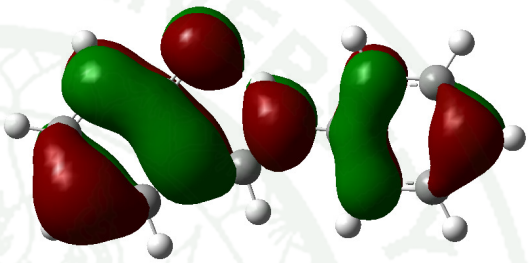
HOMO (-0.338)	**HOMO (-0.326)**

Figure 46 The theoretical frontier molecular orbitals of Compound (II) using the TDDFT/CAMB3LYP/6-311G(d,p) level of theory in acetonitrile solution.

E-form	K-form
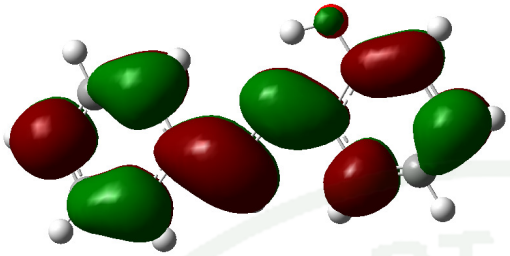	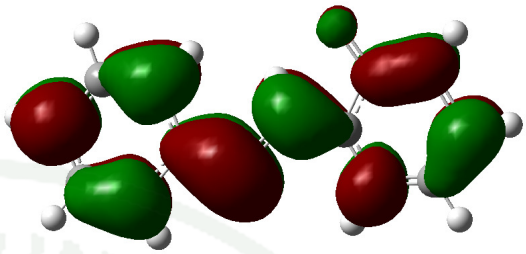
LUMO (-0.238 eV)	**LUMO (-0.231eV)**
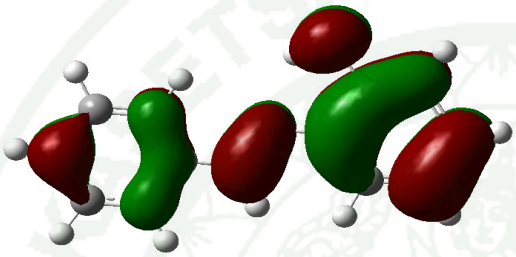	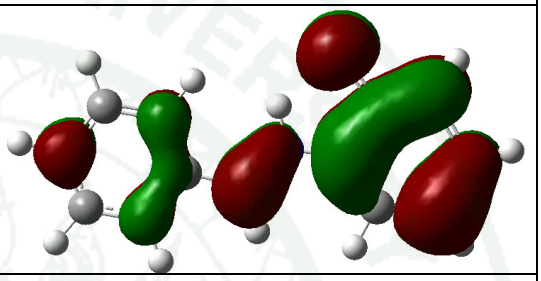
HOMO (-0.316 eV)	**HOMO (-0.331 eV)**

Figure 47 The theoretical frontier molecular orbitals of Compound (III) using the TDDFT/CAMB3LYP/6-311G(d,p) level of theory in acetonitrile solution.

2.3 Emission properties

After ESIPT process, enol*→keto*, keto* in the excited state emitted fluorescence and turned back to the keto form on ground state. Accordingly, the difference between the energies of the optimized geometries at the first singlet excited state and the ground state was used in computing the emissions (Lakowicz *et al*., 1999; Valeur *et al*., 2001). The emission calculations of three salicylaldimine schiff bases were performed vertical de-excitation of the molecules using the TDDFT method with CAM-B3LYP/6-311G(d,p) in their first singlet excited state optimized structure including conductor polarizable continuum model. The calculated emission energies, oscillator strength and transition character for keto form were summarized in Table 10.

The calculated emission result showed excited state (S_1) with the largest oscillator strength arisen from LUMO to HOMO corresponding to π^*-π de-excitation. The calculated fluorescence of K-form were noted 454, 453 and 512 nm belonging to Compound (I), (II) and (III). However, the TDDFT calculation of emission spectra was not accurate enough for comparing experiment observations. Several research had been failed to describe the emission simulation (Promkatkaew *et al*., 2013). It may be a result of limited in quantum theory either the emission or fluorescence complete with the geometry relaxation subsequent to the photoexcitation and also nonradiative decay to the ground state.

Table 10 The emission energies and oscillator strength (*f*) in acetonitrile solution by TDDFT/CAM-B3LYP/6-311G(d,p) method combined with PCM model and experimental data in the same solution (acetonitrile) for keto form of the Compound (I), (II) and (III).

Electronic transitions	E_{ex} (eV)	E_{ex} (nm)	f^a	Transition state[b]	Expt[c] (nm)
Compound I					
$S_1 \rightarrow S_0$	2.73	454	0.54	H→L (98%)	547
Compound II					
$S_1 \rightarrow S_0$	2.74	453	0.60	H→L (95%)	549
Compound III					
$S_1 \rightarrow S_0$	2.42	512	0.64	H→L (97%)	504

[a] Oscillator strength, [b] H = HOMO, L = LUMO, [c] Experimental part

3. Potential energy profiles for GSIPT and ESIPT process and conical intersection

3.1 PEC scan along the O-H bond distance

Selection of proton transfer coordinate was a crucial job for the building of ground and excited state potential energy curves (PECs). For a small system, intrinsic reaction coordinate approach (IRC) was quite handy as proton transfer reaction co-ordinate. It involved the consideration of O-H elongation distance as proton transfer reaction co-ordinate named as 'distinguished co-ordinate approach' by Sobolewski and Domcke in 1994. Many research also considered this approach for the GSIPT and ESIPT processes of various systems (Misra *et al*., 2012 and Annaraj *et a*l., 2014).

It had been demonstrated that the ESIPT process could be facilitated by hydrogen transfer in S_1 state (Lan *et la*., 2013). To further investigate, the GSIPT and ESIPT processes for Compound (I) can be most clearly presented and critically assessed through potential energy surface (PES) along the proton transfer reaction co-ordinate. Reaction path as a function of O-H bond distance was studied to understand the proposed GSIPT and ESIPT of salicylaldimine schiff base. Here we also had generated the PEC for GSIPT by calculating IRC and the ESIPT by calculating the vertical transition energies at the TDDFT/CAM-B3LYP/6-311G(d,p) level for the ground state structures at each point. The PEC was plotted using the relative energies (with respect to the lowest energy) as a function of O-H distances from 0.98 to 1.56 Å in gas phase and the potential energy diagram for Compound (I) displayed in Figure 48.

The ground state (S_0) PEC clearly showed that enol form was more stable than keto form with the minimal energies of enol form at O-H distance about 0.98 Å, The energy barrier in going from enol to keto form was 8.6 kcal/mol. Therefore, due to quite low energy barrier, it might be possible to have GSIPT under thermal condition. Noted that the energy barrier for the reverse process, keto to enol conversion, was 0.3 kcal/mol. It was also quite low to occur at room temperature. Therefore, at ground state there would always be a mixture of keto and enol forms.

In the case of excited state PEC, the curves of S_1 and S_2 were quite similar. Interestingly, in both S_1 and S_2 states, the keto form became more stable than that of enol form and there was no any energy barrier in S_1 so the enol* → keto* transformation occurred in excited state through a barrierless path. It suggested that very large stokes shift took place during emission. After decaying to the ground state, the photo-tautomer (keto form) reverted to the original enol via reverse proton transfer barrier of 0.3 kcal/mol. This implied that although the occurrence of GSIPT from enol → keto should be very difficult more than the reverse proton transfer process from keto → enol that could take place easily, which was much favorable for ESIPT occurrence. This signal was not only the inoperativeness of a GSIPT process, but also the feasibility of an ESIPT process in salicylaldimine based.

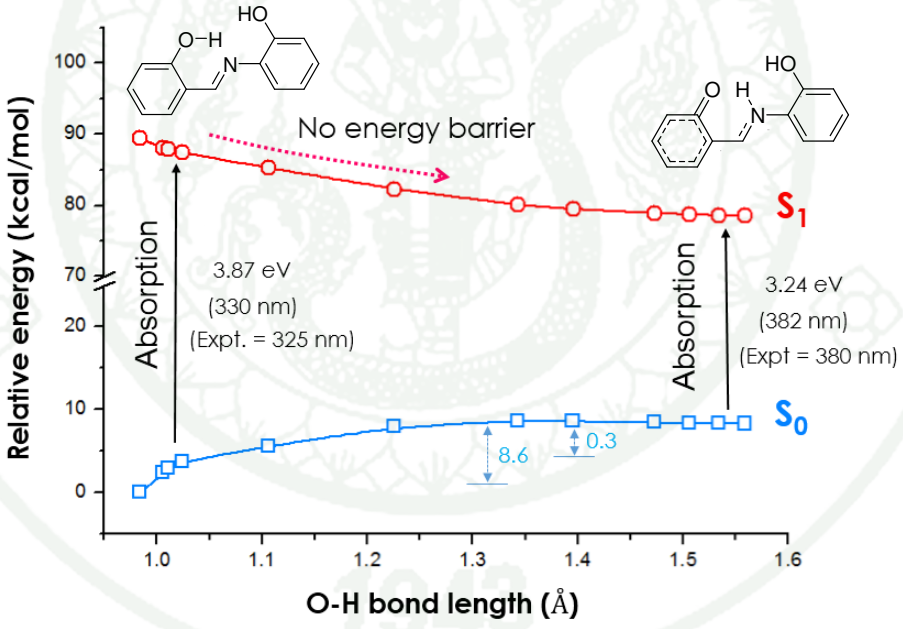

Figure 48 The calculated potential energy curve of enol form into keto form which S_0 (blue line) and S_1 (red line) state computed by CAM-B3LYP/6-311G (d,p) method as a functions of the O-H bond length (Å). The energies of S_0 state were calculated under the geometries of the corresponding S_1 state.

3.2 Alternate pathway in radiationless decay through conical intersections.

As discussed before, the best known and most thoroughly studied photochromic schiff base showed the four-level cyclic photoreaction scheme of Compound (I) which was the reaction cycle completion E→E*→K*→K→E. In fact, the photochromism of the aromatic schiff bases likely arised from an excited state intramolecular proton transfer ESIPT reaction that might be followed by a plethora of other photochemical processes such as *cis-trans* isomerizations, thermal deactivation, and internal conversion (IC) through conical intersections (CIs) or intersystem crossing (Ortiz-Sanchez *et al*., 2008). In addition, Noh and coworker (2013) reported the low fluorescence quantum efficiency of Compound (I) only 0.001 that confirmed the weak emission was observed in experimental outcome for salicylaldimine schiff base (Noh *et al*., 2013). Thus Compound (I) was investigated to gain insight into the molecular level of salicylaldimine fluorescence quenching. Potential energy surfaces were employed again to calculate the global minimum energy of the excited state with sufficient energy relaxed through the conical intersection in isolated gas phase as a function of certain dihedral angles of interest. Rotation potential curve of *cis-keto* in the ground (S_0) and first singlet excites state (S_1) were displayed in Figure 49.

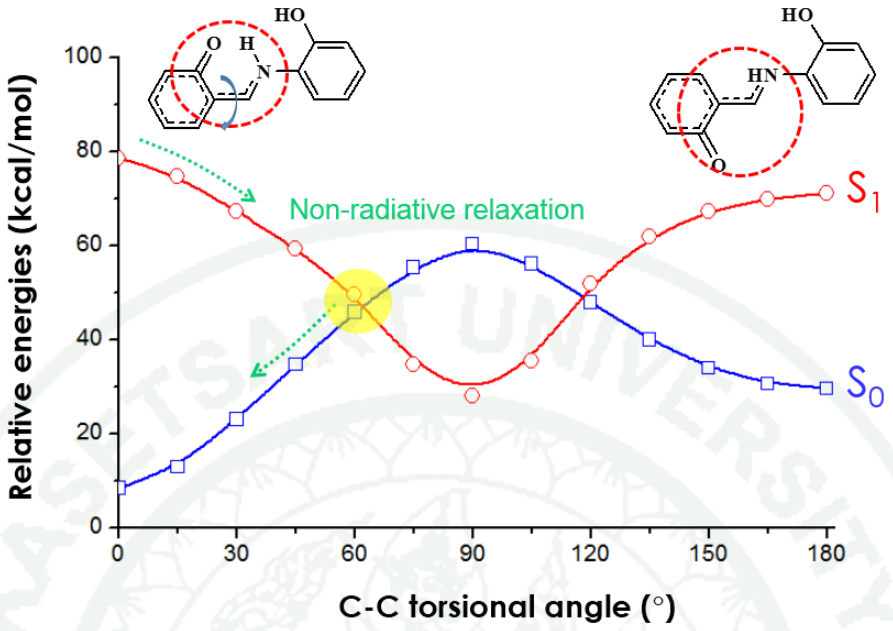

Figure 49 Rotation potential curve of *cis-keto* in the ground (S_0) and first excited state (S_1), computed by CAM-B3LYP/6-311G(d,p) method as a functions of the C-C rotation (degree). The energies of S_0 state were calculated under the geometries of the corresponding S_1 state.

The potential energy curves along the minimum energy path of the S_1 state were shown for Compound (I) in Figure 49. The energy barrier to the conical intersection was calculated almost no energy barrier and cross at about 45.8 kcal/mol. These calculations qualitatively explained the experimental fact that activation energies occurred on the non radiative relaxation or turned to global minimum energy (29.5 kcal/mol) of *tran-keto* tautomer.

Figure 50 depicted the potential energy profile Compound (I) which included Figure 48 and 49 into one graph for explanation GSIPT and ESIPT mechanism consisting of relaxed one dimensional energy paths along the O-H bond length in Figure 49 (left) as well as the torsional angle (0-180°) around the central C3-C4-C5-N6 bond in Figure 49 (right). PES result showed radiation of suitable energy 350 nm placed the enol tautomer in the first singlet excited electronic state S_1. After electronic excitation,

the molecule was no longer a minimum energy structure but was in unstable conformation that might relax to an energy minimum. The system in S_1 might occur through two different channels: ESIPT and IC. An ESIPT process might form the excited *cis-keto* tautomer. However, the planar *cis-keto* tautomer was not a stable structure in S_1 and underwent out-of-plane torsions to gain some energy stability about 60°. The torsion that led to the *cis-trans* isomerization process through the C4-C5 bond, process IC was connected to a CI between S_0 and S_1. At this point, the *cis-keto* molecules might deactivate to S_0 to form either the *trans-keto* as the final photoproduct or the *cis-keto* minimum due to the very low reverse proton transfer energy barrier, would form again the enol tautomer, closing the photochemical cycle and allowing a new photoactivation to start the process again.

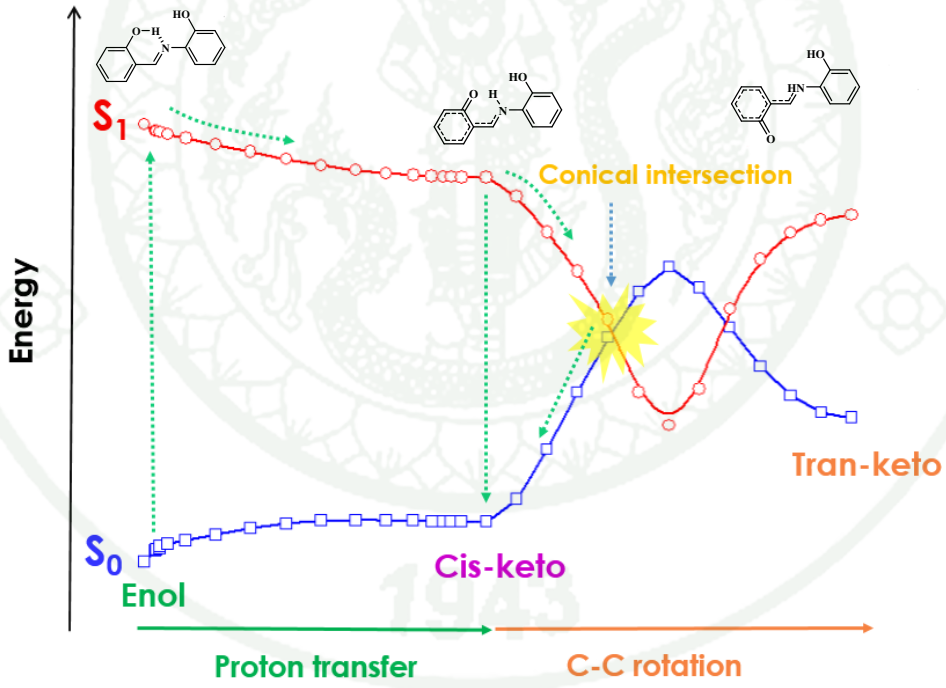

Figure 50 Potential energy curves of the S_0 state (blue line) and the S_1 state (red line), determined at the CAM-B3LYP/6-311G(d,p) level as the function of hydrogen transfer reaction path (*enol* to *cis-keto* form) and C-C torsional reaction path on the *cis-keto* to *trans-keto* form for Compound (I).

CONCLUSION

Three Salicylaldimine Schiff bases 2-(2-hydroxybenzylideneamino)phenol, 2-(hydroxybenzylidene)aniline and (Benzylideneamino)phenol were synthesized to study ground state and excited state intramolcular proton transfer. For experiment, Compound (I), (II) and (III) containing the phenolic proton next to nitrogen of imine group showed pH dependent behavior in acetonitrile:aqueous solution, the enol form presented in the acidic solution while the keto form presented in the basic solution. The schiff bases I, II and III also showed a single prominent emission in polar solvents and dual emission with large stokes shift in non-polar and aprotic solvents due to excited state intramolecular proton transfer (ESIPT).

Calculation results based on CAM-B3LYP and TD/CAM-B3LYP with 6-311G(d,p) basis set proved to be an efficient tool for explaining the experimental finding. Frontier molecular orbitals explained the probability of density electron delocalization in HOMO and LUMO on ESIPT process. Potential energy curves for GSIPT and ESIPT confirmed the cycle of ESIPT through barrierless energy led to red emission band which was the significant property in wide applications; furthermore, PES scan along the C-C bond torsion exposed the alternative pathway in radiationless decay through conical intersection. The presence of the S_0/S_1 conical intersection provided the efficient and fast decay process of excited state, resulting the low quantum yield of fluorescence in solution.

LITERATURE CITED

Annaraj, B., S. Pan, M.A. Neelakantan and P.K. Chattaraj. 2014. Dft Study on the Ground State and Excited State Intramolecular Proton Transfer of Propargyl Arm Containing Schiff Bases in Solution and Gas Phases. **Computational and Theoretical Chemistry** 1028 (0): 19-26.

Chatziefthimiou, S.D., Y.G. Lazarou, E. Hadjoudis, T. Dziembowska and I.M. Mavridis. 2006. Keto Forms of Salicylaldehyde Schiff Bases: Structural and Theoretical Aspects. **American Chemical Society** 110 (47): 23701-23709.

Doroshenko, A.O., A.Y. Matsakov, O.V. Nevskii and O.V. Grygorovych. 2012. Excited State Intramolecular Proton Transfer Reaction Revisited: S1 State or General Reversibility? **Journal of Photochemistry and Photobiology A: Chemistry** 250 (0): 40-49.

Fang, T.-C., H.-Y. Tsai, M.-H. Luo, C.-W. Chang and K.-Y. Chen. 2013. Excited-State Charge Coupled Proton Transfer Reaction Via the Dipolar Functionality of Salicylideneaniline. **Chinese Chemical Letters** 24 (2): 145-148.

Fegley, M.E.A., S.S. Pinnock, C.N. Malele and W.E. Jones Jr. 2012. Metal-Containing Conjugated Polymers as Fluorescent Chemosensors in the Detection of Toxicants. **Inorganica Chimica Acta** 381 (0): 78-84.

Jacquemin, P.-L., K. Robeyns, M. Devillers and Y. Garcia. 2014. Reversible Photochromism of an N-Salicylidene Aniline Anion. **Chemical Communications** 50 (6): 649-651.

Jayabharathi, J., V. Thanikachalam, K. Jayamoorthy and M.V. Perumal. 2011. A Physiochemical Study of Excited State Intramolecular Proton Transfer Process: Luminescent Chemosensor by Spectroscopic Investigation Supported by Ab Initio Calculations. **Spectrochimica Acta Part A: Molecular and Biomolecular Spectroscopy** 79 (1): 6-16.

Jayabharathi, J., V. Thanikachalam, K. Jayamoorthy and N. Srinivasan. 2013. Synthesis, Spectral Studies and Solvatochromism of Some Novel Benzimidazole Derivatives – Esipt Process. **Spectrochimica Acta Part A: Molecular and Biomolecular Spectroscopy** 105 (0): 223-228.

Jayabharathi, J., K. Vimal, V. Thanikachalam and V. Kalaiarasi. 2014. Photophysical and Excited-State Intramolecular Proton Transfer of 2-(1-(3,5-Dimethylphenyl)-1h-Phenanthro[9,10-D]Imidazol-2-Yl)Phenol: Dft Analysis. **Spectrochimica Acta Part A: Molecular and Biomolecular Spectroscopy** 125 (0): 290-296.

Joshi, H., F.S. Kamounah, C. Gooijer, G. van der Zwan and L. Antonov. 2002. Excited State Intramolecular Proton Transfer in Some Tautomeric Azo Dyes and Schiff Bases Containing an Intramolecular Hydrogen Bond. **Journal of Photochemistry and Photobiology A: Chemistry** 152 (1–3): 183-191.

Kim, S., J. Seo and S.Y. Park. 2007. Torsion-Induced Fluorescence Quenching in Excited-State Intramolecular Proton Transfer (Esipt) Dyes. **Journal of Photochemistry and Photobiology A: Chemistry** 191 (1): 19-24.

Kim, Y.H., S.-G. Roh, S.-D. Jung, M.-A. Chung, H.K. Kim and D.W. Cho. 2010. Excited-State Intramolecular Proton Transfer on 2-(2[Prime or Minute]-Hydroxy-4[Prime or Minute]-R-Phenyl)Benzothiazole Nanoparticles and Fluorescence Wavelength Depending on Substituent and Temperature. **Photochemical & Photobiological Sciences** 9 (5): 722-729.

Koll, A. 2003. Specific Features of Intramolecular Proton Transfer Reaction in Schiff Bases. **International Journal of Molecular Sciences** 4 (7): 434-444.

Lan, X., D. Yang, X. Sui and D. Wang. 2013. Time-Dependent Density Functional Theory (Td-Dft) Study on the Excited-State Intramolecular Proton Transfer (Esipt) in 2-Hydroxybenzoyl Compounds: Significance of the Intramolecular Hydrogen Bonding. **Spectrochimica Acta Part A: Molecular and Biomolecular Spectroscopy** 102 (0): 281-285.

Laurent, A.D., Y. Houari, P.H.P.R. Carvalho, B.A.D. Neto and D. Jacquemin. 2014. Esipt or Not Esipt? Revisiting Recent Results on 2,1,3-Benzothiadiazole under the Td-Dft Light. **RSC Advances** 4 (27): 14189-14192.

Li, G.-Y., G.-J. Zhao, Y.-H. Liu, K.-L. Han and G.-Z. He. 2010. Td-Dft Study on the Sensing Mechanism of a Fluorescent Chemosensor for Fluoride: Excited-State Proton Transfer. **Journal of Computational Chemistry** 31 (8): 1759-1765.

Lin, W.-C., S.-K. Fang, J.-W. Hu, H.-Y. Tsai and K.-Y. Chen. 2014. Ratiometric Fluorescent/Colorimetric Cyanide-Selective Sensor Based on Excited-State Intramolecular Charge Transfer –Excited-State Intramolecular Proton Transfer Switching. **Analytical Chemistry** 86 (10): 4648–4652

Martínez-Máñez, R. and F. Sancenón. 2003. Fluorogenic and Chromogenic Chemosensors and Reagents for Anions. **Chemical Reviews** 103 (11): 4419-4476.

Moghadam, A.J., R. Omidyan and V. Mirkhani. 2014. Photophysics of a Schiff Base: Theoretical Exploration of the Excited-State Deactivation Mechanisms of N-Salicilydenemethylfurylamine (Smfa). **Physical Chemistry Chemical Physics** 16 (6): 2417-2424.

Moghadam, A.J., R. Omidyan, V. Mirkhani and G. Azimi. 2013. Theoretical Investigation of Excited State Proton Transfer Process in the N-Salicylidene-2-Bromoethylamine. **The Journal of Physical Chemistry A** 117 (4): 718-725.

Mohammad, R.B. and M. Ali. 2011. Dft Study of Solvent Effects on Tautomerization of 4-(2-Thiazolylazo)-Resorcinol. **International Journal of Physical Sciences** 6 (24): 5726-5730.

Ortiz-Sánchez, J.M., R. Gelabert, M. Moreno and J.M. Lluch. 2008. Electronic-Structure and Quantum Dynamical Study of the Photochromism of the Aromatic Schiff Base Salicylideneaniline. **The Journal of Chemical Physics** 129 (21): -.

Özdemir, N. 2013. Quantum Chemical Investigation of the Intra- and Intermolecular Proton Transfer Reactions and Hydrogen Bonding Interactions in 4-Amino-5-(2-Hydroxyphenyl)-2h-1,2,4-Triazole-3(4h)-Thione. **Journal of Molecular Modeling** 19 (1): 397-406.

Padalkar, V., P. Ramasami and N. Sekar. 2013. A Combined Experimental and Dft-Tddft Study of the Excited-State Intramolecular Proton Transfer (Esipt) of 2-(2′-Hydroxyphenyl) Imidazole Derivatives. **Journal of Fluorescence** 23 (5): 839-851.

Park, S., S. Kim, J. Seo and S. Park. 2008. Application of Excited-State Intramolecular Proton Transfer (Esipt) Principle to Functional Polymeric Materials. **Macromolecular Research** 16 (5): 385-395.

Patil, V.S., V.S. Padalkar, A.B. Tathe and N. Sekar. 2013. Esipt-Inspired Benzothiazole Fluorescein: Photophysics of Microenvironment Ph and Viscosity. **Dyes and Pigments** 98 (3): 507-517.

Paul, B.K., A. Samanta and N. Guchhait. 2010. Influence of Chlorine Substitution on Intramolecular Hydrogen Bond Energy and Esipt Barrier: Experimental and Theoretical Measurements on the Photophysics of 3,5-Dichlorosalicylic Acid. **Journal of Molecular Structure** 977 (1–3): 78-89.

Prabhu, S., S. Saravanamoorthy, M. Ashok and S. Velmathi. 2012. Colorimetric and Fluorescent Sensing of Multi Metal Ions and Anions by Salicylaldimine Based Receptors. **Journal of Luminescence** 132 (4): 979-986.

Prasad De, S., S. Ash, S. Dalai and A. Misra. 2007. A Dft-Based Comparative Study on the Excited States Intramolecular Proton Transfer in 1-Hydroxy-2-Naphthaldehyde and 2-Hydroxy-3-Naphthaldehyde. **Journal of Molecular Structure: THEOCHEM** 807 (1–3): 33-41.

Promkatkaew, M., S. Suramitr, T. Karpkird, M. Ehara and S. Hannongbua. 2013. Absorption and Emission Properties of Various Substituted Cinnamic Acids and Cinnamates, Based on Tddft Investigation. **International Journal of Quantum Chemistry** 113 (4): 542-554.

Roohi, H., F. Hejazi, N. Mohtamedifar and M. Jahantab. 2014. Excited State Intramolecular Proton Transfer (Esipt) in 2-(2′-Hydroxyphenyl)Benzoxazole and Its Naphthalene-Fused Analogs: A Td-Dft Quantum Chemical Study. **Spectrochimica Acta Part A: Molecular and Biomolecular Spectroscopy** 118 (0): 228-238.

Shigemitsu, Y., T. Mutai, H. Houjou and K. Araki. 2012. Excited-State Intramolecular Proton Transfer (Esipt) Emission of Hydroxyphenylimidazopyridine: Computational Study on Enhanced and Polymorph-Dependent Luminescence in the Solid State. **The Journal of Physical Chemistry A** 116 (49): 12041-12048.

Song, P., J.-X. Ding and T.-S. Chu. 2012. Td-Dft Study on the Excited-State Proton Transfer in the Fluoride Sensing of a Turn-Off Type Fluorescent Chemosensor Based on Anthracene Derivatives. **Spectrochimica Acta Part A: Molecular and Biomolecular Spectroscopy** 97 (0): 746-752.

Spörkel, L., G. Cui, A. Koslowski and W. Thiel. 2013. Nonequilibrium H/D Isotope Effects from Trajectory-Based Nonadiabatic Dynamics. **The Journal of Physical Chemistry A** 118 (1): 152-157.

Swager, T.M. 1998. The Molecular Wire Approach to Sensory Signal Amplification. **Accounts of Chemical Research** 31 (5): 201-207.

Wang, J. and Y. Pang. 2014. A Simple Sensitive Esipt on-Off Fluorescent Sensor for Selective Detection of Al3+ in Water. **RSC Advances** 4 (12): 5845-5848.

Wang, L., W. Qin, X. Tang, W. Dou and W. Liu. 2011. Development and Applications of Fluorescent Indicators for Mg^{2+} and Zn^{2+}. **The Journal of Physical Chemistry A** 115 (9): 1609-1616.

Wu, K., Y. Gao, Z. Yu, F. Yu, J. Jiang, J. Guo and Y. Han. 2014. A Facile Fluorescent Chemosensor Based on Naphthalene-Derived Schiff Base for Zinc Ions in Aqueous Solution. **Analytical Methods** 6 (11): 3560-3563.

Xie, N. and Y. Chen. 2006. Design and Synthesis of a Selective Chemosensor for Zn^{2+}. **Chinese Journal of Chemistry** 24 (12): 1800-1803.

Zhao, J., S. Ji, Y. Chen, H. Guo and P. Yang. 2012. Excited State Intramolecular Proton Transfer (Esipt): From Principal Photophysics to the Development of New Chromophores and Applications in Fluorescent Molecular Probes and Luminescent Materials. **Physical Chemistry Chemical Physics** 14 (25): 8803-8817.

APPENDICES

Appendix A

^{1}H-NMR in $CDCl_3$

2-(2-hydroxybenzylideneamino)phenol (Compound I)

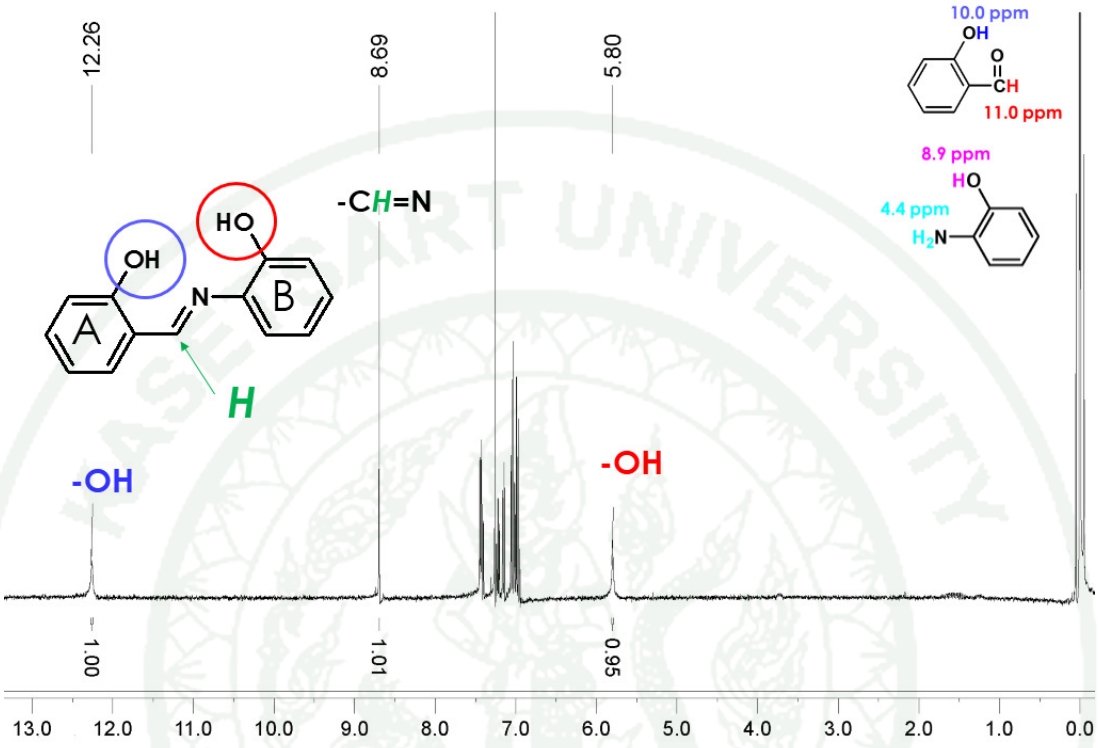

Appendix Figure A1 ^{1}H-NMR spectrum of 2-(2-hydroxybenzylideneamino)phenol (Compound I).

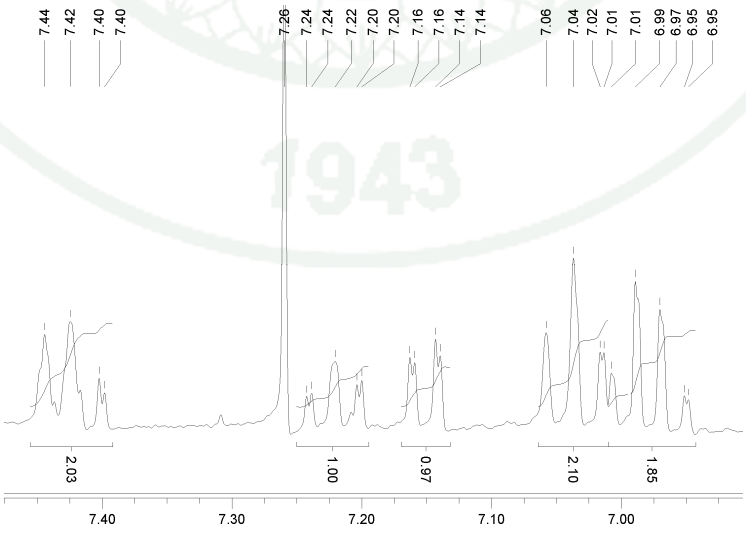

Appendix Figure A2 ^{1}H-NMR signals on aromatic ring of Compound (I)

2-(hydroxybenzylidene)aniline (Compound II)

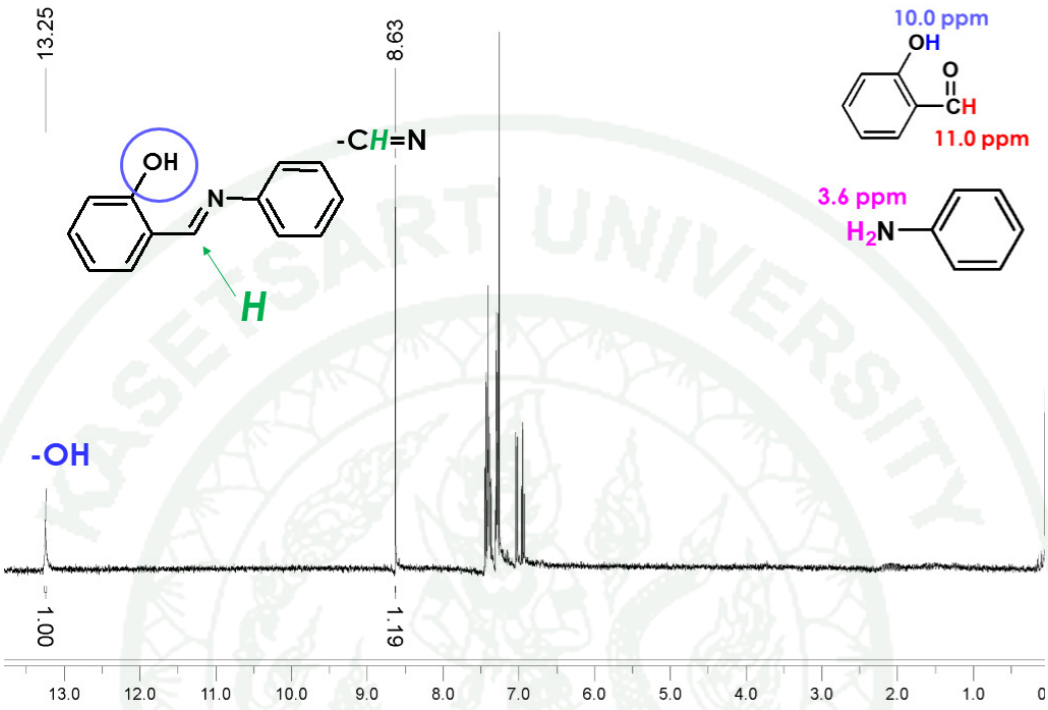

Appendix Figure A3 ^{1}H-NMR spectrum of 2-(hydroxybenzylidene)aniline (Compound II)

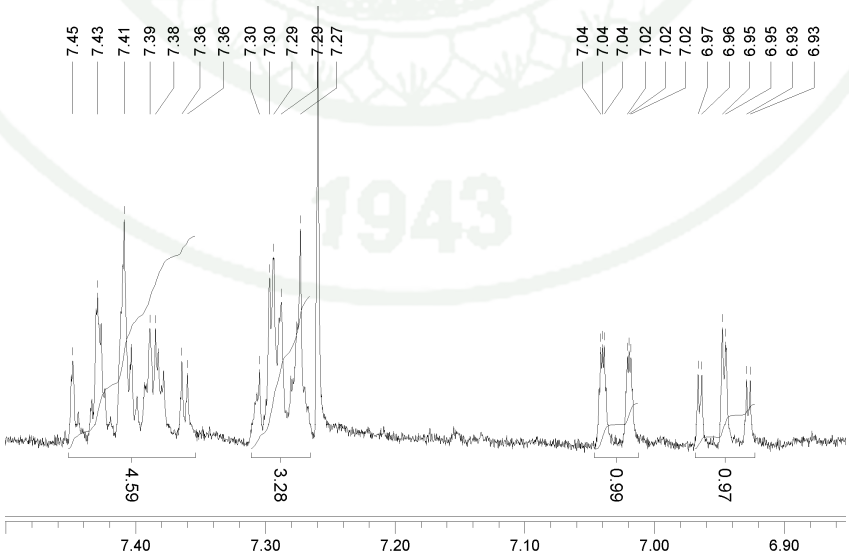

Appendix Figure A4 ^{1}H-NMR signals on aromatic ring of Compound (II)

(Benzylideneamino)phenol (Compound III)

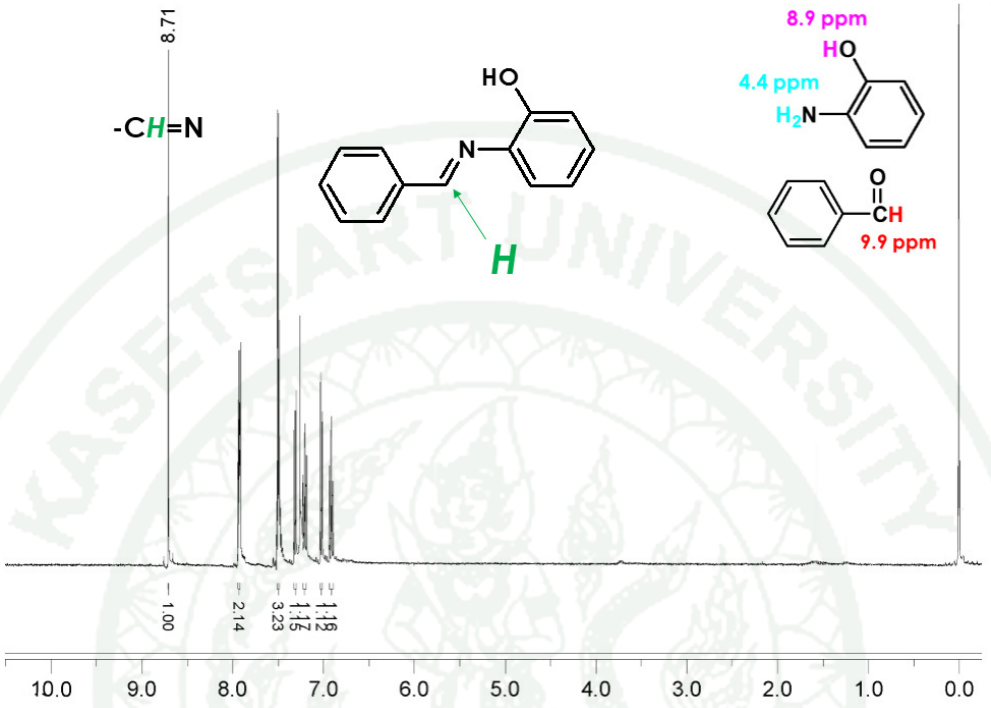

Appendix Figure A5 ^{1}H-NMR spectrum of (Benzylideneamino)phenol (Compound III).

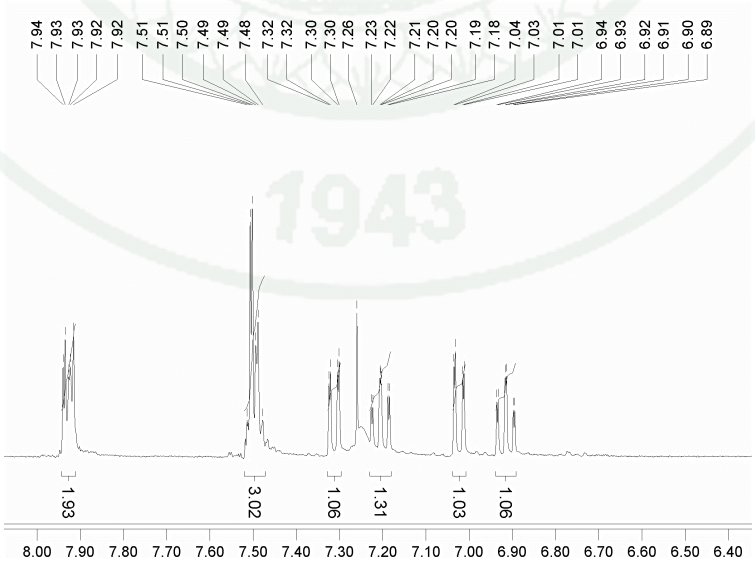

Appendix Figure A6 ^{1}H-NMR signals on aromatic ring of Compound (III)

Appendix B

FT-IR Spectroscopy

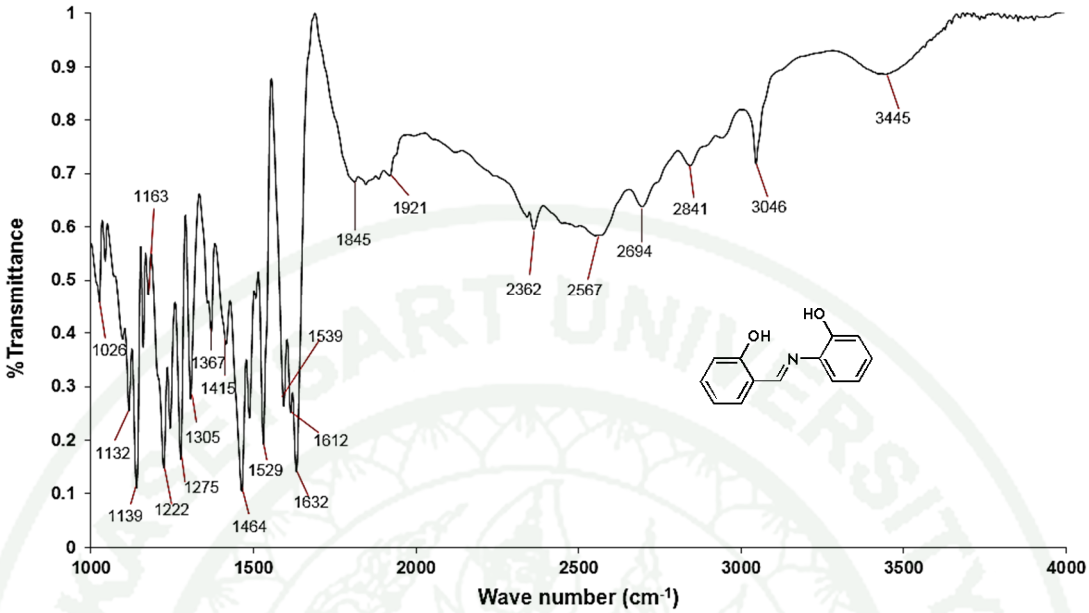

Appendix Figure B1 FT-IR spectrum of 2-(2-hydroxybenzylideneamino)phenol (Compound I).

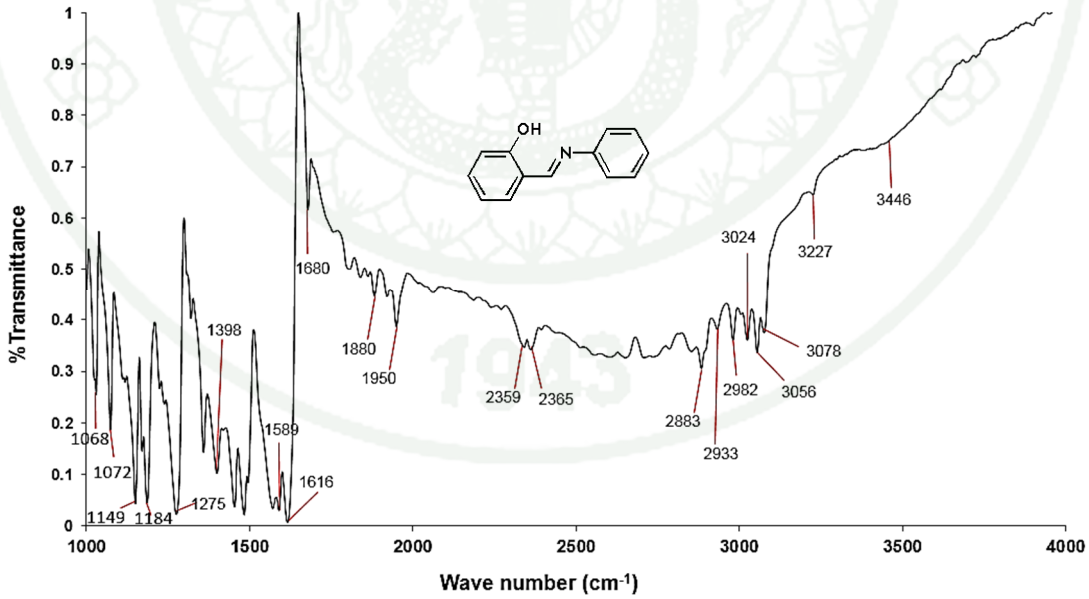

Appendix Figure B2 FT-IR spectrum of 2-(hydroxybenzylidene)aniline (Compound II)

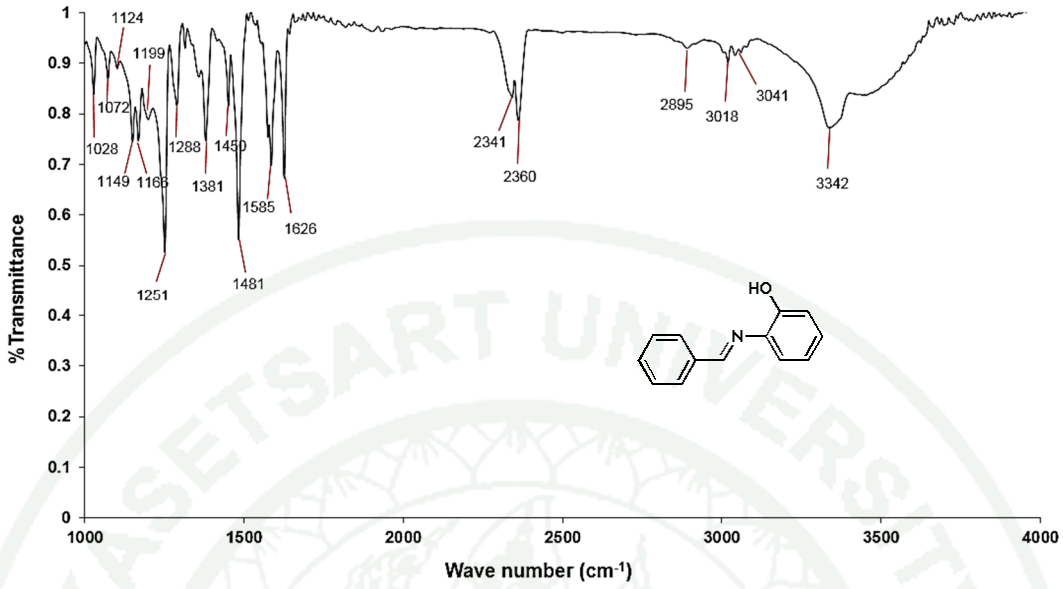

Appendix Figure B3 FT-IR spectrum of (Benzylideneamino)phenol (Compound III).

Appendix C

Molecular structure for optimization in quantum calculation with the relative energies

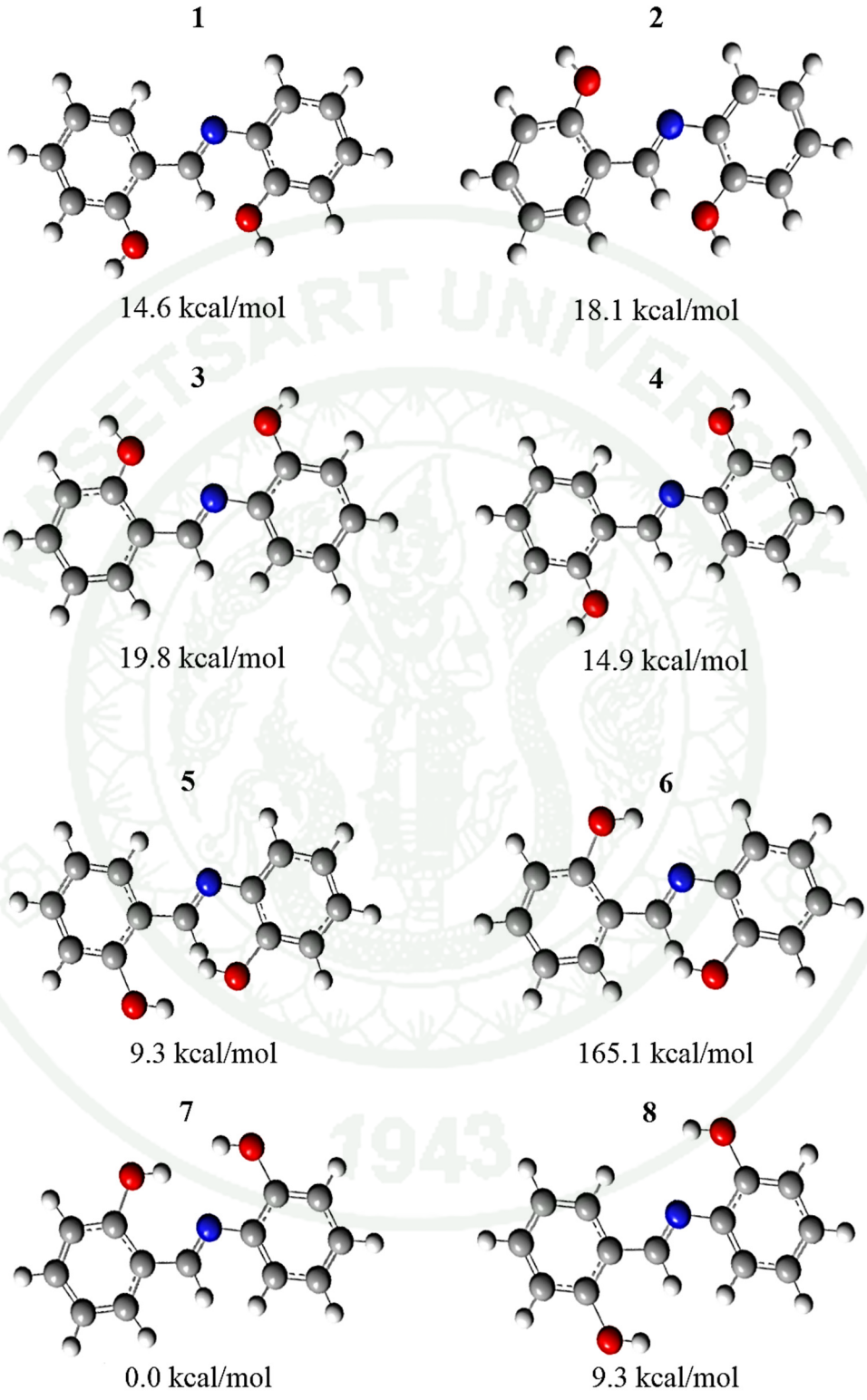

Appendix Figure C1 Possible conformations of Compound (I) were optimized by CAM-B3LYP/6-311G (d,p) including relative energies.

Appendix D

Optimized structure in enol, transition state and keto form of Compound (II) and (III)

2-(hydroxybenzylidene)aniline (Compound II)

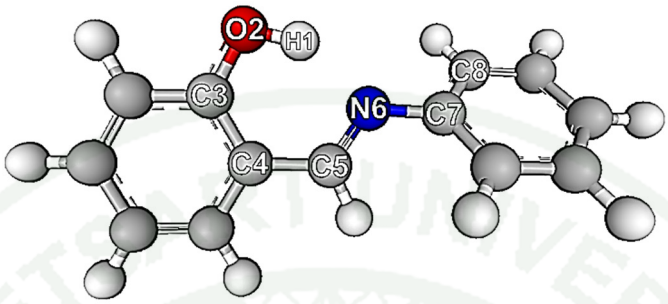

(a) E-form

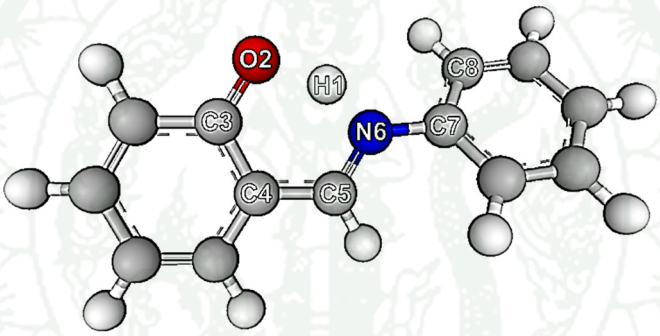

(b) TS-form

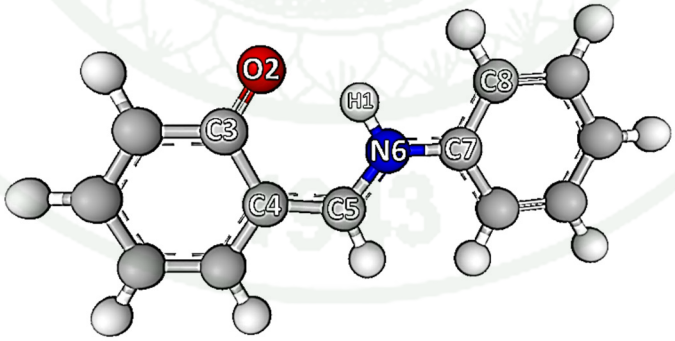

(c) K-form

Appendix Figure D1 Optimized structures of Compound (II) (a) E-form, (b) TS and (c) K-form which calculated in gas phase by CAM-B3LYP with 6-311G(d,p) basis set.

(Benzylideneamino)phenol (Compound III)

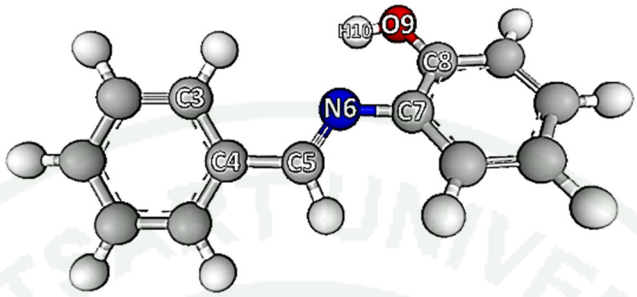

(a) E-form

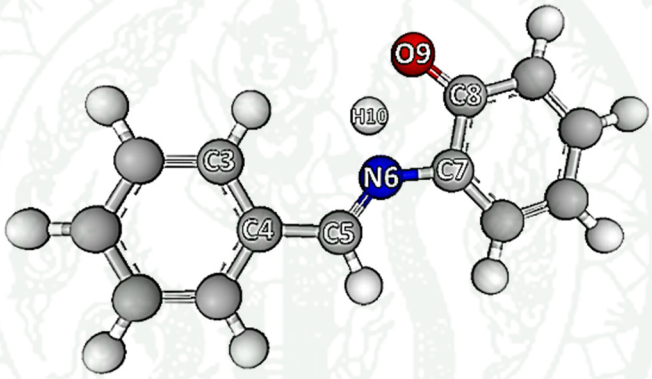

(b) TS-form

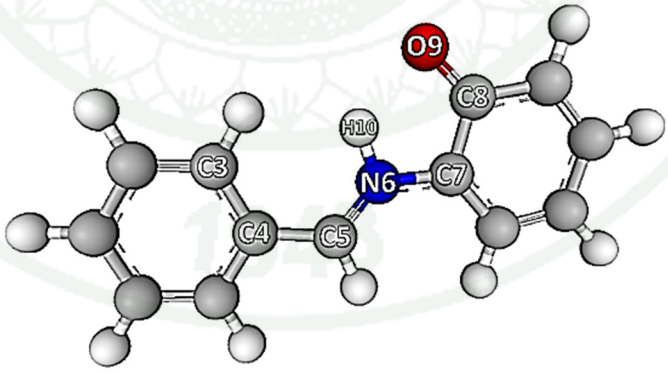

(c) K-form

Appendix Figure D2 Optimized structures of Compound (III) (a) E-form, (b) TS and (c) K-form which calculated in gas phase by CAM-B3LYP with 6-311G(d,p) basis set.

CURRICULUM VITAE

NAME : Ms. Nutjarin Klinhom

BIRTH DATE : Sep 06, 1987

BIRTH PLACE : Songkla, Thailand

EDUCATION :

YEAR	INSTITUTE	DEGREE/DIPLOMA
2006-2009	Silpakorn Univ.	B.Sc. (Chemistry)
2011-Present	Kasetsart Univ.	M.S. (Chemistry)

POSITION/TITLE : Postgraduated student

WORK PLACE : Faculty of science, Kasetsart University

SCHOLARSHIP :
- Laboratory of Computational and Applied Chemistry (LCAC)
- The National Research University Project of Thailand (NRU)
- Kasetsart University Research and DeverlopmentInstitute (KURDI)

PUBLICATION :

1. Proceeding

Nutjarin Klinhom, Supa Hannongbua and Songwut Suramitr **Theoretical Study on Sensing Mechanism of Salicylaldimine Based Chemosensor: Excited state Proton Transfer.** 17th International Annual Symposium on Computation Science and Engineering (ANSCSE17), Khon Kaen University, Khon Kaen, Thailand, 27-29 March 2013.

Theoretical Study on the Sensing Mechanism of Salicylaldimine Based Chemosensor: Excited-State Proton Transfer

Nutjarin Klinhom[1,2,3], Supa Hannongbua[1,2,3] and Songwut Suramitr[1,2,3,c]

[1] Laboratory for Computational and Applied Chemistry, Department of Chemistry, Faculty of Science and Center of Nanotechnology, Kasetsart University Research and Development Institute, Kasetsart University, Bangkok 10900, Thailand
[2] NANOTEC Center for the Design of Nanoscale Materials for Green Nanotechnology, Kasetsart University, Bangkok 10900, Thailand
[3] Center for Advanced Studies in Nanotechnology and its Applications in Chemical, Food, and Agricultural Industries, Kasetsart University, Bangkok 10900, Thailand

[c] E-mail: fsciswsm@ku.ac.th email; Fax: +66 2 562 5555 ext.2176; Tel. +66 2 562 5555 ext.2227

EXTENDED ABSTRACT

Both intermolecular and intramolecular hydrogen-bonding interactions induce an excited-proton transfer (ESPT), are proposed to account for the fluorescence sensing mechanism of a fluoride chemosensor, 2-(2-hydroxybenzylideneamino) phenol. The time-dependent density functional theory (TD-DFT) method has been applied to investigate the varied electronic states. The present theoretical study of this chemosensor, as well as its anion and fluoride complex, has been conducted with a view to monitoring its structural and photophysical properties. The proton of the chemosensor can shift to fluoride in the ground state but transfers from the proton donor (OH group) to a proton acceptor (NH group) in the first singlet excited state.

Keywords: Computational Science, Computational Conferences.

INTRODUCTION

A chemosensor is a molecular device designed to detect a specific molecule or class of molecules. Research in this field shows considerable advances with the advent of diverse methods for analyze detection and new developments in the field of molecular recognition.[1] The development of chemosensors for specific chemical species is an important research area within the field of supramolecular chemistry. One of the most appealing approaches involves the construction of colorimetric sensors, species that would allow the so-called 'naked-eye' detection without resort to any spectroscopic instrumentation.

In recent years, designing molecular systems for sensing anions and cations with ''naked-eye'' detection is an attractive goal. Such system generally contain some combination of substrate recognition functionality (receptor) and optical signal reporter group (chromophore) which are designed to permit the detection of substrates via binding-induced changes in absorption properties.

Anions are ubiquitous throughout biological systems and play a fundamental role in a wide range of chemical and biological processes.[2] However, the recognition and sensing of anions have been interest due to the importance of anions in biological, industrial and environment processes.[3] Among the interests in biologically functional anions, Fluoride is the smallest and most electronegativity anion. It is one of particular importance owing to its established role in dental care and treatment of osteoporosis.[4] However, high level of fluoride has been associated with osteosarcoma, and some effects on the brain, such as lower IQ values.[5] Up to now, several chemosensors for F- have been reported.[3,4,5] However, the realization of both colorimetric and fluorescent measurements for F- is still a challenge.

Salicylaldimine based is colorimetric and fluorescent chemosensors for anion and cation sensing properties, 2-(2-hydroxybenzylideneamino) phenol as colorimetric chemosensor for fluoride contains an N⋯H—O intramolecular hydrogen bond in the ground state.[6]

Hydrogen-bonding interaction is the most popular and important way for chemosensors designed to detect fluoride.[7] Many neutral chemosensors containing N-H moieties enable selective anion recognition in aqueous solution. It is noted that a p-system bearing an N-H moiety may be an appropriate candidate for designing fluoride chemosensors, because the N-H moiety tends to bind the fluoride anion (F^-···H-N) through hydrogen bonding. In recent year, many studies have focus on the mechanism of such processes. The transfer of a proton (PT) in ground or excited-state proton transfer (ESPT) along the hydrogen bonds can neutralize the charge separation in intramolecular charge transfer (ICT) state. Consequently, the hydrogen-bond-induced ICT of this chemosensor can be used to detect the fluoride anion through optical responses, such as UV/Vis and fluorescence spectroscopy. Previous theoretical studies have revealed that a PT or ESPT process is often responsible for the colorimetric and fluorescent signaling of chemosensors.[8] To further understand the sensing mechanism, we could use density functional theory (DFT) and time dependent density functional theory (TD-DFT) to clarify fundamental aspects concerning the hydrogen bond formation in the S_0 and S_1 states, respectively. Accordingly, it is important to understand the detailed sensing mechanism of the interaction between the chemosensor and anions because of its clearly crucial role in determining selectivity. In the present work, we report a theoretical study relating this chemosensor, which may represent a new candidate for investigating the mechanism of fluoride reorganization. The present calculation aims to provide a complementary view on the sensing mechanism of this molecule. In particular, we have focused our attention on the mechanism regarding enol-keto tautormerization.[9] and the hydrogen-bonding interaction between this chemosensor and fluoride anion in both the ground state and the excited state.

Computational detail

Density functional theory (DFT) that is popular theoretical method, has been used efficiently and accurately in studying the mechanism of fluoride chemosensor. Time dependent density functional theory (TD-DFT) method has been confirmed to be an effective candidate to investigate the electronic spectra and electronic excited state. So in this work we use DFT and TD-DFT methods in GAUSSIAN 09 program to deal with all the electronic structure calculation including the ground state and the excited state. Hybrid functional with long-range corrections (CAMB3LYP) with 6-311G(d,p) basis set was used which is further confirmed by the good accordance of our results with the experiment ones in the current paper. All electronic structure calculations were confirmed with the absence of an imaginary mode in vibrational frequency calculations.

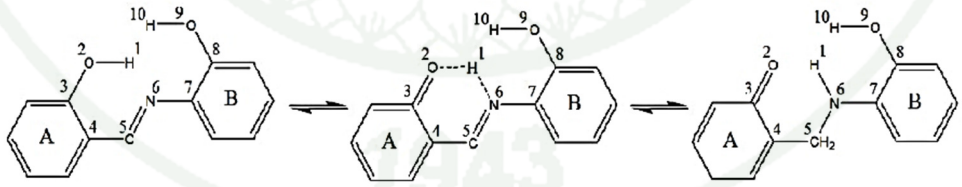

Figure 1. Structure and Atomic labelling atom of the chemosensor 2-(2-hydroxybenzylideneamino)phenol, enol and keto form.

RESULTS

The structures of enol and keto form were fully optimized by using CAM-B3LYP with 6-311G(d,p) basic set. The results show that formation of tatomerization prefer occur on aromatic A to aromatic B because the formation of transition state by six membered ring is more stable than 5 membered ring. Some of the calculated structural parameters including bond lengths, bond angle and torsional angle are shown in Table 1.

From Table 1 displays bond lengths, bond angle and dihedral angle of Enol, transition (TS) and Keto form of 2-(2-hydroxybenzylideneamino)phenol. The calculated structural parameters are in good agreement with the corresponding values reported in x-ray experiment for similar compounds.[10] It is indicated that CAMB3LYP/6-311G(d,p) calculation can use to study in system. The calculated dihedral angles demonstrate that both the keto and enol tautomers are planar. The intramolecular-hydrogen bond generates a six membered ring in both the keto and enol tautomers. This interaction is between and phenolic O-H donor N acceptor, where the hydrogen-bond length of O-H is about 0.82 Å and C3-O2 single bond is 1.34 Å in enol form. The keto and enol tautomers could be converted to each other via an intramolecular proton transfer (IPT) reaction. The enol form change in the enol-keto IPT, the most important of which are: the C2-O1 bond length decreases from 1.34 in the Enol form to 1.25 Å in the keto form. N-H hydrogen-bond length shows 1.06 Å indicating that the H-bonding interaction is relatively strong. The calculated hydrogen bond angles H1-O2-N6 in enol and keto tautomers are 146.8 and 144.6°, respectively.

Table 1. The calculated bond lengths (Å), angle (◦) and torsional angle (◦) of 2-(2-hydroxy-benzylideneamino) phenol, enol and keto form.

Parameters	Enol form		TS-A form	Keto-A form
	Calculated	X-ray*	Calculated	Calculated
Bond lengths (Å)				
O2-H1	0.98	0.82	1.29	1.56
C3-O2	1.34	1.35	1.28	1.25
C3-C4	1.41	1.41	1.44	1.46
C4-C5	1.45	1.45	1.41	1.39
C5-N6	1.28	1.29	1.31	1.32
N6-C7	1.41	1.42	1.40	1.40
C7-C8	1.40	1.38	1.40	1.40
C8-O9	1.35	-	1.36	1.36
C9-H10	0.97	-	0.97	0.96
N6-H1	1.76	-	1.20	1.06
Bond angle (◦)				
∠C4-C5-N6	123.0	121.7	120.0	123.5
∠C5-N6-C7	121.2	124.4	125.2	126.5
∠C3-O2-H1	107.5	109.5	104.1	-
∠C8-O9-H10	107.8	-	109.6	110.4
Torsional angle (◦)				
∠C3-C4-C5-N6	-3.2	0.9	-0.4	-0.215
∠C5-N6-C7-C8	145.6	-179.2	-154.5	161.9

*Zhao, L., X.-T. Dong, et al. (2012). Acta Crystallographica Section E 68(2): o429.

For investigate the excited-state proton transfer (ESPT) process, tne Enol and Keto form were calculated the excitation energy by using TD-DFT(CAM-B3LYP) with 6-311G(d,p) basis set. The absorption spectra for Enol and Keto carried out by TD-DFT(CAMB3LYP) are show in Table 2. In Table 2, we can see that $S_0 \rightarrow S_1$ transition for chemosensor is predicted at about 340 nm with large oscillator strength 0.7309. Whereas, the $S_0 \rightarrow S_1$ transition for Keto-A is also the dominant transition with the largest oscillator strength of 0.3236 lies at about 364 nm. The change in excitation from 327 to 364 indicating that transformation from enol to ketol is caused by intramolecular transfer of transition state.

Table 2. The electronic properties for chemosensor, Enol and Enol-A

Transition	Excitation			Major contributions	Expt.*
	E_{exc} (eV)	E_{exc} (nm)	*f*		
Enol					
$S_0 \rightarrow S_1$	3.79	327	0.7309	HOMO→LUMO (92%)	340
$S_0 \rightarrow S_2$	4.37	283	0.0956	H-1→LUMO (81%)	-
$S_0 \rightarrow S_3$	4.85	255	0.0397	H-2→LUMO (62%)	-
$S_0 \rightarrow S_4$	5.03	246	0.3216	H-3→LUMO (52%)	260
$S_0 \rightarrow S_5$	5.60	222	0.1128	HOMO→L+1 (40%)	-
Keto					
$S_0 \rightarrow S_1$	3.41	364	0.3236	HOMO → LUMO (97%)	-
$S_0 \rightarrow S_2$	3.84	323	0.0096	H-3 → LUMO (77%)	-
$S_0 \rightarrow S_3$	4.42	281	0.2873	H-1 → LUMO (76%)	-
$S_0 \rightarrow S_4$	4.92	252	0.0885	H-2→LUMO (71%)	-
$S_0 \rightarrow S_5$	5.46	227	0.0462	HOMO→L+1 (45%)	-

* Prabhu, S., Saravanamoorthy, S., Ashok, M., and Velmathi, S. *Journal of Luminescence*, 2012, **132**(4), 979-986.

Energy schematics in Figure 2 show the excitation energy of enol-keto tautomerization. Red arrows indicate the absorption and emission wavelength while lines represent the calculated energy of excitation from each isomer minimum in the ground and excited states. The results confirmed that excited state intramolecular proton transfer (ESIPT) occur through excited enol isomer undergoes tautomerization to an excited keto form. The excited keto then emits fluorescence when it transitions back to the keto ground state. The transition from singlet to the ground singlet of keto-A emits singlet-singlet transition wavelength photon about 457 nm.

Conclusion

In this work, structural parameters and energetic characters of both the enol and keto tautomers of the 2-(2-hydroxybenzylideneamino) phenol as well as its tautomerization mechanism have been theoretically studied using CAM-B3LYP method with 6-311g(d,p) basic set. The density functional theory (DFT) calculations showed that the enol tautomer is more stable than the keto tautomer. The calculated E_a for the keto-enol tautomerism is 11.0 kcal/mol.

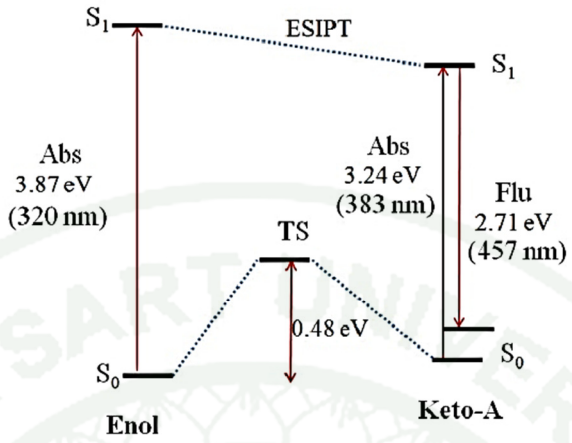

Figure 2. Energy schematics of the optimized ground and excited states of Enol, Transition state and Keto form of chemosensor.

ACKNOWLEDGMENTS

This work was supported by the Thailand Research Fund (RTA5380010 to SH and MRG5480273 to SS). SS was supported from the Asea-Uninet, the University of Vienna and Science Research Fund (ScRF), and ScAWAKE from Faculty of Science, Kasetsart University. Center of Nanotechnology Kasetsart University, Kasetsart University Research and Development Institute (KURDI), National Nanotechnology Center (NANOTEC), Laboratory of Computational and Applied Chemistry (LCAC), the Commission on Higher Education, Ministry of Education [trough ''the National Research University Project of Thailand (NRU)'' and the ''National Center of Excellence for Petroleum, Petrochemical and Advanced Materials (NCEPPAM)''] are gratefully acknowledged for research facilities. The calculations were performed in part on the Schrodinger III cluster and the VSC of the University of Vienna.

REFERENCES

1. Martínez-Máñez, R., and Sancenón, F., *Chemical Reviews*, 2003, **103**(11), 4419-4476.
2. Sun, H., Dong, X., Liu, S., Zhao, Q., Mou, X., Yang, H. Y., and Huang, W. *The Journal of Physical Chemistry C*, 2011, **115**(40), 19947-19954.
3. Odago, M. O., Colabello, D. M., and Lees, A. J. *Tetrahedron*, 2010, **66**(38), 7465-7471.
4. Peng, X., Wu, Y., Fan, J., Tian, M., and Han, K. *The Journal of Organic Chemistry*, 2005, **70**(25), 10524-10531.
5. Ambrosi, G., Formica, M., Fusi, V., Giorgi, L., Macedi, E., Piersanti, G., and Zappia, G. *Tetrahedron*, 2012, **68**(19), 3768-3775.
6. Prabhu, S., Saravanamoorthy, S., Ashok, M., and Velmathi, S. *Journal of Luminescence*, 2012, **132**(4), 979-986.
7. Li, G. Y., Zhao, G. J., Liu, Y. H., Han, K. L., and He, G. Z. *J Comput Chem*, 2010, **31**(8), 1759-1765.\
8. Song, P., Ding, J. X., and Chu, T. S. *Spectrochim Acta A Mol Biomol Spectrosc*, 2012, **97**, 746-752.
9. Massaro, R. D., and Blaisten-Barojas, E. *J Chem Phys*, 2011, **135**(16), 164306-164313

2. Poster Presentation

Nutjarin Klinhom, Supa Hannongbua and Songwut Suramitr **Theoretical Study on Sensing Mechanism of Salicylaldimine Based Chemosensor: Excited state Proton Transfer.** The 2nd Chemistry Postgraduate Symposium (ChPGS2), Department of Chemistry, Faculty of science, Kasetsart University, Bangkok, THAILAND

Theoretical Study on the Sensing Mechanism of Salicylaldimine Based Chemosensor : Excited-State Intramolecular Proton Transfer

Nutjarin Klinhom and Songwut Suramitr*
Department of Chemistry, Faculty of Science,
Kasetsart University, Bangkok, Thailand
Email address: nutjarin.k@gmail.com Tel. +66-81-8113936

Abstract Excited State Intramolecular Proton Transfer (ESIPT) are proposed to account for the fluorescence sensing mechanism of a fluoride chemosensor, 2-(2-hydroxybenzylideneamino)phenol. The time-dependent density functional theory (TD-DFT) method has been applied to investigate the varied electronic states. The present theoretical study of Enol-Keto tautomerize chemosensor has been conducted with a view to monitoring its structural and photophysical properties. Tautomerization occur by proton transfer which shift from the proton donor (OH group) to acceptor (NH group) through Excited-State Intramolcular Proton Transfer (ESIPT)

Introduction

Chemosensor is a molecular device designed to detect a specific molecule or class of molecules. 2-(2-hydroxybenzylideneamino) phenol is colorimetric and fluorescent chemosensor for fluoride ion. From its structure, it occur Enol-Keto tautomerization through Excited State Intramolecular Proton Transfer (ESIPT) which involves a hydrogen atom moving from its initial binding site to another functional group in the same molecule. To understand on chemosensor mechanism, Enol-Keto tautomer of 2-(2-hydroxybenzylideneamino) phenol was study using quantum chemical calculation

Objective

1. To investigate the structural and electronic properties of 2-(2-hydroxybenzylideneamino) phenol by using quantum chemical calculation
2. To study the tautomerization mechanism through Excited-State Intramolecular Proton Transfer (ESIPT) using CAM-B3LYP/6-311G(d,p) level of theory

Experiment

In this work we use DFT and TD-DFT methods in GAUSSIAN 09 program to deal with all the electronic structure calculation including the ground state and the excited state. Hybrid functional with long-range corrections (CAMB3LYP) with 6-311G(d,p) basis set was used. All electronic structure calculations were confirmed with the absence of an imaginary mode in vibrational frequency calculations.

Results and Discussion

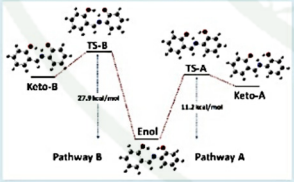

Figure 1. Relative energies of Transition state involving hydrogen transfer corresponding to Enol – Keto tautomerization of Pathway A and Pathway B

The result shows that transition state A has relative energy lower than transition state B. It conclude that 2-(2-hydroxybenzylidene amino)phenol prefer Pathway A than B

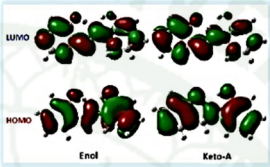

Figure 2. HOMO and LUMO orbitals of Enol-Keto tautomer (left)

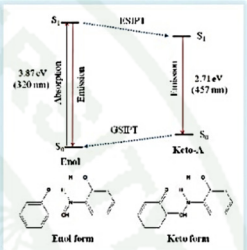

Figure 3. Schematic representation of the ESIPT process of Salicylaldimine (right)

Fig. 2, the acidic character of the phenol group and the basic character of amine group change in the excited state with excitation of the electron from HOMO to LUMO pushing the π-electronic density toward the N atom of the molecule. It is advantageous for proton transfer in excited-singlet state. For the HOMO orbital of keto tautomer shows high electron density on the O atom, this electronic distribution leads to proton transfer from the Keto to the Enol tautomer in the ground state. The schematic representation of the ESIPT process is shown on Fig. 3.

Conclusion

In this work, structural parameters and energetic characters of both the enol and keto tautomers of the 2-(2-hydroxybenzylidene amino) phenol as well as its tautomerization mechanism have been theoretically studied using CAM-B3LYP method with 6-311g(d,p) basic set. The Time-Dependent Density Functional Theory (TD-DFT) calculations showed that chemosensor occur Enol-Keto Tautomerization through Excited-State Intramolecular Proton Transfer from OH of phenyl on aromatic A to N of amino.

References

1. Prabhu, S., Saravanamoorthy, S., Ashok, M., and Velmathi, S. *Journal of Luminescence*, 2012, 132(4), 979-986.
2. Kim, Y. H., Roh, S. G., Jung, S. D., Chung, M. A., Kim, H. K., and Cho, D. W. *Photochem Photobiol Sci*, 2010, 9(5), 722-729.

Acknowledgement

I would like to thank National Research University Project of Thailand (NRU), Kasetsart University and Kasetsart University Research and Development Institute (KURDI).